In situ DNA synthesis in porous silicon for biosensing applications

Jenifer L. Lawrie

Dissertation

Submitted to the Faculty of the

Graduate School of Vanderbilt University

in partial fulfillment of the requirements

for the degree of

DOCTOR OF PHILOSOPHY
in

Interdisciplinary Materials Science

December, 2012

Nashville, TN

Committee:

Sharon M. Weiss; Department of Electrical Engineering and Computer Science, Department of Physics and Astronomy

Richard F. Haglund, Jr.; Department of Physics and Astronomy

Paul E. Laibinis; Department of Chemistry and Biomolecular Engineering

Deyu Li; Department of Mechanical Engineering

Michael P. Stone; Department of Chemistry

Dedications

To Ben, Isaac, and Evelyn

Acknowledgements

I am very thankful for all of those whom I have had the pleasure to work with on this project. I would like to express my thanks to Professor Sharon Weiss for her guidance on this research as my academic advisor. Professor Weiss's support and questions continually push me to investigate further and probe deeper into my research. Her encouragement and critiques have helped me to acquire experimental, analytical, and presentation skills during the five years I have worked in her laboratory. This dissertation also would not have been possible without the support of Professor Laibinis, who provided significant guidance, advice, and equipment to the work of DNA synthesis.

I would also like to express my gratitude to Professors Haglund, Li, and Stone for serving on my Ph.D. committee and for their expertise throughout my time here at Vanderbilt. Each member of my committee has provided vital feedback during each Committee meeting, and aided greatly in the development of my research. Additionally, Professor Richard Mu, my advisor during my time at Fisk University, has aided my growth as a scientist from the moment I stepped into his lab, and encouraged me on the path towards completing my Ph.D. dissertation.

I have had the pleasure to work with a number of post-docs, graduate students, and undergraduate students during my time at Vanderbilt University. I would especially like to thank Dr. Guoguang Rong and Dr. Zhou Xu, who both provided extensive training and technical discussion. I would like to thank other member of the Weiss Group, past and present, particularly Dr. Xing Wei, Girija Gaur, Yang Jiao, Judson Ryckman, Dr. Jeremy Mares, Shweta Bhandaru, Gilbert Rodriguez, Dayana Abd Rahman, and Yiliang

Zhao. I would additionally like to thank Professor Bridget Rodgers, Bobby Harl, and Dr. Ben Schmidt for their expertise and assistance with X-ray photoelectron spectroscopy and surface analysis of porous silicon samples. Dr. Steve Vilt and Professor Kane Jennings provided valuable guidance on selecting and synthesizing monomers for substrate functionalization. Dr. Amanda Furtado from Professor LeVan's research group also provided assistance in completing and interpreting nitrogen adsorption isotherms for analyzing porous silicon surface area. Finally, some analysis was completed in the Vanderbilt Institute for Nanoscale Science and Engineering facilities. I owe many thanks to Professors Anthony Hmelo and Dmitry Koktysh for technical assistance and training.

Finally, I would never have made it this far without the love and support of my family. My husband, Ben, has been by my side throughout this endeavor, always ready to provide feedback, look for solutions, or simply commiserate after a bad day of experiments. Our parents and siblings have been a constant presence in our lives, despite the distances separating us, and have gone above and beyond in encouraging me in my research. My children, Isaac and Evelyn, are my joy and inspiration. They make the tough days in research worth working past, and the good days in the lab worth celebrating.

This work was generously supported in part by Army Research Office, Project #W911NF-08-1-0200, and a Vanderbilt University Discovery Grant.

TABLE OF CONTENTS

TABLE OF FIGURES

PREFACE

Porous silicon optical structures have generated significant interest in recent years for biological applications such as drug delivery, environmental monitoring, and chemical sensing. The enormous internal surface area in porous silicon of up to a few hundred square meters per cubic centimeter provides a significant advantage for capturing and detecting gaseous, chemical, and biological species. The pore diameters, the porosity, and the thickness of the porous layers can be carefully controlled by tuning the fabrication conditions in order to produce high quality optical structures. For a waveguide structure, the light is guided in the plane of the thin film, facilitating the integration of such a sensor, along with source and detector components, into lab-on-a-chip devices. Varying the effective porous silicon optical thickness by biorecognition events in the waveguide results in a shift in the reflectance resonance, and allows for quantitative analysis of the target biomolecules.

In an effort to increase the sensitivity of porous silicon waveguide sensors, we have utilized in situ synthesis of DNA oligonucleotide bioreceptors, in contrast to the traditional method of infiltrating and attaching bioreceptor molecules on the internal surfaces of the pores. Applying this commercial, solid-phase synthesis method using phosphoramidite protected nucleic acids, DNA oligos are immobilized in the waveguide in higher densities than allowed via the traditional method. As a result, DNA conformation, flexibility, and length do not play a role in bioreceptor density. The increased sensitivity of in situ prepared porous silicon waveguide sensors has been demonstrated for short oligo targets.

This work demonstrates the use of porous silicon waveguides for label-free detection of target DNA oligos, with the lowest detection limits reported in the nanomolar range. Bioreceptor and target molecule infiltration for a given waveguide porosity has been shown to depend directly on the DNA oligo length. The pore size, DNA bioreceptor density and length, and target size and aspect ratio play a significant role in molecule infiltration and detection sensitivity of porous silicon waveguide sensors. Using synthesized DNA oligos in porous silicon as aptamers, highly selective detection of the small molecule target adenosine and ochratoxin A has also been demonstrated. This first demonstration of DNA aptamer-based sensing within porous silicon may be expanded to other small molecule targets of interest, combining the high selectivity of aptamer detection schemes with the sensitivity and filtering capabilities afforded by mesoporous silicon waveguide sensors.

Chapter 1

1. INTRODUCTION TO BIOSENSING

1.1 Definition and classification of biosensors

Although reports of biosensing devices have only occurred over the past 50 years, humans have essentially been performing biological and chemical detection for millennia. Antibodies in our immune system identify and neutralize foreign invaders; enzymes in our taste buds distinguish between sour and sweet; and olfactory receptor neurons can recognize thousands of different scents. With improved technology and understanding of biological organisms in the last century, researchers have looked toward many of these highly efficient and highly specialized bio-mechanisms as inspiration for new sensing devices. Evolution has produced bio-recognition molecules of unmatched specificity. As a result, the vast majority of biosensing devices utilize a bio-recognition system either taken directly from a living organism, or designed to mimic their function.

When it comes to building biosensing devices in the laboratory, a signal transducer is required in order to take the reaction of the bioreceptor, which selectively binds the molecule of interest, and convert it to a measurable signal. Bioreceptors have an affinity for and ability to capture a molecule of interest. For signal transduction, there are a number of methods available, generally falling under the categories of optical, electrochemical, or mass-related transduction [1-4]. Of these categories, optical transduction is by far the most widely utilized, given the variety of spectrochemical properties available to be recorded for any given material. Optical transducers reported in the literature include absorption, reflection, transmission, fluorescence, Raman, and surface enhanced Raman scattering. It is in the area of optical signal transduction that the

unique optical properties of silicon play a crucial role in the development of new and innovative biosensing devices [5-7].

Typically, biosensors and lab-on-a-chip devices are classified by either their bioreceptor unit or their transduction method. Depending upon the desired application, there is a large variety of possible bioreceptors and transducer materials, and each transduction method may be utilized with a number of different bioreceptor-target systems. Figure 1.1 illustrates the variety of bioreceptor and transducer options available for building biosensing devices. Examples of these sensing device combinations will be discussed in this chapter. Sensing devices discussed throughout this dissertation will be classified by their transducer microstructure, and by the accompanying spectroscopy technique used to detect the analyte of interest.

This chapter will begin with a basic overview of the variety of bioreceptor molecules and transduction mechanisms frequently employed in sensor devices. The distinctions and inherent advantages and disadvantages of labeled and label-free biosensing will be outlined. In this work, the aim is to highlight the role of silicon photonics in biosensing applications for small molecule detection. As such, an outline of the major classes of silicon photonic biosensing devices classified by the specific signal transduction method utilized will be included. A discussion of the current challenges in small molecule and oligonucleotide detection in silicon photonic sensing devices and the motivations for the thesis will conclude this chapter.

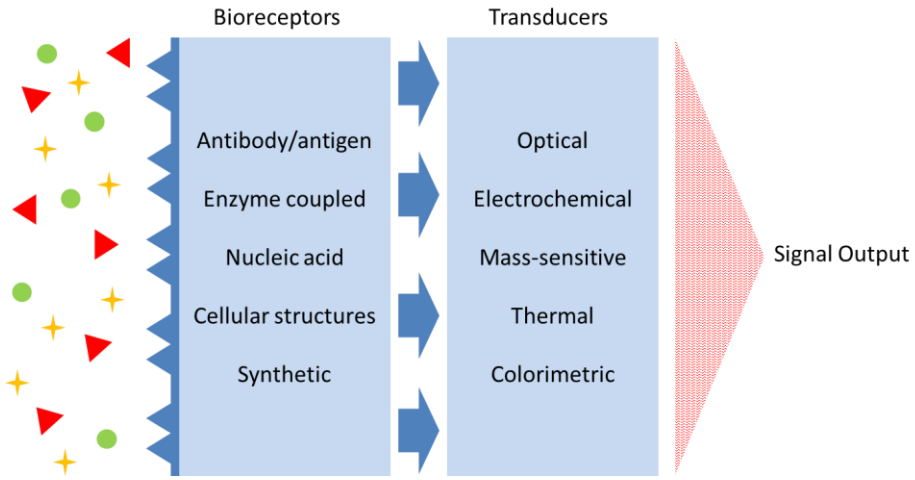

Figure 1.1 Classification of biosensors by type of bioreceptor or transducer. At the bioreceptor, a chemical change occurs selectively in the presence of target biomolecules. The transducer transforms this interaction into a quantitative, electronic signal which can be collected and analyzed.

1.1.1 Common classes of bioreceptors

Figure 1.2 below illustrates the binding mechanisms of a number of bioreceptor-target binding interactions. A bioreceptor (also referred to as probe or sense molecule) has the ability to preferentially bind to the target molecule of interest. The most commonly utilized bioreceptor structures found in sensing devices are derived or designed from biological organisms: antibodies, enzymes, nucleic acids, and other cellular structures. In principle, any biomolecule or molecular assembly that displays the ability to selectively capture a target molecule could be used as a bioreceptor. It can be challenging however to maintain the functionality of these biologically derived or inspired structures as they are attached and utilized on various substrate surfaces or in different sensing media. Each of these categories will be described in further detail below.

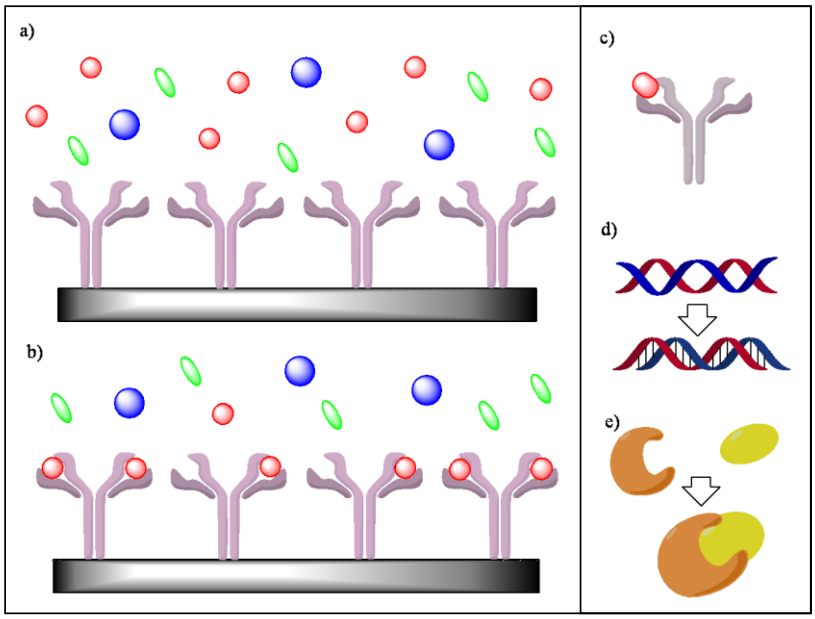

Figure 1.2: On the left, selective capture of target biomolecules by bioreceptors attached to a surface is illustrated. (a) A sensor surface functionalized with antibody molecules (i.e. bioreceptors) is exposed to a solution containing target and mismatched antigens. (b) Only the target antigens are bound to the immobilized antibodies. On the right, examples of common bioreceptor and target pairs are shown: (c) antibody and antigen pair, (d) DNA as a receptor for a complementary DNA oligo, and (e) an enzyme and target protein.

The antibody-antigen bio-recognition system is often viewed as a gold-standard in biosensing. Antibodies are complex proteins, which may be composed of hundreds of amino acid subunits, and corresponding antigen targets typically must exceed 5000 Da in order to prompt an immunogenic response. In such a system, the biological molecules known as antibodies act as a receptor site toward a large protein target molecule, in what is often described as a "lock and key" fit. The "lock and key" refers to the antibody's specific conformation, which allows for binding of the target antigen based upon specific characteristics such as size, geometric conformation, and active chemical functional groups. In a typical antibody/antigen biosensor, the antibody molecules are immobilized on the surface and are capable of selectively binding a target antigen. Although

antibody/antigen binding has remarkably high specificity, some of the major challenges of antibody-based biosensor are achieving proper orientation of the antibodies onto sensor surface and the lifetime and stability of antibodies in sensing media.

With a few exceptions, enzymes are generally a specific type of protein – a biological macromolecule composed of amino acids. Some enzymes are composed only of amino acids, while others include co-factors (often transition metal ions) or co-enzymes (complex organometallic molecules). Often, enzymes are selected for use in biosensors for their specific binding capability or catalytic activity. Catalytic activity in particular can impart unique properties to a biosensing device, as enzyme-coupled reactors can be designed to modify the bioreceptor mechanism. For example, ligand binding at the receptor may change the activity of an enzyme. Additionally, biosensors using enzyme bioreceptors can potentially show very high sensitivity toward a particular target, since the biorecognition event is not a one-to-one binding, but rather an enzymatic activity. For example, consider a glucose sensing fiber-optic device that has the enzyme glucose oxidase immobilized on the surface. Instead of directly sensing glucose, a detector measures the presence of oxygen in solution; the level of oxygen changes when the enzymatic reaction between glucose and glucose oxidase occurs [8].

Nucleic acids are a common choice for biorecognition molecules, where the hybridization event involving deoxyribonucleic acid (DNA) or ribonucleic acid (RNA) is detected. For DNA sensors, the hybridization reaction between the biorecognition element and target molecule results from the pairing up of complementary bases on corresponding oligos, with cytosine (C) bases in the oligo binding guanine (G) on the complement, and adenine (A) bases binding thymine (T) on the complement molecule.

Nucleic acids have also been of considerable interest for biochip technologies that use nucleic acids as bioreceptors for detecting molecules other than complementary DNA strands. When nucleic acid structures are engineered for the detection of non-nucleic acid targets, they are referred to as aptamers. This topic will be addressed further in Chapter 5. The considerable flexibility in defining a nucleic acid sequence and length, allows for the generation of a large library of DNA sequences, which increases the likelihood of finding a suitable bioreceptor for a particular target of interest.

Cellular structure bioreceptors encompass a broad category that could include anything from using non-enzymatic transport proteins for target molecule binding to bioluminescent proteins for toxin detection in bacteria. When using cellular structures as bioreceptors, an entire cell or micro-organism may be included in the sensor, or just a particular cell component. A few examples of such biorecognition systems are the protein cytochrome c' used for nitric oxide detection [9] and lipopeptides for virus detection [10].

1.1.2 Common classes and examples of signal transducers

Just as critical as the bioreceptor for biosensor fabrication is the transducer element. The transducer translates the chemical binding event at the receptor into a measureable signal, from which quantitative information about the target capture can be collected. By far, the most common class of signal transducers is optical. As an example, for enzyme-based biosensors there is a large body of research utilizing optical transduction methods [11] – including absorptiometry [12], luminometry [13, 14], chemiluminescence [15], scattering [16], and surface plasmon resonance [17].

A number of electrochemical sensors have also been described, and play an important role in chemical and biomedical sensing elements [18-21]. One of the most

prolific biosensing devices containing an electrochemical transducer is undoubtedly the home glucose sensor [22]. Generally, electrochemical transduction occurs via conductivity, capacitance, potentiometric, amperometric, or voltammetric sensing [2, 4, 18, 20, 21]. These systems require an electrochemical cell with a standard electrode arrangement. They can be found applied in both in vivo and in vitro applications. Modern electrochemical sensors utilizing antibody or nucleic acid bioreceptors for early cancer detection have been described in the literature [20]. Simple, disposable DNA-based electrochemical biosensors for detection of both nucleic acid sequences and small molecule targets have been reported [23].

Additionally, many sensors utilize mass-sensitive signal transducers. Typically, these systems rely on surface acoustics, piezoelectric response, or a microcantilever device [3]. Several commercial devices utilize quartz crystal microbalances to detect biomolecule binding [24, 25]. Mass-sensitive transduction methods typically are not as sensitive as optical transduction, mainly as a result of the larger surface area required for mass-sensitive transduction schemes [26]. In recent years however, mass sensors have been developed that not only respond to target capture, but also provide molecular characterization information such as charge density, viscosity, elasticity modulus, and molecular conformation. Similarly, silicon microcantilever devices have shown high sensitivity and the ability to analyze certain molecular characteristics such as charge upon target binding [27].

1.1.3 Labeled vs. label-free biosensors

In addition to the standard classifications by receptor and transducer, biosensors are very commonly separated into the broad categories of “labeled” and “label-free”.

Generally, this designation indicates the source of the transduced signal produced upon biorecognition. In some sensing systems, a target molecule or structure undergoes a chemical work-up to attach a specialized tag or label which is utilized for detection; these sensing systems are now known as labeled sensors. The designation of labeled sensor was first introduced in 1990 with the development of the first commercial label-free optical biosensor – Biacore – to contrast the label-free method of molecular detection that does not require special tags or labels. Before label-free systems were commonly available, the most common sensing platforms for biomolecule detection involved enzyme-linked immunoassays or immunofluorescence assays. Complex chemistry attaching enzymes, fluorescent labels or radiometric labels can make labeled biosensing a time consuming endeavor. Additionally, any labels attached will invariably modify the structures of the receptor or target, ultimately affecting the kinetics of the binding event. Labeled sensing is typically not performed in real-time, meaning that kinetic and thermodynamic analysis cannot be performed. Despite these notable disadvantages, there is one major advantage to labeled biosensors – high sensitivity. Labeled sensing schemes with reported detection limits in fM levels have been reported [6].

Over the last two decades, label-free biosensing techniques have grown substantially. A broad spectrum of devices has been described in the literature and commercially developed systems are available. Most label-free biosensing devices rely on changes in optical properties – particularly surface plasmon resonance and attenuated total reflectance – but mass-sensitive, acoustic, and calorimetric label-free detection schemes have also been described. In an optical label-free biosensor, signal is often generated by a change in effective refractive index of the substrate as binding of target

biomolecules occur. Measurement in such systems may be by reflection, transmission, or by molecular adsorption fingerprints. A number of commercial label-free biosensing systems have been developed since the 1990's. GE's Biacore utilizes an surface plasmon resonance-based arrays on which oligonucleotides [28] and a number of other targets have been detected. ForteBio's Octet measurement system relies on interferometry layers on a disposable fiber optic sensor requiring no microfluidics [29]. An example of a mass-sensitive label-free device is Attana System's quartz microbalance sensors [30]. The xCelligence system from Roche Applied Sciences operates via electrochemical transduction of the binding event [31], and has been used in cellular pharmaco-toxicology applications.

1.2 Porous silicon optical biosensors

Although porous silicon was first reported in 1956 [32], interest in the material was rather limited until its room temperature photoluminescence was observed [33]. Since then, there has been considerable interest in the integration of porous silicon components into optoelectronic devices, and more recently biochemical devices, based on the tunable nature of the physical and optical properties of the material. The pore diameters, which can range from nanometers to microns in size, as well as the porosity and thickness of the porous layer, can be tuned depending upon the formation conditions, typically in an electrolyte containing hydrofluoric acid. When the pore diameter is much smaller than the wavelength of light, porous silicon can be treated as an effective medium for which the refractive index is a weighted average of the refractive indices of separate components of the composite matrix [34]. Adjusting the porosity of the silicon allows for a wide range of refractive indices to be achieved. Depending on the conditions, a

refractive index range of approximately 1.15 to 3.30 can be produced by appropriate tuning of the fabrication conditions. Multilayer thin film structures, such as Bragg mirrors, rugate filters, microcavities, and waveguides can be formed by simply varying the porosity through electrochemical etching. Since the etching preferentially proceeds at the pore tips where the electric field is concentrated and charge carriers are present, under most conditions the previously formed porous silicon layers are not etched further as the formation of subsequent layers proceeds. As a result, sharp interfaces between porous silicon layers of different porosity (different refractive index) are produced.

Over the past several years, there has been an increasing level of interest generated in the biological applications of porous silicon, such as drug delivery, environmental and chemical sensing, and filters for molecular separations. One of the most significant advantages of porous silicon is the enormous internal surface area, which can range up to a few hundred square meters per cubic centimeter. Since many more biological molecules can attach to porous silicon compared to planar materials, its structure provides a significant advantage for capturing and detecting gaseous, chemical, and biological species. In the following sections, several different porous silicon optical structures are discussed for their application as biosensors. A more focused discussion of porous silicon for DNA detection is presented in Section 3.1.2.

1.2.1 Porous silicon photoluminescence biosensors

Some of the earliest sensing work using porous silicon took advantage of the photoluminescence of the material, in particular, room-temperature photoluminescence, which was first observed for porous silicon in the early 1990's. Porous silicon emits a broadband luminescence centered in the red portion of the electromagnetic spectrum.

While photoluminescent tags are commonly used in labeled biomolecule detection, the examples that follow are all label-free systems, where the biorecognition event induces a change in the natural photoluminescent properties of the material. Porous silicon biosensors using photoluminescence transduction have been developed for organic solvents, explosives, and hazardous wastes.

There are a limited number of reports of detection of biomolecules due to porous silicon photoluminescence, likely due to the greater measurement error compared with the other methods described in this chapter. The photoluminescence of porous silicon is known to be highly sensitive to a number of molecular species, via mechanisms such as electron transfer and interfacial charging, while exposed to biological media, which makes it difficult to account for background effects and drift in the photoluminescence peak [35]. Nevertheless, biosensors utilizing photoluminescence as the transduction method have been reported based on both photoluminescence quenching and spectral shifts. Immunocomplex formation between an antibody and antigen within a porous silicon matrix has been observed to quench the material's photoluminescence [36], and a similar quenching mechanism was observed for DNA hybridization in porous silicon [37]. In both reports, the photoluminescence quenching was attributed to a non-radiative recombination mechanism. Resonance shifts in the photoluminescence spectra of porous silicon microcavities when functionalized and subsequently exposed to target bacteria[38] and DNA oligos [39] have also been reported. The microcavity structure is described in detail in Section 1.2.4.

1.2.2 Single-layer thin films – optical reflectance

The most basic transduction method utilizing porous silicon is based on the change in effective optical thickness of porous silicon films upon a binding event between receptor and target molecules in a single-layer thin film, as illustrated in Figure 1.3. This sensing mechanism takes advantage of the difference between the phase of light reflected at the top and bottom interfaces of a porous silicon layer. A reflectance spectrum for such a porous silicon thin film shows a characteristic Fabry-Perot interference pattern; the fringe spacing is dependent upon the optical thickness of the porous silicon layer. Infiltration of bioreceptors into the pores, and the subsequent biorecognition reaction with a target molecule results in a change in the optical thickness of the thin film due to the increase in the effective refractive index as the biological target replaces air in the pores. Detection of a specific molecular species is possible due to appropriate surface chemistry preparation in the pores, as discussed in Section 2.1.2.

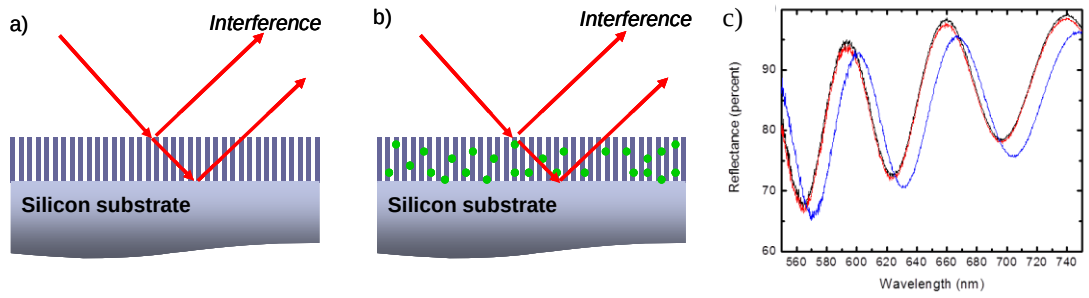

Figure 1.3 Single layer porous silicon film on silicon substrate. Characteristic Fabry-Perot interference patterns are produced through reflectance measurement (a). Infiltration of the porous silicon film with biomolecules (b) increases the effective refractive index of the layer, and results in a shift in the interference fringes. The change in reflectance spectrum upon infiltration with biomolecules is demonstrated (c).

A porous silicon interferometric biosensing device was first introduced by Sailor and colleagues in 1997, a breakthrough which sparked significant interest in porous silicon as a platform for optical biosensing [40]. A porous silicon thin film was fabricated via electrochemical etch, oxidized, and functionalized with a chemical linker. Either DNA oligonucleotides or proteins were attached as bioreceptors in the films. To monitor the DNA hybridization or protein interaction, the reflectance spectrum was taken before and after exposure to the target molecule of interest, and the Fabry-Perot fringes were monitored. In the initial work by Sailor and colleagues, a blue-shift (e.g. shift to shorter wavelengths) in the interference pattern - instead of the expected red-shift (e.g. shift to longer wavelength) corresponding to an increase in optical thickness - was observed. This blue-shift of the DNA was later attributed to the corrosion of the porous silicon layer upon exposure to the analyte solution [41]. This unanticipated dissolution of the film, however, resulted in a sensitivity that remains unmatched in similar single layer porous silicon sensors using optical reflectance measurements. Detection limits in the sub-picomolar range were observed [40]. Recently it has been shown that labeling DNA oligonucleotides with charge-carrying metal complexes can increase the porous silicon corrosion rate, thus improving the sensitivity of the detector. With a labeled system in a single-layer interferometer sensor, detection limits in the sub-micromolar range can be achieved for a number of bioreceptor and target pairs [42].

The dissolution of the porous silicon thin film, and thus the blue-shift of the Fabry-Perot spectrum, can be prevented by selecting appropriate surface passivation chemistry. Essentially, the observation of a blue-shift indicates that the surface was not effectively passivated against chemical attack by the analyte solution. By adjusting the

oxidation or silanization conditions appropriately, the surface dissolution in analyte is prevented, allowing for unambiguous detection of the target molecules through a red-shift in the Fabry-Perot optical signature. This red-shift in the optical reflectance spectrum has been observed for affinity interactions [43], protein-protein interactions [44], DNA hybridization [45], and small molecule binding [46] in single layer porous silicon. These systems, however, are considerably less sensitive than those relying on porous silicon dissolution. Typical detection limits of red-shifted sensors are in the micromolar range [5].

In recent years, there has been further development of Fabry-Perot optical materials for biosensing, such as two-layer interferometric biosensors with different pore sizes in each layer. A major limitation of the single-layer devices is the drift observed in the effective optical thickness of the thin film due to complex media being introduced and inferring with the sensor. Drift can be difficult to account for in real-time measurements, and has a significant impact on sensor performance. The two-layer architecture provides a top porous layer for the biorecognition event to occur within, and adds a bottom porous layer to act as the reference layer. The porosity, and correspondingly pore size, of the bottom layer is sufficiently small to exclude biomolecules based upon size, ensuring that the target biorecognition event occurs only in the top porous layer. When reflectance data is taken for these two layer systems, the three superimposed interference patterns that result (i.e. due to top layer, bottom layer, and combined layers) allow for a built-in control to compensate for signal drift by separately providing data on the binding, adsorption, and partitioning in the layers. Size-dependent filtration and molecular detection was demonstrated using the bovine serum albumin (66kDa) and sucrose (0.34

kDa). The porosities of the layers were tuned such that the larger BSA molecule could only penetrate the top porous layer, but the smaller sucrose molecule could access both the top and bottom pores [47].

1.2.3 Bragg mirrors

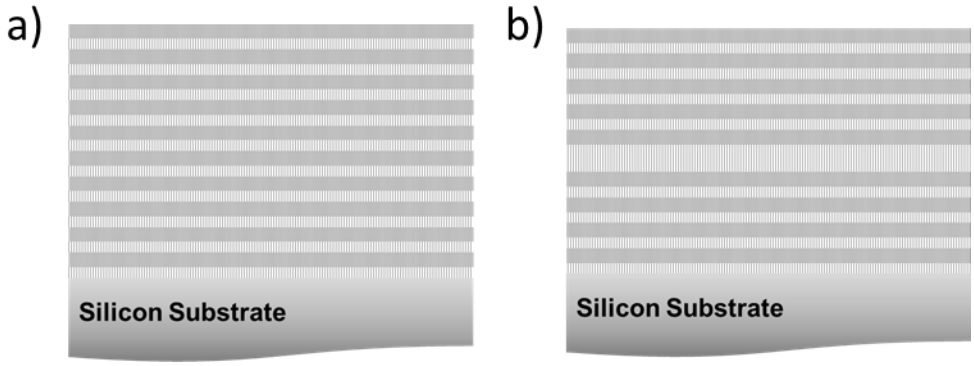

Figure 1.4: The Bragg mirror consists of alternating layers of high index and low index porous silicon (a). The Microcavity consists of similar alternating layers of high and low index, but a defect cavity is introduced into the middle of the structure, breaking the periodicity (b).

Bragg mirrors are a class of one-dimensional photonic crystal that have been produced in porous silicon for biosensing. Fabrication builds upon the methods discussed in the previous section. By periodically changing the applied current density during the electrochemical etch using a step function; alternating layers of high and low porosities of porous silicon are obtained as shown in Figure 1.4. The condition $\lambda/4$ for the optical thickness is typically applied to the Bragg mirrors, and gives a near 100% reflectance band over the spectral region of interest, centered at the designed wavelength λ. When biomolecules infiltrate into the porous layers, there is a red-shift in the wavelength of the stop-band, allowing one to monitor changes in the reflectance spectrum of the Bragg mirror to detect the presence of biomolecules.

Some limited work in biosensing with Bragg mirrors has been done, including a set of theoretical [48] and experimental analyses comparing the sensitivity of Bragg mirrors to single-layer porous silicon layers [49]. When a sucrose solution was introduced to the different porous silicon architectures, experiments suggested that Bragg mirror biosensors may be more sensitive than single layer biosensing structures [49].

1.2.4 Microcavities

Introduction of a defect layer in the middle of a Bragg mirror results in a porous silicon architecture known as a microcavity as shown in Figure 1.4. The defect layer is simply a layer that has a different optical thickness than either of the repeated two-layers that form the Bragg mirror. A resonant microcavity is often formed within a Bragg mirror, with an optical thickness that is an integer multiple of $\lambda/2$. Breaking up the periodicity of the Bragg mirror with the resonant cavity results in a sharp resonance feature in the reflectance spectrum, located within the Bragg stop band at the designed wavelength λ. This resonance occurs as light becomes trapped and resonates in the defect in the microcavity [50]. The resonance can be quite sharp and narrow, which suggests that a microcavity may be a highly sensitive system capable of detecting very small shifts in the optical spectrum. As a result, microcavities have received considerably more attention than Bragg mirrors for biosensing applications. Sub-nanometer line width cavity resonances are possible in microcavities with optimized parameters [51].

As with the Bragg mirror, in order for the microcavity to be effective in biosensing applications, the pore size must be sufficiently large to allow for infiltration of the target biomolecules into the pores. In particular for the microcavity, the biomolecules must pass into the defect layer deep within the Bragg mirror layers (typically > 1 μm) if

any signal from the sensor is to be measured. This limits the possible applications of Bragg mirrors and microcavities in macromolecule detection. In order to expand the list of potential target molecules, techniques have been developed to expand the pore openings found in microcavity architectures. One such technique employs post-anodization etching of porous silicon in an alkaline solution [52], which was shown to enlarge the pores and allow infiltration of protein into the defect layer. Pore widening does, however, result in a broadening of the cavity resonance, which compromises the ultimate detection limit of the sensor. For macromolecules such as proteins, optimizing and etching a porous silicon microcavity with larger pores by utilizing n-type silicon has been shown to be an effective way to preserve reasonable optical quality of microcavity sensors with pore diameters of approximately 100nm [53, 54]. Similar microcavity structures have also shown promise in label-free detection of specific antigens in serum and whole blood samples, indicating that the inherent size exclusion properties of these sensors could prove effective in direct point-of-care analysis of complex biological samples [55].

1.2.5 Rugate filters

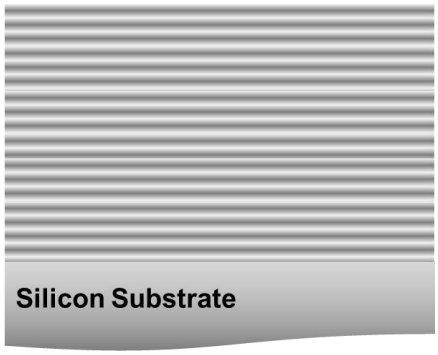

Figure 1.5: In a porous silicon rugate filter, porosity varies in a sinusoidal manner between high and low porosity. The structure is fabricated by applying an etch current varying sinusoidally in time.

As opposed to the step-wise variations in porosity to achieve porous silicon microcavities, rugate filters are produced by sinusoidal variation of the current density applied during the electrochemical etch as illustrated in Figure 1.5. The resulting reflectance spectrum of a rugate filter is characterized by a relatively narrow high-reflectance stop-band with suppressed side lobes. Similar to the architectures previously described, small changes to the effective optical thickness of the porous matrix will result in a shift of the characteristic reflectance stop-band. Thus the optical reflectance characteristics again allow the porous silicon to act as a signal transducer upon biorecognition and binding of the target molecule. One significant advantage of the rugate filter over Bragg mirrors or microcavity sensors is the low contrast between the high and low porosity layers. Generally, the porosity variation is less than one percent, meaning the difference in diffusion rates for the biomolecules varies little from one layer to another.

Porous silicon rugate filters have received considerable interest in the literature for their application in detecting enzymes. Sailor and colleagues utilized a rugate filter architecture in their "smart dust" microparticles [56]. The porous layers in their work were functionalized via methylation, which prevented the infiltration of large biomolecules into the pores. The protein zein was subsequently adsorbed onto the upper surface of the porous silicon. Exposure to the enzyme pepsin led to digestion of the zein, breaking the protein into smaller peptide fragments which could easily filter into the rugate filter's pores. As these digestion products infiltrated into the pores, a red-shift in the reflectance spectrum was observed. This device showed a color change visible to the

naked eye when protease concentration was higher than 14μM. The detection limit of this "smart dust" towards protease was 7μM [57]. Gao and colleagues were able to replicate this system using gelatin instead of zein, and detected the presence of the enzyme gelatinase [58]. Rugate filters with the ability to detect protease via digestion products could have applications in biological laboratories, possibly in the development of petri dishes with a built-in system to monitor the health of cell cultures by the presence of protease.

An alternative system for protease detection in rugate filters was developed by Kilian and colleagues [59]. Instead of adsorption on the top surface of the porous matrix, short peptides were covalently immobilized in the internal surfaces of the porous silicon matrix. Subsequent exposure to the target protease resulted in a blue-shift of the stop-band, as the peptides within the matrix are digested and the resulting small fragments are washed out of the sensor. Because a single protease may digest many peptides within the sensor, a low detection limit of 7.2pM of protease was achieved. Similar systems have been developed for detection of protein loading, cellular processes, and other small biomolecules.

1.2.6 Waveguides

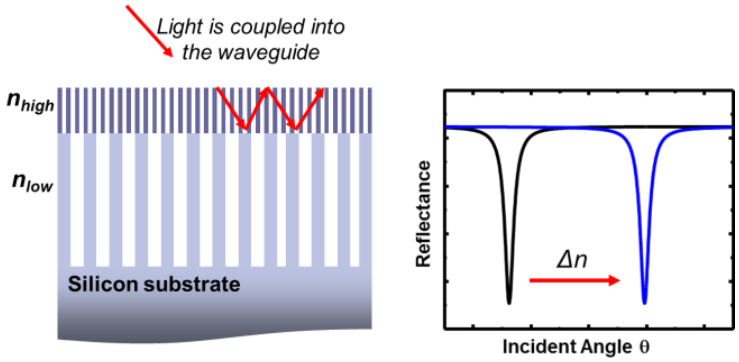

Figure 1.6: At left, the waveguide structure is illustrated, with a high refractive index layer of porous silicon above a low index cladding layer of porous silicon. Under specific conditions, an incident beam may be coupled into the waveguide layer and will propagate by total internal reflection within that high index, low porosity layer. The conditions at which a mode match will occur are dependent upon the effective refractive index of the porous silicon layer. At right a typical graph showing the shift to higher resonance angle upon the change in refractive index of the waveguide layer.

Porous silicon waveguides for biosensing are a relatively recent advance [60], although porous silicon waveguides were used for solvent detection as early as 1998 [61]. A significant advantage of the waveguide structure is that light is guided in the plane of the thin film, facilitating the integration of such a sensor, along with source and detector components, into lab-on-a-chip devices. Additionally, the active sensing layer in a porous silicon waveguide is the top porous layer, eliminating the infiltration difficulties that can plague Bragg mirrors, rugate filters, and microcavities, where biomolecules must filter through many layers of both high and low porosity. As a result, waveguide sensors display electric field localization, sharp resonance peaks, and a thin sensing layer, qualities that facilitate fast response and a high sensitivity detection of molecules.

A prototypical porous silicon waveguide consists of a waveguide layer of low porosity (high refractive index) porous silicon in which light is guided via total internal reflection, bounded by a cladding layer of high porosity porous silicon (low refractive

index) as shown in Figure 1.6. Porous silicon waveguides have also been demonstrated using a single layer of porous silicon with a low index polymer cladding [62, 63]. A prism or grating [64] can be used to couple light into the waveguide from the top. Under the proper conditions (e.g. angle of incidence, wavelength of light) a characteristic dip, or peak, in the reflectance spectrum appears. Varying the effective porous silicon optical thickness by biorecognition events in the waveguide results in a shift in the reflectance resonance, and allows for quantitative analysis of the target biomolecules present.

Previous work has demonstrated that compared to SPR platforms, porous silicon waveguides may show higher sensitivity by attenuated total reflection measurements [60]. In a porous silicon waveguide, guided waves propagate through the material overlapping with the region in which molecular binding events occur, unlike SPR sensors in which an evanescent, exponentially decaying wave interacts with bound molecules; hence, the strength of interaction between light and target molecules is higher in the porous silicon waveguide. Weiss and colleagues demonstrated the use of p-type porous silicon waveguides for detection of target DNA oligos of 8-, 16-, and 24-mer in length, with the lowest detection limit projected to be in the nanomolar range [62, 63, 65]. Bioreceptor and target molecule infiltration for a given waveguide porosity was shown to be dependent upon the DNA oligo length [66].

1.3 Current challenges in label-free small molecule and oligo detection

Even with the many advances in label-free sensing described in previous sections, many challenges remain, particularly in the area of small molecule detection. A major obstacle is that, given their relatively low mass, small molecule targets often cannot generate sufficient signal in a label-free platform. In SPR immunoassay sensors for

example, direct detection of antigenic targets may be possible, but such systems generally display poor sensitivity or low signal. Frequently high mass labels are attached to target antigens or competitive immunoassays are developed or signal enhancement via nanoparticle conjugation will be introduced to improve small molecule detection. In such systems however, the advantages of a label-free sensing approach – no pre-sensing work-up, real-time kinetics analysis – are forfeited.

The high surface area to volume ratio in porous silicon allows for the immobilization of a large number of bioreceptors within the porous matrix, increasing the likelihood of target capture and detection. As noted in the previous section, a major advantage of porous silicon is its ease of integration with standard semiconductor processing and well-described tunable morphology. By changing fabrication parameters, structures with pore sizes ranging from a few nanometers to several microns can be achieved, uniform porosity layers with controlled thickness approaching the thickness of the starting silicon substrate are possible, and switching between discrete layers of different porosity or forming uniform gradients between high and low porosity as etching progresses down into a silicon wafer have been described. The variation in possible pore sizes can allow for the infiltration of biomolecular targets of interest while excluding larger, contaminating species. However, with very small targets – such as nucleic acids or small molecules – challenges of bioreceptor molecule preparation remain.

Previous work in the Weiss group has demonstrated that infiltrating porous silicon waveguides with bioreceptors can be challenging, even when the waveguide pore diameters are up to five times larger than the bioreceptor size [67]. In this case, the aspect ratio and charge on DNA bioreceptors may have resulted in a significant barrier to

infiltration into porous silicon. If porous silicon waveguides are to be utilized in biosensing applications while retaining their high sensitivity and selectivity, alternatives to simple bioreceptor infiltration for pore wall functionalization must be realized. In addition, the desired small pore diameters of the porous silicon waveguide limit the possible classes of bioreceptor that may be used for target capture. In order to expand porous silicon waveguide usage to applications involving small molecules that are captured using a larger molecule bioreceptor, it is likely that the bioreceptors for these small molecules will need to be synthesized from the bottom up within the mesopores in order to circumvent the inherent size-selecting properties of the porous silicon.

1.4 Objectives of the dissertation

The objective of this dissertation is to implement and optimize a method of DNA synthesis into porous silicon optical structures for use as nucleic acid bioreceptors within a label-free optical sensing platform. This work will demonstrate that in situ synthesis of DNA bioreceptors and tuning of DNA surface density allows for unmatched detection sensitivity for oligo sensing in porous silicon waveguides. Additionally, the in situ synthesis method allows for longer oligo sequences to be achieved in mesoporous waveguides than could be infiltrated by traditional attachment methods. These longer DNA oligos may be used as aptamers for the detection of small molecule targets. The chapters to follow will each examine one of the objectives below:

- Demonstrate synthesis of DNA oligonucleotides in porous silicon waveguides, and compare to traditional porous silicon functionalization with infiltrated, pre-synthesized DNA oligonucleotides (Chapter 2).
- Observe the selective detection of target oligonucleotides by in situ synthesized DNA bioreceptors within the waveguides (Chapter 3).

- Optimize DNA bioreceptor surface coverage within porous silicon in order to reduce steric crowding effects and increase sensitivity toward target biomolecules (Chapter 4).

- Utilize in situ synthesized DNA bioreceptors in porous silicon as aptamers for detection of small molecule targets (Chapter 5).

Chapter 2

2. POROUS SILICON WAVEGUIDE FABRICATION AND FUNCTIONALIZATION

2.1 Porous silicon waveguide preparation and measurement

2.1.1 Waveguide fabrication

In a waveguide structure, light is guided in the plane of the thin film, facilitating the integration of such a sensor, along with source and detector components, into lab-on-a-chip devices. The porous silicon waveguides used in this work were fabricated by traditional electrochemical etching techniques, using 15% hydrofluoric (HF) acid in ethanol as the electrolyte [67]. The waveguide consists of a low porosity (high refractive index) porous silicon layer in which light is guided via total internal reflection, bounded by a cladding layer of high porosity porous silicon (low refractive index) and air as shown in Figure 2.1. In other work, porous silicon waveguides have been demonstrated using a single layer of porous silicon with a low index polymer cladding [62, 63].

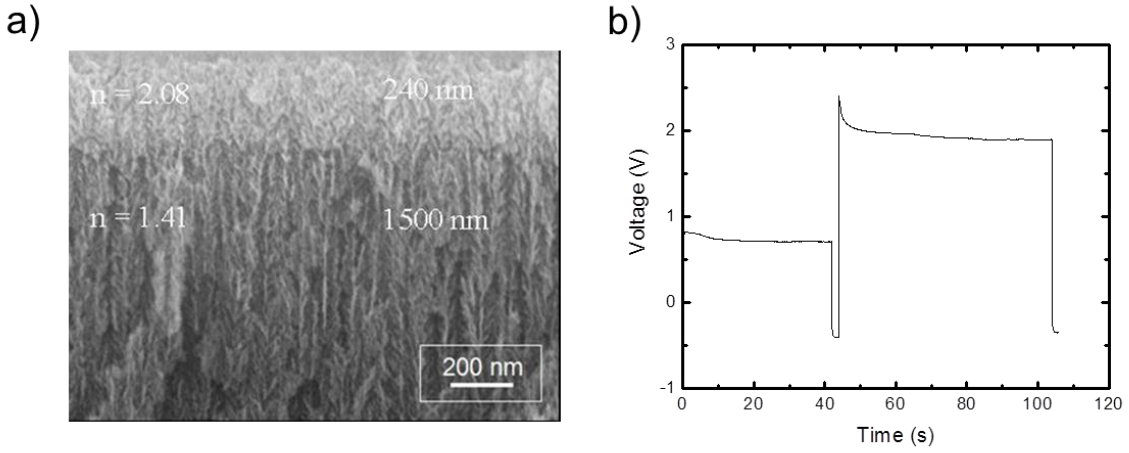

Figure 2.1: Two layer porous silicon waveguide structure fabricated by electrochemical etch in HF solution. At the resonance condition, light is guided in the top (high index) layer. The cladding layer (low index) is below (a). Lower applied voltage across the electrochemical cell results in the high index, low porosity layer, whereas higher applied voltage produces the low index, high porosity layer.

The development and details of the electrochemical etching parameters to form the porous silicon layers in hydrofluoric acid electrolyte with desired thickness and porosities have been developed previously in the Weiss group [65, 67]. Electrochemical etch in porous silicon is by far the most commonly used method of porous silicon fabrication. In his process, hydrogen-terminating silicon surfaces are immersed in the HF electrolyte and a current is applied perpendicular to the wafer surface. Applied current drives holes within the silicon matrix towards the exposed HF electrolyte solution. At the surface, successive nucleophilic attacks by the fluoride ions in solution at silicon-hydrogen bonds occurs, forming two new silicon-fluorine bond and allowing for H_2 to be released to the solution. The polarization of the Si-F species leaved the neighboring Si-Si bonds susceptible to further nucleophilic attack by fluoride ions. When a silicon tetrafluoride ion is formed, dissolution of this anion into the electrolyte after reaction with additional HF to the stable SiF_6^- occurs. In this manner, silicon atoms are dissolved from the substrate surface. The process occurs directionally as a result of the applied electric field. Hole transfer takes place at the interface between the silicon and the solvent. As pore tips begin to form, electric field is concentrated at these regions, initiating further etching. Holes are depleted from the side walls of the pores as they travel directionally to the wafer-electrolyte surface, minimizing pore widening effects and ensuring that the etch propagates primarily in one direction. Although some questions about the details of the mechanism remain, it has been described in detail in a number of texts [68-73].

For this work, p-type silicon wafers (~0.01 Ω cm) were chosen to enable mesopore formation. Before anodization, the native oxide layer was removed by soaking

for one minute in the 15% HF solution in ethanol, followed by ethanol rinsing. This procedure was used to facilitate the pore initiation process. Anodization then proceeded as detailed in Table 2.1. Samples are immobilized in a Teflon etch cell and exposed to electrolyte. The low current is applied first, forming the high refractive index, low porosity layer. After the desired thickness is achieve, current is turned off for two seconds. The high current is subsequently applied, forming the low refractive index, high porosity layer below. Current application and timing for each etch step in the waveguide fabrication is automated through a Keithley Instruments SourceMeter using Labview.

Layer	**Current density (mA/cm^2)**	**Etch time (sec)**	**Thickness (nm)**	**Post-KOH Refractive Index**
Waveguide	5	42	240	1.77
Cladding	48	60	1500	1.32

Table 2.1: Etch parameters for porous silicon waveguide fabrication. Resulting refractive index and thickness values (measured by SEM) are included for each layer following 30 min KOH pore opening process.

Following HF electrochemical etch, the substrates are exposed to a 1.5 mM solution of potassium hydroxide (KOH) in ethanol for 30 min. This solution is prepared from a 9mM stock solution of KOH dissolved in water, which is diluted 5:1 with ethanol. The 30 minute incubation takes place in a sealed petri dish with full immersion of the substrate to limit evaporation of the solvent. At the end of the etch time, the KOH etch solution is pipetted out of the container, and the substrate is covered with ethanol for an

additional 5 minute soak. Finally, samples are removed from incubating solution and washed thoroughly with ethanol. Care is taken to ensure that samples do not dry out before having been thoroughly rinsed, as salt crystallization may occur within the pores. After washing, samples are dried under nitrogen. The resulting pore diameters were 20-30 nm, estimated from SEM images.

2.1.2 Optical measurement techniques

A Metricon 2010 prism coupler was used to evanescently couple 1550 nm light from a diode laser into the porous silicon waveguide (Figure 2.2), although grating coupling [64] could also be used. Light couples into the waveguide at a resonant angle that corresponds to a wavevector match between the incident light and the propagating waveguide mode. This resonant angle directly correlates to the effective refractive index of the porous silicon waveguide, as shown in Equation 1,

$$k_0 n_p \sin\theta = k_0 n_{eff} \tag{1}$$

where n_p is the refractive index of the prism, θ is the angle of incidence within the prism, and n_{eff} is the effective index of the waveguide mode, which is related to the refractive index of the porous silicon film. The presence and quantity of DNA or other molecules inside the waveguide is determined by monitoring the resonant angle θ that satisfies Equation 1. Molecular DNA attachment inside the pores causes the refractive index of the porous silicon to change, leading to a change in the effective index of the waveguide mode and a corresponding shift of the resonant angle. The magnitude of the resonance shift increases as a function of the quantity of molecules immobilized in the

pores. The waveguide allows particularly sensitive detection of small molecules since the electric field is primarily confined in the top porous silicon layer; hence the most sensitive sensing region (i.e. top waveguideing layer) is the layer that is most easily accessible to infiltrates. Given the fast response time and strong field confinement observed in porous silicon waveguides, even small concentrations of molecules attached in the pores result in a measurable shift of the coupling angle.

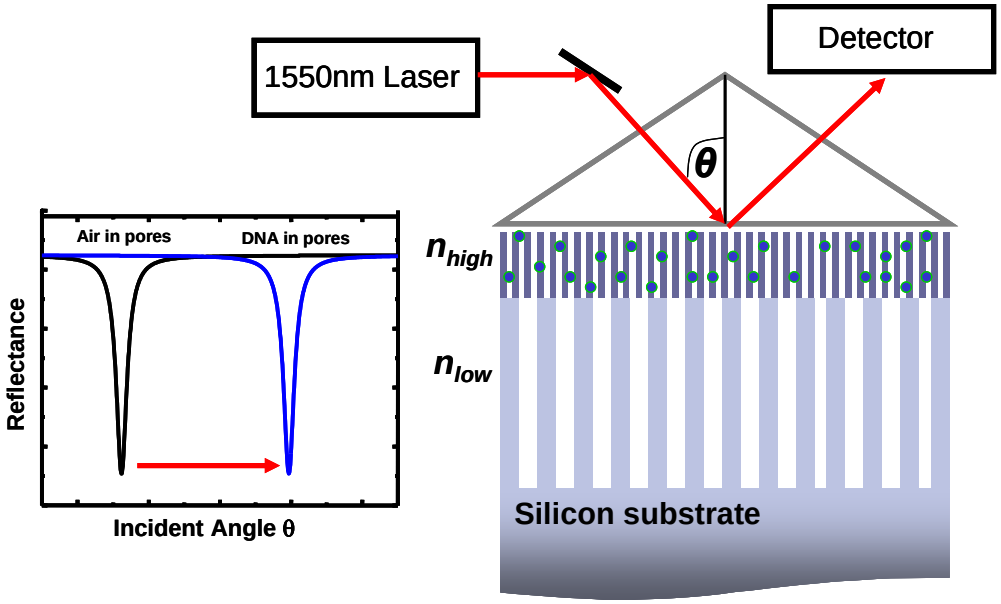

Figure 2.2: Schematic of prism coupler configuration for measurement of a porous silicon waveguide sample with DNA. The source is a 1550 nm diode laser. For most incident angles, light reflects off the prism base into the detector. For one particular angle (i.e., resonance angle), light is evanescently coupled into the waveguide. The inset graph shows typical attenuated total reflectance spectra characterized by a dip in reflectance at the resonance angle; the resonance shift to higher angle that occurs upon the introduction of biomolecules such as DNA into the waveguide is illustrated.

2.1.3 Porous silicon waveguide passivation

Porous silicon waveguides for biosensing are a relatively recent advance [60], although porous silicon waveguides were used for solvent detection as early as 1998 [61]. Of critical importance in the development of porous silicon biosensing platforms and

devices is the silicon surface preparation, allowing for appropriate passivation of the material towards aqueous solutions and functionalization for recognition of the biomolecule target. Passivation of the surface to provide a stable material for detection in a variety of biological solutions is especially important for porous silicon due to its biocompatibility, which causes degradation in physiologic fluids [74]. Detection of a number of biomolecules of interest, particularly in lab-on-a-chip flow cells, occurs in physiologic fluids. Surface degradation could lead to dramatic changes in effective optical thickness, which would significantly affect sensor performance and reliability [75]. This effect becomes amplified with the high surface-to-volume ratio in porous silicon.

Immediately after fabrication, porous silicon architectures have silicon-hydride terminated pore walls. The silicon-hydride bond is highly susceptible to oxidation under ambient conditions, so immediate stabilization of the material is required. Given the disparity between the near infrared refractive indices of silicon oxide (n = 1.45) and silicon (n = 3.5), fixing the silicon to oxygen ratio in the sensing layers of the material is critical. There are two general methods of surface passivation currently utilized in silicon photonics. The first method involves controlled growth of an oxide layer on the porous silicon architecture, and the second method involved passivation of the surface via formation of silicon-carbon bonds.

The more common method for porous silicon passivation is the growth of an oxide layer. The popularity of this method is more likely a reflection of the method's relative ease and repeatability, and not necessarily the quality of the resulting surface. An oxide layer on the surface of the silicon matrix can be produced thermally or by ozone.

The thickness of the oxide layer grown thermally depends upon the temperature and time for oxidation, as well as the oxygen content of the furnace. Growth of a sufficiently thick surface oxide layer prevents further changes in the effective optical thickness due to ambient conditions, but may not be sufficient to protect the surface from dissolution in aqueous solutions. After oxidation, silane chemistry is frequently utilized to form a protective alkyl silane monolayer on the silicon surface, further limiting attack on the silicon matrix by water molecules. Using alkyl silanes, the silicon sensor architecture can be tuned to sense a range of targets by selecting an appropriate distal functional group on the silane monomer, providing appropriate attachment groups for many different bioreceptors. The major advantage of silane attachment is that it can be performed under ambient conditions; however, there is a strong tendency for silanes to form multilayers instead of monolayers, and the polarity of the silicon-oxygen bond formed upon silanization is highly susceptible to hydrolysis [41].

For many applications, oxidization and silanization provide an appropriately passivated and functionalized surface for sensing. An alternative surface preparation method exists in hydrosilylation. The procedure involves exposing the hydride-terminated silicon to an alkene or alkyne, forming a very stable alkyl monolayer on the surface. Because the resulting silicon-carbon bond is non-polar, this method forms a far more stable monolayer than with silanization. Additionally, since there is no possibility for cross-linking, this method does not result in multilayer formation [76]. Surface passivation by hydrosilylation does have a major limitation in that it must occur under inert atmosphere, as formation of silicon oxides on the surface of the matrix will significantly compromise the quality of the monolayer formed. Hydrosilylation has been

demonstrated as a highly effective surface preparation technique for biosensing, and has been used to attach a number of bioreceptors to various porous silicon architectures [77]. Figure 2.3 illustrates the difference in surface attachment between silanized and hydrosilylized silicon surfaces. Note that both surface functionalization methods are generally only a starting point for bioreceptor attachment, and further surface chemistry is often required for sensing.

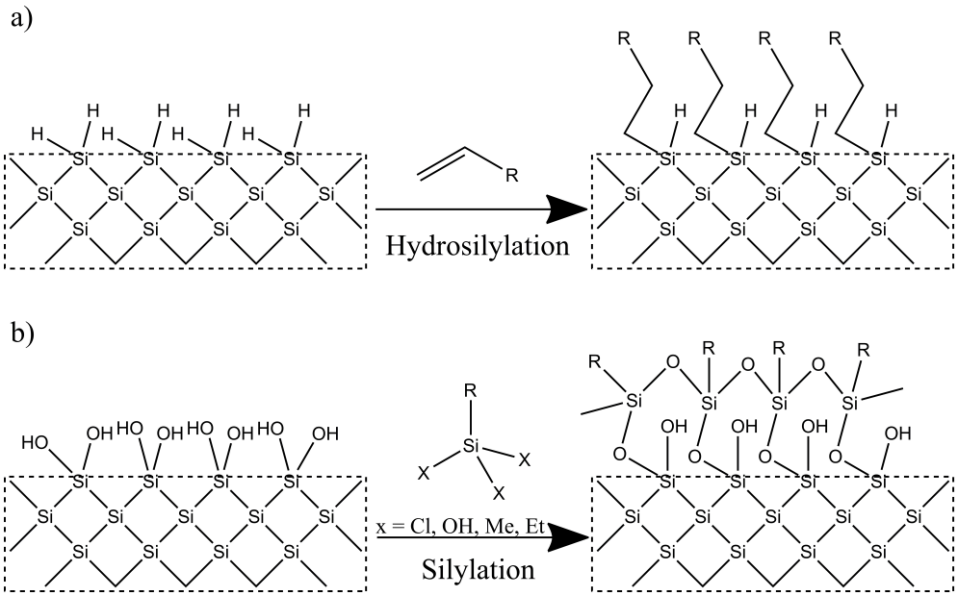

Figure 2.3: Sample reactions for porous silicon surface passivation. (a) Hydrosilylation reactions, involving either alkene or alkyne reagents, form silicon-carbon bonds. (b) Silylation (or silanization) reactions attach silane molecule to oxidized porous silicon via linkage to surface oxygen.

2.1.4 Importance of surface chemistry

For some applications, including drug delivery, the biocompatibility of porous silicon is a highly desirable property; the dissolution of porous silicon to silicic acid in aqueous solution can be used as a timed release mechanism [74]. In biosensing devices, however, the dissolution of porous silicon in aqueous solutions and physiologic fluids is

detrimental to the sensitivity and lifetime of the sensor. Thus, a critical part of porous silicon biosensor design is passivation of the material to limit in-solution fouling and degradation [41, 42, 77]. A number of surface treatment and passivation techniques for porous silicon have been reported in the literature. The most commonly utilized approach begins with oxidation (thermal or chemical) of freshly etched, hydrideterminated porous silicon. Subsequent silanization of the surface produces a protective coating and introduces surface functionality for biosensing via the choice of silane molecule. An alkylsilane may be attached to the oxidized porous silicon surface via vapour phase deposition, organic solution phase, or aqueous solution phase [78]. While the popularity of the oxidation and silanization passivation technique likely stems in part from its simplicity (typically a one-pot reaction performed in air), there are several drawbacks. Repeatability of the process can be difficult, and the resulting Si-O-Si bonding at the silane/substrate interface leaves the material susceptible to degradation of the surface due to nucleophilic attack. This nucleophilic attack occurs when one of the electron pairs in a solvent water molecule attacks the polar covalent Si-O surface bond, releasing silane from the surface and exposing the porous silicon to dissolution in an aqueous solution. One method for reducing the dissolution of silanized porous silicon is to use large molecular spacers on the substrate surface, such as long polyethylene glycol oligos, to sterically prevent water molecules from reaching the substrate surface [79]. This method, however, may not be desirable in meso- or nanoporous materials where the length of the PEG spacer could block a considerable fraction of the pore opening [66].

Alternative surface functionalization methods for porous silicon involve the formation of silicon-carbon bonds on the silicon surface [80-82]. One such method,

hydrosilylation, utilizes an alkene or alkyne molecule reaction with the hydride-terminated, freshly etched porous silicon surface [83]. This procedure results in a highly stable, non-polar silicon-carbon bond between the substrate and the coating alkyl molecule. The Si-C bond imparts much higher stability to the substrate than can be achieved through oxidation and silanization, but this method must be completed with the porous silicon substrate under inert atmosphere, making it impractical in some settings. Additionally, the efficiency of hydrosilylation is low, ranging from ~15-30%, depending upon the selected technique [84]. In addition to attaching surface coatings of functionalized organic molecules, there are also vapour-phase inorganic coatings that may be applied to the as-prepared porous silicon substrates. Using an acetylene gas furnace treatment, porous silicon can be thermally carbonized, resulting in a Si-C surface, without the attached alkyl monolayers formed during hydrosilylation [85, 86]. While thermal carbonization offers better efficiency, like hydrosilylation, this technique requires the exclusion of air and moisture from the sample before processing under a controlled atmosphere. Moreover, there have not been many reports of using a carbonized porous silicon surface for the attachment of biomolecules [87, 88].

The following work investigates conditions for achieving a thin, robust silanized coating on mesoporous silicon. The route of oxidation and silanization is chosen for its simplicity and ability to produce hydroxyl functionality in a single chemical step in air ambient. In order to mitigate the problems of multilayer formation, poor repeatability, and low stability, post-silanization treatments and washing may be utilized. In particular, a specific annealing and hydrolyzing protocol is developed for silanization with N-(3-

triethoxysilylpropyl)-4-hydroxybutyramide (TEOS-HBA), which can be used in oligonucleotide synthesis on porous silicon waveguides [89].

2.2 Porous silicon waveguide silanization

2.2.1 Silanization with N-(3- triethoxysilylpropyl)-4-hydroxybutyramide

To prepare the porous silicon waveguides in this work for in situ DNA synthesis of bioreceptors, as will be described in Section 2.3, the waveguides were thermally oxidized in a furnace under atmosphere at 800°C for 30 minutes. Surfaces were functionalized via silanization with 95% purity N-(3- triethoxysilylpropyl)-4-hydroxybutyramide (TEOS-HBA), obtained from Gelest; the structure of this silane is shown in Figure 2.4 A 4% solution of TEOS-HBA was prepared by combining 1900 μL ethanol, 100 μL DI water, and 83 μL of TEOS-HBA. The porous silicon waveguide samples were incubated in the silane solution for 16 hours. Samples were immersed completely in silanizing solution and stored overnight in a lidded petri dish to limit evaporation for the duration of the incubation. Following silanization, samples were then rinsed with ethanol and placed in an oven for annealing under atmosphere. Figure 2.4 shows the shift in resonance angle measured by reflectance for a range of weight percent TEOS-HBA in the ethanol and water solution. The magnitude of the resonance shift increases with increasing silane concentration below about 3% suggesting that monolayer coverage of the silane is not achieved for the lower concentration solutions. Above approximately 3%, the resonance shift begins to stabilize, suggesting that monolayer coverage of the silane is achieved in the pores. For silanization experiments, a 4% TEOS-HBA solution is selected to reach the maximum monolayer coverage while minimizing

the challenges seen in higher percent silane solutions, such as aggregation and multilayer formation [90].

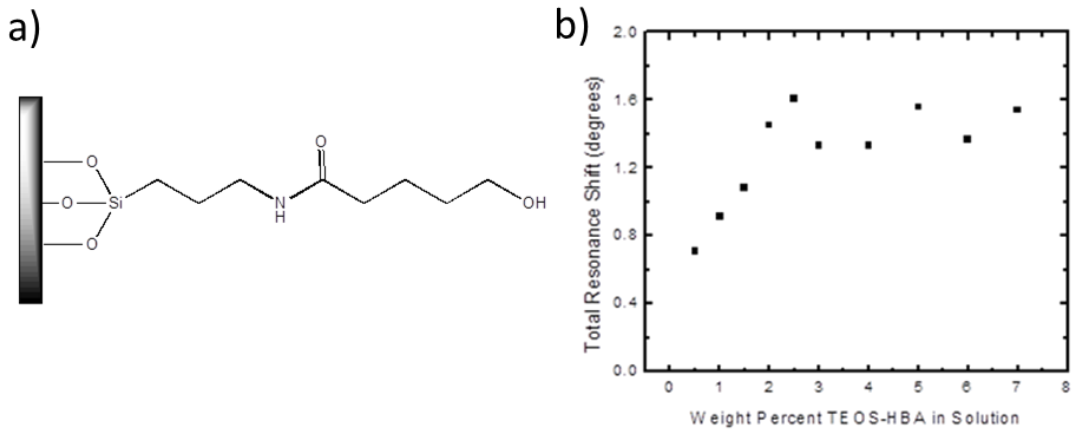

Figure 2.4: (a) Schematic of a porous silicon substrate functionalized with the TEOS-HBA silane molecule used to prepare the surface for in situ DNA synthesis. The –OH functional group introduced on the surface acts as the 5'- terminal hydroxyl group in the phosphoramidite synthesis cycle to be described in section 2.4. (b) Shift in porous silicon waveguide resonance angle measured after exposure to different weight percent of alkyltriethoxysilane in solution. A smooth concentration dependence is not achieved. Above 4% silane in solution, the resulting shift in resonance appears to near saturation, suggesting that all available binding sites on the surface have been filled.

As compared with similar silanes for silicon functionalization, the quality of the TEOS-HBA silane monolayer was found to be highly sensitive to annealing and hydrolyzing conditions [91]. Due to its alcohol functional group, the silane is likely to form weakly bound multilayers on the silicon surface, which must be removed before the DNA synthesis begins [90]. If they remain on the surface, these weakly bound multilayers may detach during the DNA synthesis and hybridization, compromising the later measurements which will be discussed in Section 2.2.2.

2.2.2 Optimization of anneal and hydrolyzing steps

Following silanization, annealing and hydrolyzing of the silanized surface was performed in order to further passivate the substrate and stabilize the silane coating [75]. Annealing was performed in a furnace in atmosphere. Afterwards, waveguides were rinsed with ethanol and water, and dried under nitrogen. Samples were hydrolyzed by soaking in deionized water at room temperature. During hydrolyzing, samples could be removed from the water soak and measured via prism coupling. After removal from the water soak, samples were dried under nitrogen before measurement.

When hydroxide terminated silica surfaces are exposed to silanization solution, a coating of the silane molecules via self-assembly forms on the substrate. The nucleophilic attack by the surface hydroxyl groups on the alkoxy groups from the TEOS-HBA molecule in solution aids in anchoring the molecule to the substrate [90]. The result is a covalent Si-O-Si bonding pattern on the surface, which passivates the porous silicon against oxidation and corrosion [75]. Post-silanization annealing induces cross-linking between neighboring surface- assembled molecules, as illustrated in Fig. 2.5.

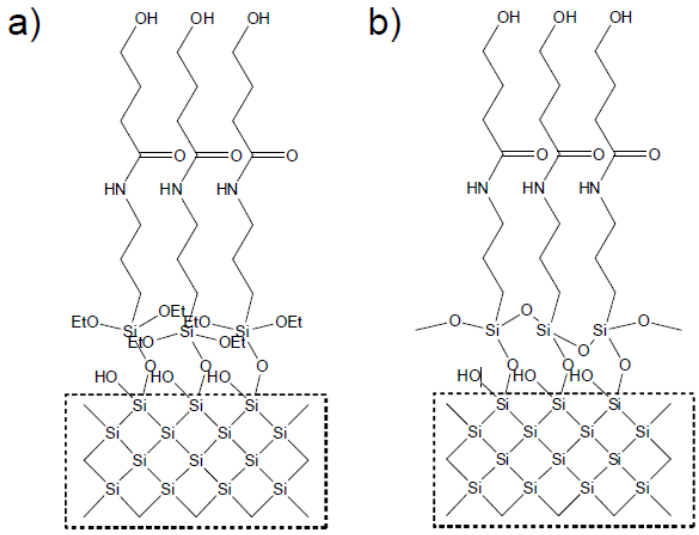

Figure 2.5: (a) Schematic showing the formation of a TEOS-HBA monolayer on oxidized silicon substrate. (b) Cross-linking between neighboring TEOS-HBA molecules occurs during the annealing process via loss of ethanol. Figure adapted from [92].

Literature reports using TEOS-HBA are limited [90, 93, 94], and the silanization procedures described vary considerably. None of the prior reports discuss the use of TEOS-HBA in nanoscale pores. To examine the effects of annealing temperature on silanization quality in porous silicon, two different annealing temperatures were selected: 100 °C and 200 °C. Additionally, two different annealing times were examined: 1 hour and 16 hours. These conditions were chosen based on similar studies performed on the commonly utilized aminopropyltriethoxysilane (APTES), which suggested that the annealing conditions (i.e. temperature and time) may have a significant impact on the quality and robustness of the resulting coating [78, 91, 95]. For each waveguide at the various conditions, the resonance angle was determined using the Metricon prism coupler, as described in Section 2.1.2, at each step: after oxidation, after silanization, after annealing, and after washing. Low temperature (100 °C) annealing of the waveguide

silanized for 16 hours led to a resonance shift of 1.402° to higher resonance angle, indicating a coating of molecules was formed on the pore walls. The magnitude of the shift was consistent in different regions of the sample. As a reference value, analysis based on the transfer matrix method and effective medium theory predicts that a perfect monolayer coating of TEOS-HBA would produce a resonance shift of 1.150°, assuming a uniform coating thickness of 0.9 nm and a coating refractive index of 1.5 [63].

Comparing the expected shift and the actual shift immediately following annealing, it is clear that the low temperature annealed TEOS-HBA coating exceeds a monolayer, likely producing islands of multilayer formation. Multilayer formation is typical for hydroxyl-terminated silanes due to hydrogen bonding and cross-linking between the hydroxyl-functional end and the triethoxysilane-functional end of another molecule in solution [90]. On planar substrates, hydrolysis and subsequent dissolution of TEOS-HBA coatings has been found to remove weakly-bound multilayers [90]. Methods of surface abrasion have also been developed to reduce the coatings to roughly monolayer coverage on the planar substrates [90, 96, 97]. Since surface abrasion is not possible within a porous material, the efficacy of simple hydrolysis in reducing the multilayer silane coverage in the porous silicon waveguide was explored. As shown in Figure 2.6, upon soaking the low temperature annealed porous silicon samples in deionized water over the course of several hours, shifts to lower resonance angles were measured, indicating a loss of material from the surface of the sensor. After 7 hours, the loss of materials ceased and the resonance peak was stable to any further dissolution. Figure 2.6 demonstrates the silanization and subsequent degradation of the functionalized porous silicon following hydrolysis and dissolution of the silane coating in water. The

difference in resonance angles corresponding to the initial oxidized surface and final silanized surface is 0.987°. This corresponds to a sub-monolayer surface coverage. Multilayer islands of TEOS-HBA may be retained on the surface, thus the actual percent of coated surface may be reduced further.

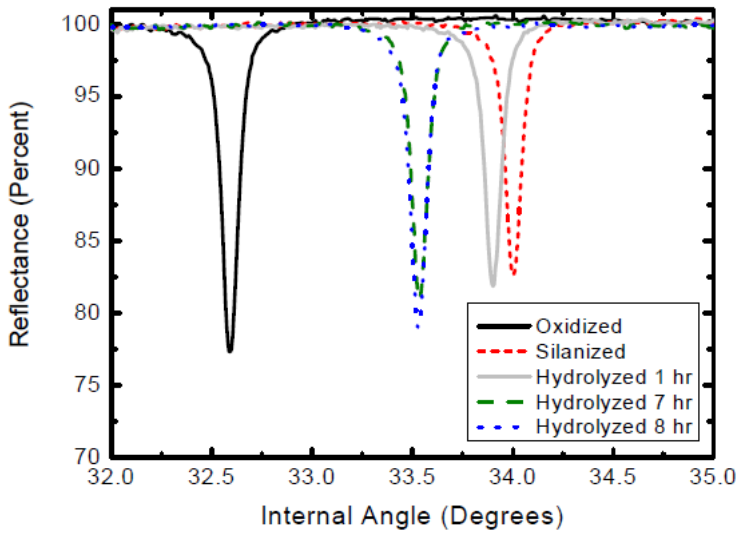

Figure 2.6: Reflectance measurements of porous silicon waveguide after oxidation (black, solid line), silanization in TEOS-HBA and annealing at 100°C for 16 hours (red, short dashed line), and different hydrolyzing times (gray solid, green dashed, and blue dotted lines). The sample is passivated against further loss of material in the water soak after 7 hours. Adapted from [92].

Figure 2.7 illustrates the typical silanization and hydrolysis profile for a TEOS-HBA silanized porous silicon waveguide that was annealed at 200 °C for 1 hour. The higher annealing temperature results in a TEOS-HBA coating that is considerably more stable towards aqueous solution; however, some material is still lost from the porous silicon surfaces during the first hour of soaking in water. After 1 hour of hydrolysis, no further shift is measured and the porous silicon is adequately passivated. The total resonance shift from oxidized baseline to stabilized sample after hydrolyzing is 1.238°

for the high-temperature annealing, compared with the post-hydrolysis total shift of 0.987° for the low-temperature annealed substrate. The larger shift in resonance angle indicates a greater surface coverage with TEOS-HBA on the porous silicon surface. This value is slightly higher than the predicted value for a monolayer, which may be attributed to some remaining multilayer regions, as posited previously. Hydrolysis after high temperature annealing is completed after one hour, while hydrolysis after low temperature annealing required nearly eight hours. Higher annealing temperatures were not investigated due the predicted flash point of TEOS-HBA at ~207 °C.

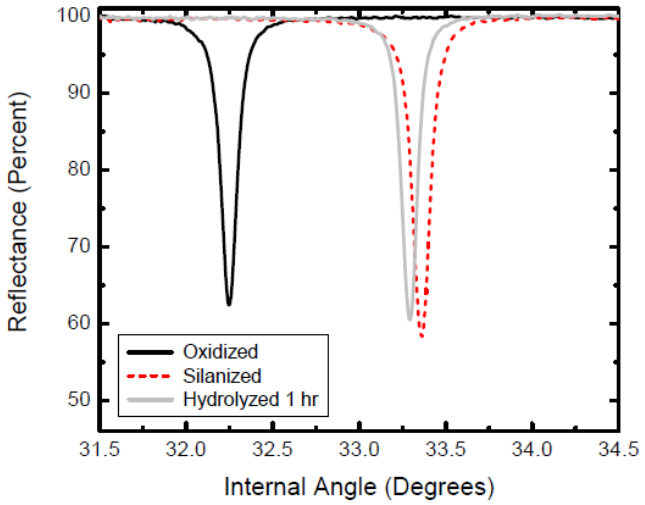

Figure 2.7: Reflectance measurements of porous silicon waveguide after oxidation (black solid line), silanization in TEOS-HBA and annealing at 200 °C for 1 hour (red dashed line), and hydrolysis for 1 hour (gray solid line). No further resonance shift is observed after longer hydrolysis times. Adapted from [92].

These experiments demonstrate that the TEOS-HBA silane on porous silicon could be stabilized on the porous silicon surface through annealing at 120°C for 16 hrs, followed by hydrolyzing the surface by soaking in DI water for 4 hrs. This extended annealing and hydrolyzing procedure produced a functionalized porous silicon surface for

which stable and repeatable resonance angle measurements were obtained after waveguide exposure to a variety of aqueous and organic reagents. This extended functionalization procedure, produces a porous silicon waveguide with long-term stability, as evidenced from the stability of resonance peaks in unaltered samples over the course of several weeks.

2.3 In situ DNA synthesis in porous silicon

2.3.1 Motivation

The development of versatile detectors for biomolecules is an active area of current research, specifically for applications in medical diagnostics and biotoxin detection. Porous silicon has become a widely studied material for this purpose over the last decade. The porous structure provides significant advantages in its ability to filter out impurities by size and its substantial increase in reactive surface area. In order to take advantage of the large internal surface area of porous silicon devices, molecules need to be effectively immobilized within the confined nanoscale pores. Consequently, a major challenge facing biosensors that utilize porous materials is the effective infiltration of molecules into the pores [66].

Synthesis of oligonucleotides in a porous template, for which the template pore size is substantially larger than the synthesized oligonucleotides, is the traditional method of producing DNA strands. After synthesis, for example in micron-sized glass pores, the DNA is cleaved from the template and collected. There have been very limited reports in the literature on DNA synthesis in porous silicon templates [98-100]. The following discussion presents the first report of in-situ DNA synthesis within a mesoporous silicon optical waveguide structure for label-free sensing. In this case, the pore size is only about fifteen times larger than the synthesized DNA (1.76nm and 3.52nm lengths for 8mer and

16mer oligos, respectively [101]). After DNA synthesis, the DNA probes are not cleaved; they remain as part of an active, functionalized sensing platform. As will be discussed in the following sections, the method of in-situ DNA synthesis in the porous silicon not only increases the probe DNA density on the pore walls compared to traditional immobilization techniques, but it also allows for flexibility in defining the probe sequence. Moreover, the detection sensitivity of the porous silicon waveguide is sufficient to detect oligonucleotides containing only a single base. Hence, combining the sensitivity of the waveguide platform with the high probe coverage obtained using the in situ DNA synthesis method, the functionalized porous silicon waveguides serve as the basis for a highly efficient sensing device.

2.3.2 Phosphoramidite chemistry

In order to take full advantage of the large surface area for sensing and the electric field confinement within the porous waveguiding layer, efficient infiltration of biomolecules into the nano- and mesoscale pore opening. For the surface chemistry and etch parameters used in this study, previous work within the Weiss Group indicated that DNA oligos must be approximately five times shorter than the pore diameter for diffusion into the pores [67]. This is a significant obstacle for developing a viable detection scheme. In order to circumvent this problem, the common commercial method of DNA phosphoramidite synthesis is applied to porous silicon waveguides.

Typically, DNA can be though of as two long polymers wound together in an anti-parallel manner and coiled around the same axis. The monomers sub-units are known as nucleotides. As shown in figure 2.8, each DNA nucleotide is comprised of a nitrogen-containing base, a deoxyribose sugar, and a phosphate group. The nitrogen-

containing bases are heterocylic aromatic compounds covalently bonded to the 1’ carbon of the deoxyribose sugar. The purine bases are guanine and adenine, and the pyrimidine bases are cytosine and thymine. The sugar is a five member ring that make up half of the DNA backbone. The carbons of the sugar are systematically named 1’ through 5’, with the prime designation serving to distinguish the deoxyribose carbons from the carbon numbering in the purine or pyrimidine ring. The final region of the nucleotide is the phosphate group, which is covalently attached to either the 3’ or the 5’ carbon of deoxyribose, and comprises the other half of the DNA backbone.

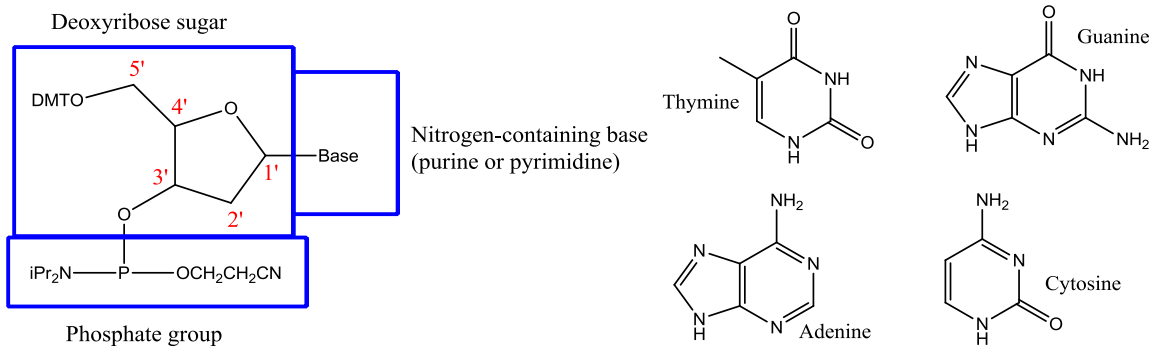

Figure 2.8: The general structure of a deoxyribonucleic acid (DNA) nucleotide. A nucleotide monomer is composed of three basic parts: the nitrogen-containing base, the deoxyribose sugar, and a phosphate group. In general, the phosphate group of a nucleotide may be attached at either the 5’ or the 3’ carbon of the deoxyribose sugar. The structures of the purine and pyrimidine bases are also shown.

After the porous silicon waveguide fabrication, thermal oxidation, and silanization with TEOS-HBA, oligonucleotide bases are attached directly to the functionalized surface through use of an Applied Biosystems Model 392 DNA Synthesizer modified to direct reagent flow onto the waveguide surface. The phosphoramidite method [102] is used, and is outlined in Figure 2.9. The waveguide is

attached to the 3'-hydroxyl end of the oligonucleotide, and subsequent nucleotide additions attach onto the 5'-hydroxyl end.

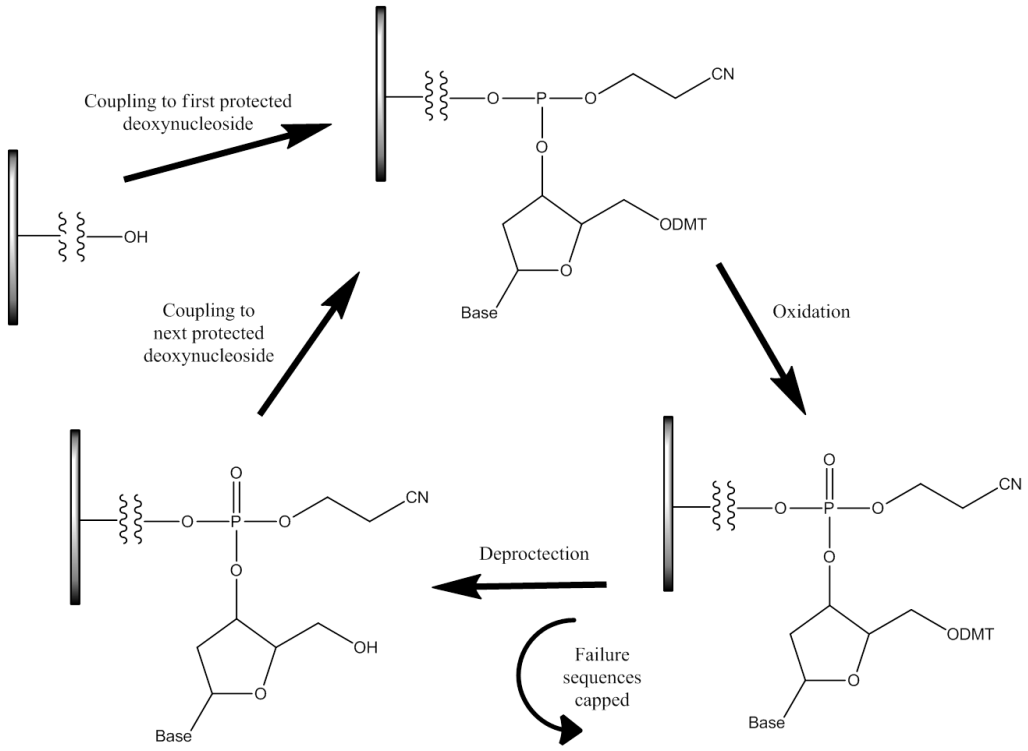

Figure 2.9: Schematic of phosphoramidite method of DNA synthesis on a solid support frequently used in commercial DNA synthesis in controlled pore glass. In this work, DNA is synthesized on silanized porous silicon waveguides. Synthesis initiates at an –OH functional end group, and DMT-protected nucleotides are added one at a time in a specified DNA sequence.

The DNA oligonucleotide cycle starts with addition of the first nucleotide with a phosphoramidite protected 3' monophosphate onto the hydroxyl-functionalized porous silicon waveguide. Tetrazole, a weak acid, is added to the flow cell chamber simultaneous with the nucleotide, protonating the nitrogen on the phosphoramidite, creating an intermediate activate toward nucleophilic attack. The nucleotide bonds to the hydroxyl head group through the formation of a phosphite bond through the 3' end of the protected nucleotide. On the 5'end of the newly attached nucleotide a dimethoxytrityl

(DMT) protecting group prevents further addition onto the chain at this step in the synthesis.

Capping follows immediately after nucleoside coupling, effectively terminating any chain that did not undergo nucleotide addition in the preceeding coupling step. At this point in the synthesis cycle, such "failure sequences" have a 5' hydroxyl end group. Introduction of acetic anhydride and 1-methylimidazole into the flow cell rapidly caps these groups by acetylation, preventing further chemistry on these chains.

In the next step of the synthesis, the generated internucleotide linkage is oxidized. An iodine, water, and pyridine are introduced into the flow cell in a tetrahydrofuran solvent. Iodine acts as an oxidizer, converting the trivalent phosphite linkage to the more stable pentavalent phosphotriester.

Finally, the dimethoxytrityl (DMT) protecting group is cleaved with the protic acid trichloroacetic acid (TCA), leaving a 5' hydroxyl terminating nucleotide. A second nucleotide with 3' a phosphoramidite protected monophosphate is introduced with the tetrazole activator, and the cycle begins again with attachment to the deprotected 5'-hydroxyl group. The cycle continues as desired to generate the oligonucleotide sequence. Figure 2.10 illustrates the step-wise growth of an oligonucleotide sequence within the mesoporous substrate.

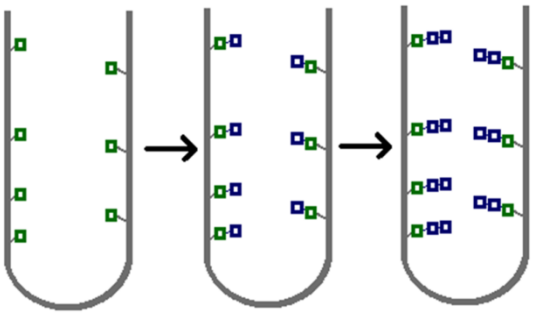

Figure 2.10: In-situ DNA synthesis. Nucleotides are attached one at a time off a silane linker monolayer. This method allows for high density of DNA to be achieved on pore walls, with little dependence on sequence length.

2.3.3 Substrate Stability in DNA synthesis solvents

One of the primary applications of synthesizing a hydroxyl-terminated substrate is to provide the requisite surface chemistry for synthesis of DNA [98, 100, 103]. Hence, it is important to test the stability of TEOS-HBA functionalized porous silicon waveguides against the various solvents used during DNA synthesis. The porous silicon samples were tested by exposure to a cycle of DNA synthesis solvents that are typically used for in situ DNA synthesis via the phosphoramidite method [102]. The solvents used during the standard phosphoramidite synthesis cycle include acetonitrile, tetrazole, dichloromethane, trifluoroacetic acid, methylimidazole, tetrahydrofuran, and iodine.

The significance of the selected post-silanization annealing temperature and time become evident when the silanized waveguides are exposed to the DNA synthesis solvents. For a porous silicon waveguide annealed at the low temperature (100 °C) for 16 hours, a large negative shift in resonance angle is observed upon exposure to the cycle of solvents, shifting by an average of -0.240°. This shift may result from porous silicon corrosion, TEOS-HBA dissolution, or a combination of the two processes. For porous silicon waveguides annealed at high temperature (200°C) for one hour, corrosion during DNA synthesis is reduced dramatically to approximately 0.063°. When the high

temperature anneal step is extended to 16 hours at 200°C, corrosion of porous silicon upon exposure to phosphoramidite synthesis solvents is almost completely eliminated, with the observed shift nearing the sensitivity of the prism coupling measurement. Table 2.1 illustrates the differences in TEOS-HBA monolayer stability under various preparation conditions.

Annealing Conditions	Corrosion in Solvents
16 hrs at 100°C	-0.240°
1 hr at 200°C	-0.063°
16hrs at 200°C	-0.010°

Table 2.1: Annealing conditions used for the silanization of porous silicon waveguides and the average observed shift in resonance angle following one cycle of a DNA phosphoramidite synthesis cycle (without nucleotide introduction). Annealing conditions for TEOS-HBA affect the stability of the surface coating towards the solvents. All samples were hydrolyzed to stability before DNA synthesis cycle was started.

Cross-linking of the TEOS-HBA monolayer by sufficient high temperature annealing, and subsequent hydrolysis and dissolution of weakly bound multilayers, stabilized the waveguide sensor against corrosion in the organic solvents utilized for DNA synthesis. As a result, the synthesis of DNA oligonucleotides in stable porous silicon waveguides functionalized with TEOS-HBA can be realized [89], and hybridization of complementary DNA oligos to the in situ synthesized DNA has been achieved, as will be discussed in Chapter 3 [104].

2.3.4 Single-base sequence additions

For the initial investigation of in situ synthesized DNA in a porous silicon waveguides, a series of eight thymine (T) oligonucleotides were synthesized in the pores. The waveguide resonance angle was measured after each T addition using the prism

coupling method described previously. As shown in Figure 2.11, a consistently increasing resonance angle was measured after the addition of each base. The first attached thymine showed a shift in resonance angle approximately twice that of the subsequent steps. The larger shift for the addition of the first base is believed to be a result of the protecting group on the first thymine, which is approximately the same size as a single base. The average shift for the first base was 0.233 degrees, and each subsequent base resulted in a shift of approximately 0.091 degrees. The maximum resolution of the prism coupler rotation stage is 0.002 degrees; the measured waveguide resonance shifts are well within the detection limit of the instrument. It should be noted that the thymine additions begin to deviate slightly from the linear fit as the oligonucleotide probe increases in length. Experiments have indicated that this deviation is a result of slight degradation of the silane linker layer, and not a result of inefficient in situ chain growth. While silane layer degradation was a concern when these initial in situ synthesis experiments were performed, subsequent work in optimizing the TEOS-HBA silane monolayer film quality through annealing and hydrolyzing eliminated this degradation problem for subsequent experiments.

From Figure 2.11, it is clear that the sensitivity of the porous silicon waveguide is sufficient to detect the addition of molecules as small as a single nucleotide. The large surface area of the porous silicon waveguide and resonant sensing mechanism enable the detection of such small molecules. This measurement would not be possible using a traditional surface plasmon resonance sensor. Furthermore, the demonstration of in-situ DNA synthesis and measurement in porous silicon waveguides is noteworthy due to the size range of the pores (20-30nm) in which the DNA was synthesized. Previous reports of

DNA synthesis on glass [66, 105] or silicon [37, 98, 99, 106] supports have been on a much larger pore scale, often in the micron range.

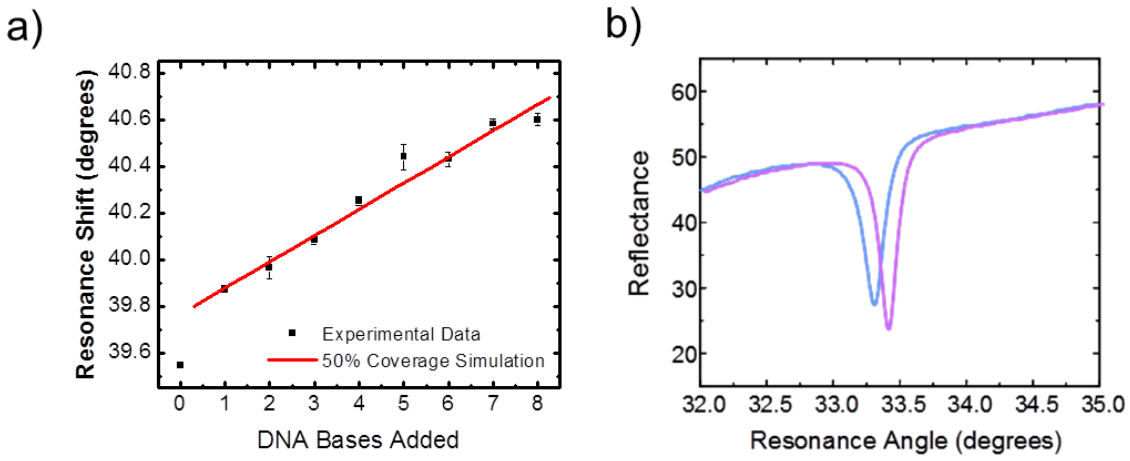

Figure 2.11: Measured porous silicon waveguide resonance shift with in-situ addition of successive single base oligonucleotides (squares). Theoretical calculations (line) demonstrating the predicted linear shift of the resonance angle if 50% pore coverage is assumed (a). Resonance angle shift demonstrated upon the addition of a single DNA nucleotide bases in a sequence on an in situ synthesized oligo (b).

One of the primary advantages of using in-situ synthesis of DNA, compared to the addition of prepared DNA strands to a silanized surface, is a substantially increased DNA density in the porous silicon. A total shift in the waveguide resonance of only 0.23° was observed when porous silicon waveguides functionalized with 3-aminopropyltriethoxysilane and sulfosuccinimidyl 4-[N-maleimidomethyl]cyclohexane-1-carboxylate were incubated in 100 μM of eight-base oligonucleotide solution (MWG Biotech) for one hour [66]. The phosphoramidite synthesis method of eight-base oligonucleotides on the porous silicon surface resulted in an average overall resonance angle shift of 0.956°, as shown in Figure 2.11. This significant difference in the magnitude of the resonance angle shift is evidence of greater DNA coverage by the

stepwise phosphoramidite method. We believe the effects of size exclusion and repulsive forces between charged oligonucleotides are magnified when pre-synthesized eight-base oligonucleotides are infiltrated into the pores instead of only single oligonucleotides. Each eight-base oligonucleotide has a length of approximately 1.8 nm, while the porous silicon pore size is 20 nm. The advantage of the phosphoramidite method over direct addition is even more significant for the immobilization of larger oligonucleotides in these pores. Tuning of porous silicon materials parameters (e.g., pore size) will also allow the fabrication of biosensors for molecules covering a wide range of sizes [107, 108].

In order to estimate the degree of pore surface coverage by the in situ synthesized probe DNA oligonucleotides, calculations of the expected resonance shift for different numbers of DNA bases and different percentages of surface coverage were performed, following the approach described in [65]. The calculations assume that each thymine nucleotide can be modeled as a 2.2 Å molecule [101] with a refractive index of 1.5 [109]. The magnitude of the waveguide resonance shift scales with the magnitude of the effective refractive index change induced by the oligonucleotides, which scales with the number of thymine bases attached and the percent of the porous silicon internal surface area covered by the DNA. As shown in Figure 2.11, the experimental data are fit well by the theoretical calculations assuming 50% pore coverage by probe DNA. The slope of the linear theoretical curve is a direct indication of the magnitude of the refractive index change induced by the addition of single oligonucleotides covering 50% of the available surface area. We note that the theoretical curve takes into account the addition of the DMT protecting group added along with the first thymine by adjusting the initial resonance shift position.

Figure 2.12 shows the evolution of the waveguide resonance shift during in situ synthesis of DNA molecules up to 24 bases in length. The data points in the figure are a concatenation of measurements from several different samples. Hence, the somewhat abrupt slope changes may be due, in part, to sample-to-sample variation. Nevertheless, the overall trend is clear that the resonant coupling angle progressively increases as additional bases are introduced into the porous silicon waveguides. Based on the magnitude of the resonance shifts, we estimate approximately 50% surface coverage for 8mer in situ synthesized DNA molecules, as discussed previously, 40% surface coverage for 16mer molecules, and 35% coverage for 24mer molecules. Hence, because the size of the protected, single DNA nucleotides is small enough to be unhindered by size of the pore opening, the surface coverage of the in situ assembled DNA molecules with up to 24 bases is only slightly dependent on the final DNA molecule size. The synthesis of larger DNA molecules is possible and will be discussed in Chapter 5. The size-dependence of the surface coverage of in situ synthesized DNA molecules is in direct contrast to the trend reported previously for infiltration of pre-synthesized DNA molecules into porous silicon waveguides. The percent surface coverage falls off sharply for DNA molecules composed of more than 16 bases, as shown in Figure 2.12. Moreover, the shift due to 8mer DNA molecules when infiltrated as pre-synthesized 8-base molecules instead of single base molecules that assemble in the pores is only ~10%. This difference in surface coverage achieved via in situ synthesis leads to binding and detection of a larger resonance shift upon hybridization to target, as will be described in Chapter 3.

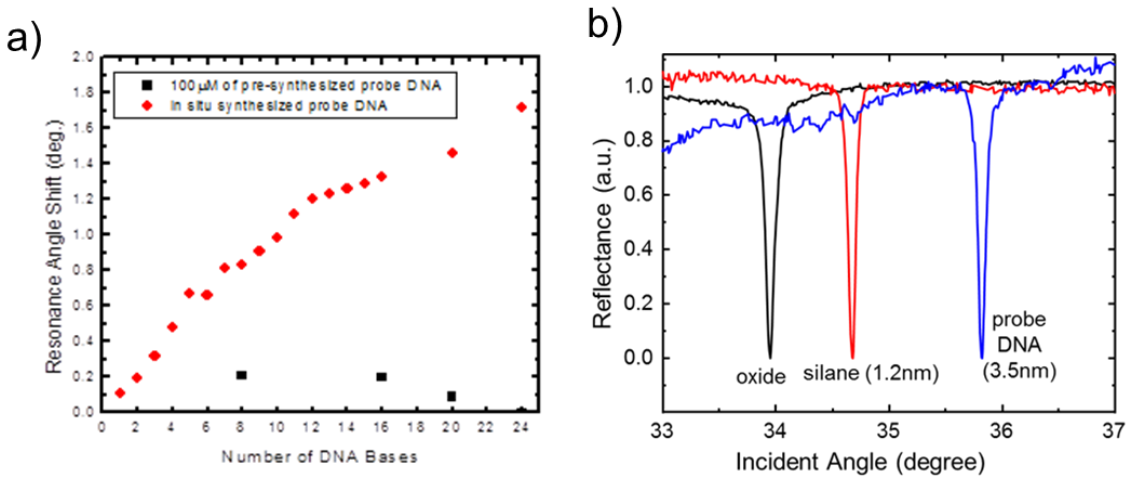

Figure 2.12: Resonance shift upon infiltration of probe DNA into porous silicon waveguides (a). Black square data points give the shift due to infiltration and immobilization of pre-synthesized DNA probes, ranging from 1.76 to 5.28 nm length. Red circular data points give the shift observed when probe DNA of the given length is synthesized base-by-base in the waveguide using the in situ method. Data for the in situ synthesis contains a correction factor that reduces the measured shift by 0.012° to account for the presence of a DMT protecting group which does not appear on the infiltrated probe. Figure adapted from [110]. In situ synthesis is utilized to circumvent infiltration challenges. Upon functionalization with monolayer of biomolecules, the shift in resonance angle scales with biomolecule size (b).

2.3.5 SIMS confirmation of DNA infiltration

In working with a porous silicon waveguide structure, the significant advantage of increased total surface area is dependent upon efficient infiltration of reagents and molecules into the porous structure. In order to further demonstrate the presence of the TEOS-HBA silane linker and oligonucleotide probe following in-situ DNA synthesis, secondary ion mass spectrometry (SIMS) analysis was performed on waveguide samples by Professor Michael Molinari at the University of Reims. France. As demonstrated in Figure 2.13, while the SIMS data below cannot be interpreted quantitatively, the presence of both carbon and nitrogen atoms in the waveguide are a strong indication that silane and/or oligos are able to infiltrate deep into the top and bottom layers of the waveguide. Also valuable is a comparison of the SIMS data from a DNA probe synthesized inside a

porous silicon waveguide using the in-situ method compared with traditional whole probe DNA attachment in a porous silicon waveguide. Note that the presence of the carbon and nitrogen in the in-situ sample appears greater. This agrees well with previous results indicating superior surface coverage with the in-situ DNA synthesis.

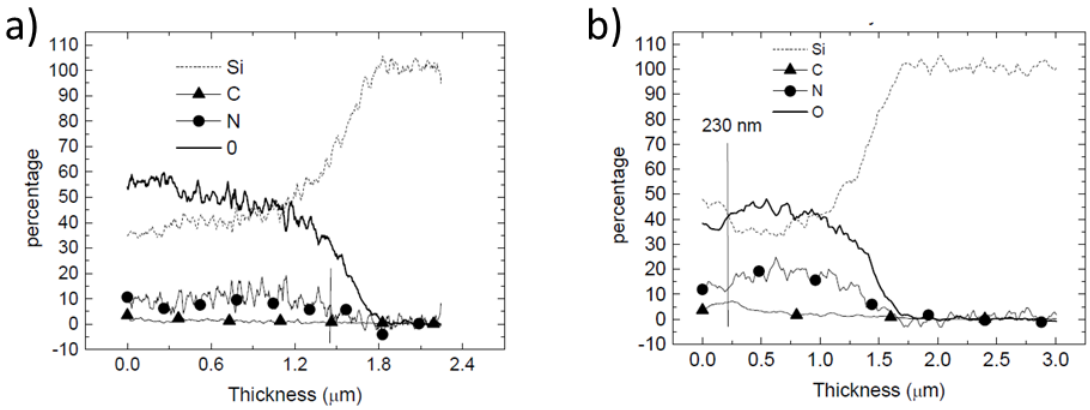

Figure 2.13: For the traditional method of direct DNA infiltration, the amount of carbon and nitrogen in the waveguide and cladding layers is only slightly above background (a). For the in the in-situ synthesized DNA in the porous silicon waveguide, a considerable difference can be observed between the presence of carbon and nitrogen in the pores compared with elsewhere (b). Figure adapted from [104].

Chapter 3

3. OLIGONUCLEOTIDE SENSING WITH POROUS SILICON WAVEGUIDES

3.1 Sensing of DNA-DNA hybridization

3.1.1 Introduction to DNA hybridization

Hybridization of an oligonucleotide bioreceptor to a complementary target oligonucleotide is the most vital component of a nucleic acid based biosensing device. This binding mechanism is used for the detection and analysis of specific DNA sequences, particularly in applications in clinical diagnostics, environmental analyses, food safety and monitoring, and forensic analysis. Prior to the advent of polymerase chain reaction for DNA amplification [111], considerably more time consuming and expensive methods such as radiolabeling DNA targets were standard. With the introduction of polymerase chain reaction (PCR), small quantities of target DNA could be replicated to increase concentration and improve signal. Later, fluorescent labeling of DNA targets allowed for optical biosensing.

Typically, DNA is thought of as a double-stranded helical macromolecule. The double-stranded structure however can be separated into single stranded DNA (ssDNA) subunits, which are complementary to one another. When these two ssDNA sequences are brought together, they will form a duplex with a high degree of efficiency and specificity. For this reason, one ssDNA of this duplex can be used as bioreceptor to detect the presence of the second, complementary, ssDNA of the pair. When the ssDNA bioreceptor is associated with a signal transducer, the hybridization event can be translated into a measurable signal. Figure 3.1 below illustrates the transition from single to double stranded DNA upon hybridization.

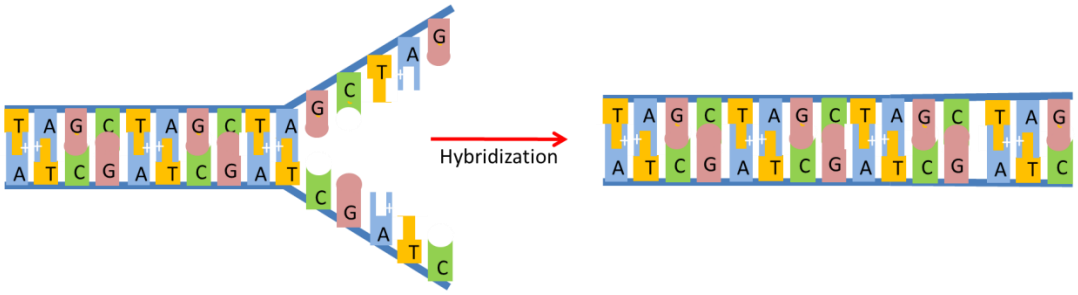

Figure 3.1: Two single strand DNA oligos will hybridize if specific binding between complementary base pairs (C to G, A to T) occurs. Hydrogen bonding between base pairs is the basis for hybridization to form the DNA duplex.

Hybridization is a complex interaction resulting from hydrogen bond formation between nucleotides on adjacent positions on complementary DNA strands. Hybridization can be affected by ionic strength of the buffer solution, oligo sequence and length, and temperature, both in solution-phase hybridization [112, 113] and when anchored to a substrate surface [114, 115]. Given that DNA hybridization is a reversible process, and the influences of the factors listed above have been well characterized, DNA denaturing or melting – the separation of the double strand DNA into two single strands – is an important property in DNA analysis. A number of algorithms (discussed further in Section 3.1.3) have been developed to quantitatively predict DNA thermodynamics for a given sequence and solution conditions [116-118]. The property of DNA-DNA hybridization upon thermal cycling is central to the PCR process, a technique in molecular biology with applications in diagnostics, genetic fingerprinting, and DNA-based phylogeny [119, 120]. The sequence-sensitive thermodynamics of the DNA-DNA denaturing and re-hybridization allows for single-base mismatch detection of ssDNA pairs [121-124].

3.1.2 DNA hybridization detection in porous silicon

Oligonucleotides (including DNA) are a target of interest in biosensing research both for the potential applications in genomics, sequencing, and biohazard identification, and also as a model system for small molecule detection. Several research groups have utilized label-free porous silicon biosensing platforms for the detection of DNA sequences. The porous silicon scaffolds range from single layers to multilayers to gold particle modified porous structures, and transduction mechanisms previously demonstrated include optical (PL and reflectance) and electrical.

The first demonstration of DNA detection on porous silicon biosensors also happens to contain the lowest reported detection limits, observing DNA hybridization with target concentrations ranging from 1 fM to 1nM [40]. This work by Lin et. al. utilized a single layer porous silicon films to which a DNA oligo bioreceptor was attached. Exposure to the target DNA induced a concentration dependent blue-shift in the reflectance spectrum. To date, however, this low detection limit for DNA targets has not been replicated by other researchers. Similar work has looked at DNA oligo detection in Bragg mirror reflector microarrays, and DNA targets were detected in concentrations of tens of micromoles [125-127]. In these experiments from the De Stefano group, Bragg reflector microarrays were attached to microfluidic systems, and detection limits were predicted to be as low as 77nM for target DNA in buffer solution, but detection of DNA at this low concentration was not experimentally detected. The De Stefano group consistently observes a red-shift in the Bragg reflector spectrum for attachment of biomolecular targets.

Several researchers have investigated porous silicon micro- and meso- structures as substrates for DNA electrochemical sensors [128-130]. In one case, DNA targets were detected in nano- to micro- molar concentrations by transducing the hybridization of DNA into a chemical oxidation of guanine by Ru(bpy)(3)(2+), the reduced form of which is then detected electrochemically [131]. Electrical impedance spectroscopy was used for label-free electrical detection of free DNA targets in free-standing macroporous silicon single-layers, with detection limits in the sub-micromolar range [130]. Label-free electrochemical DNA biosensors have also been used for the identification of oligonucleotide sequences specific to pathogens, such as Salmonella Enteritidis [132-135].

There have been reports of detecting DNA with porous silicon optical biosensors by incorporating a signal enhancement mechanism. As noted previously, some reports of label-free reflectance detection of oligonucleotides depend upon a blue-shift in the reflectance spectrum, indicating a DNA concentration dependent degradation of the porous silicon substrate [40, 43]. The authors postulated that this porous silicon corrosion occurs via significantly enhanced surface oxidation when negatively charged target DNA is in close proximity to the pore walls. Based on their analysis of the porous silicon corrosion mechanism, the Voelcker group has developed single layer mesoporous silicon sensors for in which corrosion is enhanced by electron transfer from a transition metal complex label attached to DNA targets [5, 42].

In the Weiss group, freestanding porous silicon waveguides have been developed for optical measurements [62], along with techniques for optimizing waveguide parameters for improved target sensing [136]. A detection limit of 42nM was predicted

for the 24mer ssDNA target [62]. In porous silicon waveguides attached to silicon substrates, light has been coupled into waveguides both by prism [65] and grating coupling [64, 137] for optical detection of DNA hybridization, with typical experiments performed at micromolar concentrations. For these experiments, pre-synthesized DNA probes were utilized.

3.1.3 Selecting DNA sequences for hybridization

In order to simplify hybridization dynamics for DNA-DNA binding within porous silicon substrates, sequences were selected to have melting temperatures well above room temperature, but with minimal self-dimerization or hairpin sequences. Melting temperatures need to be high enough to ensure that the efficiency of duplex formation remains high for DNA in room temperature or physiologic conditions. Higher guanine and cytosine content in DNA sequences leads to higher melting temperature due to the greater number of hydrogen bonds contained in a G-C pairing compared to an A-T pairing. Selecting longer sequences is another alternative for achieving higher melting temperatures. As sequences increase in length however, the likelihood of intramolecular interactions increases. In general, the more base pairs that may be involved in an intramolecular (hairpin) interaction, the higher the energy barrier is for the intermolecular hybridization to the complementary target. This can considerably slow the hybridization kinetics. For this reason, all sequences used in the following section have been analyzed for melting temperature, self-dimerization, and hairpin formation using a DNA thermodynamics algorithm available from Integrated DNA Technologies (www.idtdna.com) known as Oligo Analyzer.

For all 8mer sensing experiments, a sequence composed of eight guanine bases was employed. This sequence is selected for the increased melting temperatures achieved with high purine (G and C) base content. With eight purine bases in sequence, the melting temperature algorithms predict a melting temperature of 58.8 ºC under the HEPES buffer conditions of 150mM NaCl and 5mM $MgCl_2$. It is desirable to have a melting temperature above room temperature so that incubation and detection may be completed at room temperature without concern for a high degree of DNA duplex dissociation, as will occur near the melting temperature. With a short sequence of 8mer in length and without variety in bases, there is no potential for self-dimerization or hairpin formation.

For longer sequences, including the 16mer sequences used for the experiment described later in this chapter, better stability may be achieved by avoiding too high a purine content and varying the oligo sequence. The probe sequence 5'- TAG CTA TGG TCC TCG T-3' has a 50% GC content, resulting in a melting temperature of 65.9°C, high enough to allow for sensing and measurement at room temperature. The corresponding target sequence must also be checked for potential intermolecular self-dimerization that could interfere with detection, as ssDNA targets could bind to one another before exposure to the receptor. The sequence displays a low potential for intramolecular hairpin formation. All potential hairpins in the selected sequence have a Gibb's free energy greater than zero, as calculated by the IDT-DNA Oligo Analyzer tool, indicating that intramolecular hairpins will not form spontaneously under the incubation conditions at room temperature and pressure. Sequences of interest analyzed for melting temperature, self-dimerization, and hairpins can then be synthesized on porous silicon waveguide

substrates by specifying the sequence in the Applied Biosystems DNA Synthesizer for automated DNA bioreceptor synthesis.

3.1.4 8mer DNA detection experiments

Once the desired oligonucleotide bioreceptor is attached to the porous silicon surface via in situ synthesis, it may be used for detection of the complementary oligonucleotide sequence. Complementary (also referred to as antisense or target) sequences are generated from the bioreceptor sequence. For the complementary DNA, a 100% anti-parallel sequence substituting in the paired purine or pyrimidine in the probe sequence is utilized. For example, a probe sequence 5'-GAT CTG-3' would be the 100% complement to the sequence 5'-CAG ATC-3', as the 5' end of the probe aligns with the 3' end of the complement, forming base pairs G-C, A-T, T-A, and so forth. To design a non-complementary (or mismatch) sequence, an oligo is generated in which no base pair match can occur with the probe. For example, 5'-TGC GAA-3' is a complete mismatch for the previous example probe. It is essential, however, to maintain a consistent melting temperature for target and mismatch oligos, to minimize experiment to experiment variances in hybridization thermodynamics.

The probe DNA is prepared for sensing by deprotection in a 50:50 v/v solution of ethylenediamine and ethanol for 30 min. Once the probe is deprotected it is active for hybridization. The porous silicon waveguide is exposed to a DNA target in buffer solution. Porous silicon waveguides with DNA probes are exposed to both complementary DNA target sequences as well as the noncomplementary sequences in order to assess the selective binding ability of the oligonucleotide probe. DNA

hybridization on the porous silicon surface is monitored by prism coupling measurements as described in Section 2.1.2.

In order to demonstrate selective detection of DNA target molecules, a porous silicon waveguide functionalized with TEOS-HBA and an in-situ 8-mer oligonucleotide probe was exposed to 50μM solution of complementary and noncomplementary 8-mer sequences in HEPES buffer solution. The target DNA sequence (5'-CCC CCC CC-3') is 100% complementary to the synthesized probe. The non-complementary DNA (5'-AAA AAA AA-3') is a 100% mismatch towards the DNA probe. Porous silicon waveguides were incubated in DNA solutions for one hour at room temperature, and sealed in a petri dish to maintain elevated humidity and limit solvent evaporation. Incubation was followed by a rinse with buffer, then water, and drying under nitrogen. As shown in Figure 3.2, upon exposure to the complementary target DNA solution, a blue-shift in the resonance angle was observed by attenuated total reflectance measurements. Exposure to noncomplementary oligo solution also produced a shift in the resonance angle, although significantly smaller. This suggests some residual non-complementary binding occurred under the noted experimental conditions.

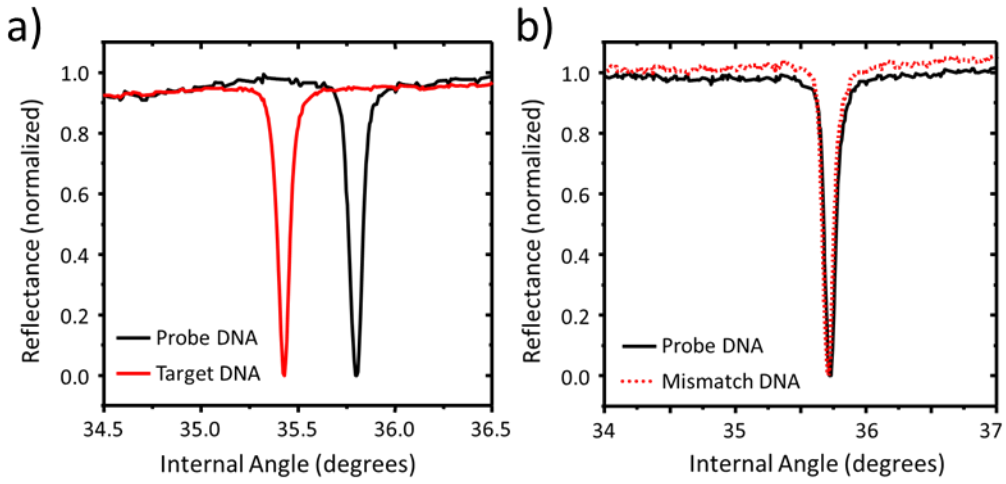

Figure 3.2: (a) Exposure to 50μM of 8mer target DNA in buffer solution produces a blue-shift in the reflectance spectrum. Exposure to 50μM of 8mer mismatch solution produces only a nominal shift (b). This result demonstrates the selective binding of DNA targets.

Given angular resolution limit of the Metricon instrument of 0.002°, the waveguide has an estimated detection limit of ~250 nM of complementary DNA. The shift resulting from hybridization of DNA is a shift to lower resonance angle, indicating a lower effective refractive index in the waveguide mode. This could be accounted for by a loss of material, consistent with an oxidative etching of the pore walls [40] as discussed in Section 3.1.2. The proposed mechanism for this blue-shift is a corrosion of the doped porous silicon walls upon the introduction of target DNA with its negatively charged backbone [41]. Importantly, the data in Figure 3.2 demonstrates clear selectivity toward the complementary sequence, and data presented in Figure 3.3 concentration dependence to the magnitude of the resonance shift. Hence, after a calibration curve, such as that in Figure 3.3, is obtained, it is possible to estimate the concentration of DNA exposed to the porous silicon waveguide based only on the magnitude of the resonance shift.

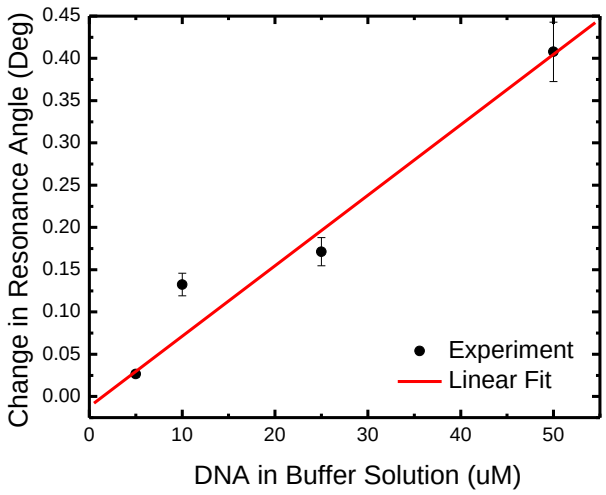

Figure 3.3: Measured change in resonance angle of porous silicon waveguide functionalized with synthesized 8-mer probe molecules upon exposure to a range of 8-mer DNA targets in HEPES buffer.

3.1.5 16mer DNA detection experiments

For exposure to a given concentration of target DNA, it is expected that longer DNA sequences will cause larger resonance shifts upon hybridization. Using the techniques described in the previous section, porous silicon waveguides were prepared with in situ synthesized 16mer DNA probes (see Section 3.1.3) and exposed to 10μM of the complementary 16merDNA target. DNA hybridization in the pores produced an average change in resonance angle of 0.39°, as shown in Figure 3.4, which corresponds to a sensitivity of 0.039°/μM. This sensitivity for the 16mer probe is greater than for the 8mer probe (see Figure 3.3), which showed an average shift of 0.14° upon exposure to 10 μM of the complementary 8mer sequence. The changes in resonance width are due in part to the coupling conditions, including air gap thickness, which were not changed during the course of the experiment. This resulted in different levels of coupling efficiency for different waveguide effective indices.

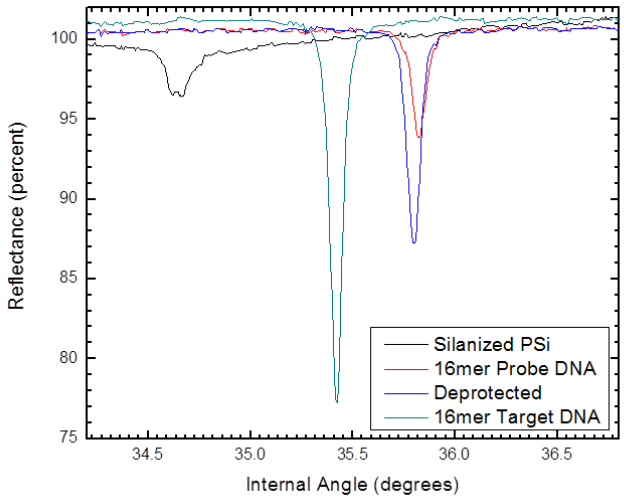

Figure 3.4: Observed shift in resonance upon 16mer DNA functionalization and hybridization to target. The resonance peak shifts to higher angle as the DNA bioreceptor is attached by in situ synthesis. Deprotection of the DNA probe activates the DNA towards hybridization and results in a shift to lower angle as the DMT protecting group is removed. Hybridization to target DNA results in shift to lower resonance angle as the negatively charged backbone of target DNA induces oxidative corrosion on the porous silicon waveguide.

3.2 Sensing of DNA-PNA hybridization

3.2.1 Introduction to PNA

The consistent blue-shift observed upon hybridization of DNA bioreceptors to DNA targets was in agreement with much of the previous literature on oligonucleotide detection in label-free porous silicon sensing devices [40, 42, 43]. Given the well supported hypothesis connecting the rigid, negatively charged backbone of the DNA target with the corrosion, there is potential to eliminate the corrosion upon target binding by utilizing a neutral oligonucleotide target species. To explore this opportunity peptide nucleic acids (PNA) [138-140] were utilized in the place of deoxyribonucleic acid in the following set of experiments.

Peptide nucleic acids are a form of artificially synthesized polymer intended to mimic the structure of DNA and RNA with numerous applications in molecular biology and medicinal therapeutics. As is apparent from the name, the structure of peptide nucleic acids differs from that of deoxyribonucleic acid in the macromolecule's backbone, where peptide bonds connect repeating units of N-(2-aminoethyl)-glycine instead of a deoxyribose sugar backbone. PNAs contain no charged phosphate groups. For this reason, it is expected that a PNA target will not induce porous silicon corrosion by the oxidation method. The PNA oligos maintain the same base-pairing abilities, as the bases A, G, T, and C may be attached off the peptide backbone just as they would be in DNA. Since the nucleic acid part of the oligos remain so similar, ssPNA and ssDNA will readily hybridize. In fact DNA-PNA binding is more robust than DNA-DNA binding because there is no electrostatic repulsion between the parallel backbones. The PNA oligos are also stable over a wider range of pH and buffer compositions, as counter ions are not necessary to stabilize the molecule in solution. Figure 3.5 illustrates the structural differences between DNA and PNA.

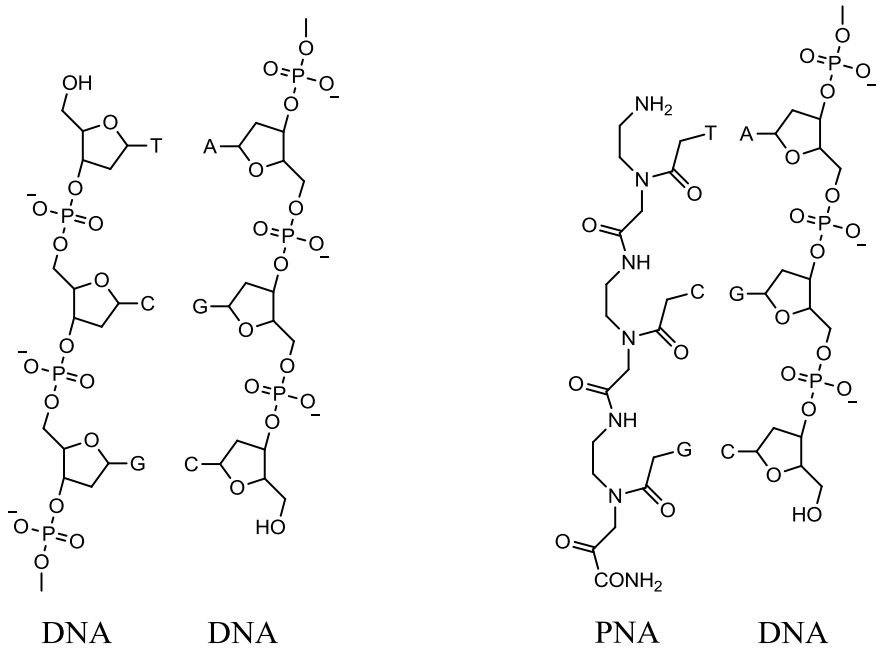

Figure 3.5: On left, the binding between DNA-DNA oligos. The DNA backbone is composed of alternating deoxyribose sugars and a negatively charges phosphate group. The bases attach to the sugar group, and hybridization occurs via hydrogen bonding between complementary bases on parallel ssDNA oligos. On right, the DNA target is replaced with a PNA target, and DNA-PNA binding is shown. Bases are attached to the neutral peptide backbone, and line up closely with the complementary bases on the parallel ssDNA. Hybridization occurs via hydrogen bonding.

Peptide nucleic acids used in this work were synthesized by Bio Synthesis Inc. and all sequences were designed as previously described for DNA experiments. The 8mer and 16mer PNA targets contained base sequences identical to those used in the DNA-DNA hybridization experiments. PNA samples were received lyophilized, and were diluted in buffer or water to form stock solutions for sensing experiments. When not in use, stock solutions were stored at -4°C to prevent degradation of the molecules. Before use, PNA stock solutions were thawed completely and diluted into desired solution concentrations in buffer or water. Before porous silicon sample incubation in PNA solutions, the solutions were heated above the predicted melting temperatures in order to reduce oligo aggregation. It should be noted that the lack of electrostatic repulsion between probe and target oligos in a DNA-PNA duplex result in higher melting

temperatures than in the corresponding DNA-DNA duplex. There are a number of methods to predict DNA-PNA melting temperature for specified sequences. Generally, at the buffer conditions used in this work, an increase of approximately 1°C in the melting temperature should be expected per base pair over the melting temperature of the DNA-DNA duplex [141, 142].

3.2.2 PNA detection experiments

Following incubation for 1 hour in target PNA solutions, porous silicon waveguides that were oxidized, silanized, and loaded with in situ synthesized probe DNA molecules were rinsed with buffer and deionized water, and then dried under nitrogen gas. Changes in the reflectance spectrum for the functionalized waveguides are monitored by prism coupling. Figure 3.6 compares the resonance shift observed after exposure to complementary 8mer DNA and PNA solutions for two standards porous silicon waveguide sensors. Note that the upon exposure to 8mer DNA target, the resonance angle shifts to lower angle, while exposure to 8mer PNA target shifts the resonance to a higher angle. This suggests that the DNA-induced corrosion is the source of the observed blue shift. The neutral charge PNA yields the expected increase in porous silicon refractive index due to material addition to the pores. Detection of DNA targets occurs via a different mechanism: negative-charge induced oxidative corrosion of porous silicon.

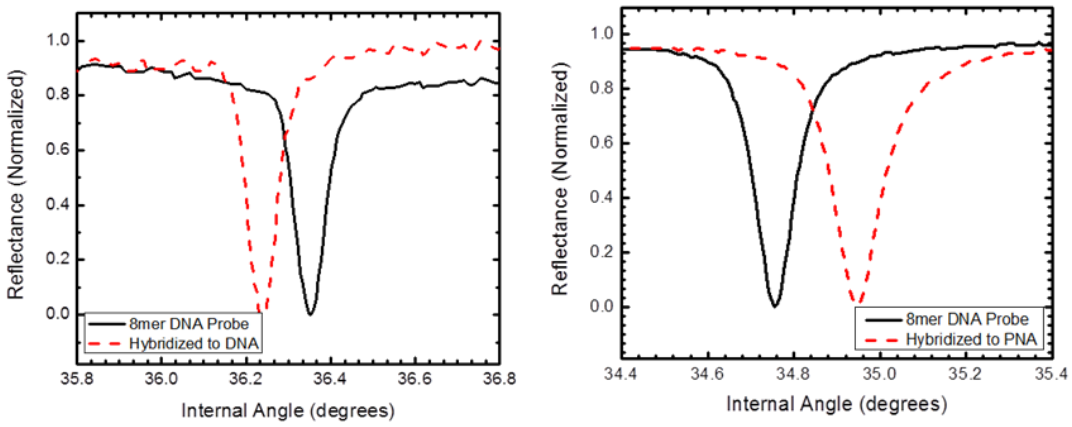

Figure 3.6: On left, DNA-DNA hybridization is detected by a shift to lower angle in the reflectance spectrum, indicating the 8mer target-DNA induced oxidation of porous silicon waveguide. On right, DNA-PNA hybridization is detected by a shift to higher resonance angle, indicating the pore filling by target PNA and subsequent increase in the effective refractive index of the waveguide layer. In both experiments, waveguides were incubated in 10μM of oligo in solution for one hour. Adapted from [110].

The detection sensitivity of the in situ functionalized porous silicon waveguide towards PNA was investigated through exposure of the waveguide to different concentrations of target analyte. Figure 3.7 shows that the waveguide resonance shifts to higher angle with increasing concentration, indicating that the effective refractive index of the waveguides layer is increasing as more PNA target is bound within the porous matrix. The sensitivity of PNA detection appears to be similar to that observed for 8mer DNA hybridization. A significant difference between DNA and PNA detection however, is that PNA binding in porous silicon waveguide optical sensors in non-destructive. Because DNA-DNA detection results in oxidation-induced surface corrosion, substrates have a very limited lifetime, and baseline drift and sample breakdown severely limit sample reusability. For DNA-PNA detection however, the target capture and signal generation are non-destructive. Experiments have shown that the DNA-PNA duplex on porous silicon waveguides may be annealed to remove target PNA, and the sensor reused

for hybridization. Porous silicon waveguides for PNA detection have been annealed and reused more than 10 times. Extrapolating from these results, it is expected that PNA functionalized sensors exposed to target DNA oligos would exhibit similar reusability.

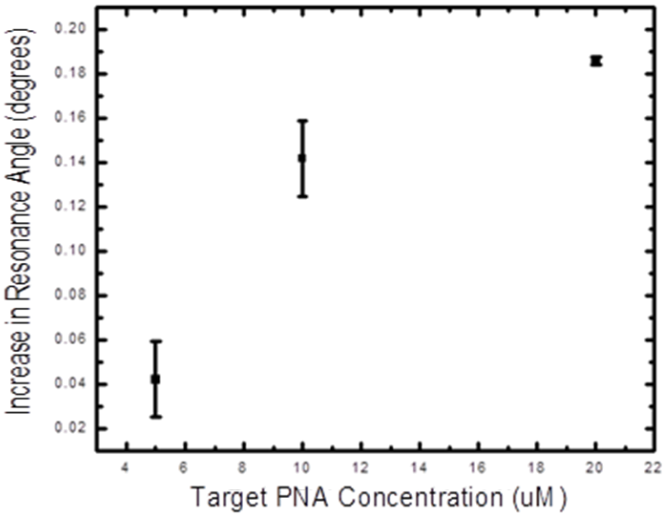

Figure 3.7: Concentration dependence for hybridization of complementary 8mer PNA targets in porous silicon waveguides. The detection sensitivity for PNA targets is similar to that observed for 8mer DNA detection.

In addition to in situ synthesis of 8mer DNA for binding of target 8mer PNA, a similar experiment was performed using 16mer sequences. The 16mer sequences previously described for DNA were synthesized within porous silicon waveguides via the in situ phosphoramidite method. Porous silicon waveguides were subsequently exposed to target 16mer PNA solution, and the changes in the reflection spectrum were monitored by prism coupling. In Figure 3.8, the shift in resonance angle observed for 8mer PNA targets is compared to the shift in resonance from 16mer PNA targets.

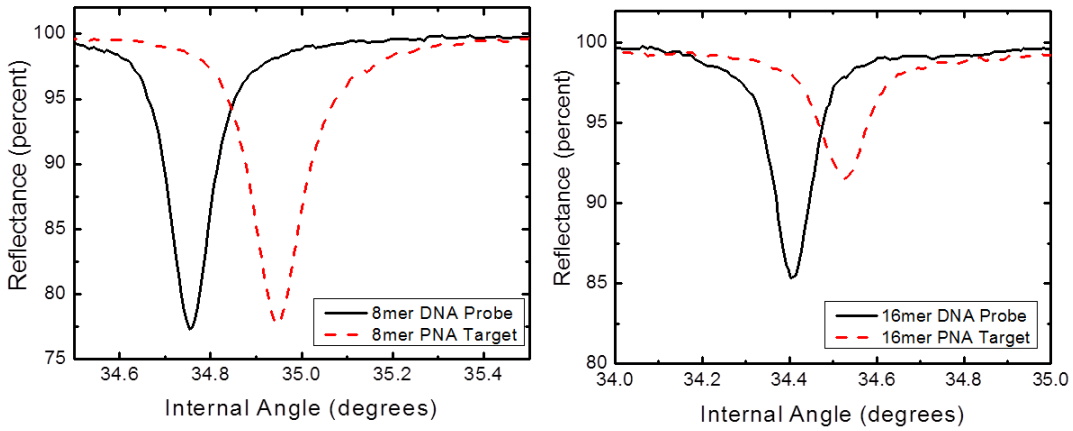

Figure 3.8: Resonance shifts upon hybridization with 100% complementary PNA sequences for 8mer (left) and 16mer (right) DNA probes. Hybridization to the 8mer probe produces a shift of 0.194°, while hybridization to the 16mer probe results in a shift of 0.122°. Adapted from [110]

Interestingly, the magnitude of the resonance shift for 8mer and 16mer PNA hybridization to the respective DNA probes is similar in the ~20 nm pore diameter porous silicon waveguides. If all of the probe molecules capture a target PNA molecule, then a resonance shift of nearly equal magnitude to that shown by the waveguide after probe DNA attachment (Figure 2.11) would be observed; consequently, the 16mer hybridization would be expected to yield a larger resonance shift than 8mer hybridization. However, given the size-dependent infiltration difficulties previously described in mesoporous silicon (Figure 2.11), we do not expect nor do we observe a comparable magnitude shift for the probe and target molecules. Moreover, the data in Figure 3.8 suggests that 16mer PNA suffers much more significantly from size-dependent infiltration challenges such that the shift due to hybridization of 16mer PNA is slightly less than that due to hybridization of 8mer PNA. While the in situ synthesis method allowed the 16mer probe to be synthesized in the pore with very little hindrance, the full size 16mer target molecule infiltrated into the pores with a much lower efficiency; steric

crowding of the 16mer probe is also a concern in this case. These issues will be examined in detail in the following chapter.

3.2.3 Comparison to DNA-DNA hybridization

The previous work demonstrates that porous silicon waveguide optical biosensors have the potential to use two distinct sensing mechanisms: concentration dependent oxidative corrosion for negatively charged targets or concentration dependent pore filling for neutral targets. For both sensing mechanisms, a number of target concentrations were tested and sensitivity curves developed for the 8mer target oligonucleotides. In each case, detection limits can be expected to be in tens to hundreds of nanomolars for target oligo solutions. In Figure 3.9, the two different sensing mechanisms are graphed together, with an initial resonance peak set to the zero position on the x-axis, where the initial peak is from a sample with in situ synthesized 8mer DNA bioreceptor, deprotected and prepared for target hybridization. When exposed to a neutral PNA target, resonance shifts to the right. When exposed to a negatively charged DNA target, resonance shifts to the left.

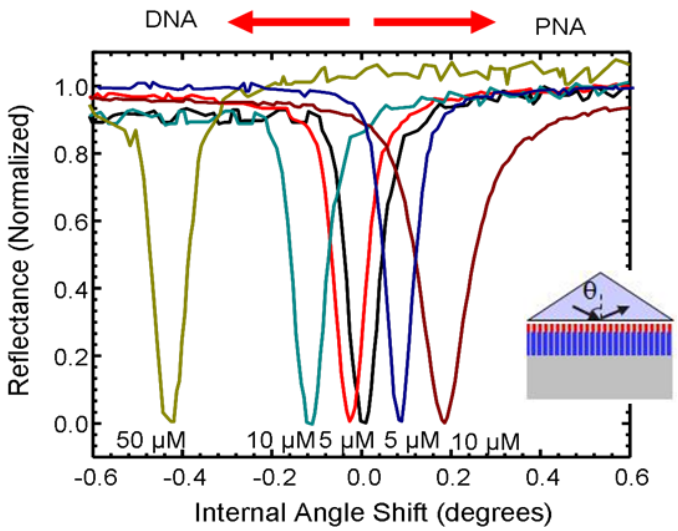

Figure 3.9: Target nucleic acid molecules, regardless of charge, produced an identifiable response compared to mismatched sequences that produced no resonance shift. DNA (negatively charged) hybridization leads to a resonance shift to lower angle, while PNA (neutral species) hybridization leads to a resonance shift to higher angle. Figure inset shows prism coupled to a porous silicon waveguide, representing the measurement setup. Internal angle θ, which is related to the modal index, is indicated.

Chapter 4

4. TUNED DNA PROBE DENSITY FOR IMPROVED SENSITIVITY

4.1 Motivation

In principle, DNA hybridization is a process of reaching a thermodynamic equilibrium between the bioreceptor oligos and the free target oligos in solution. When bioreceptors are bound to a surface, this picture becomes considerably more complicated. In some configurations, the receptor and target may not be able to hybridize under standard incubation times because of kinetic or steric effects making the receptor inaccessible to the target oligo [143]. This may be due to the oligonucleotide sequence or to the surface probe density. There are a number of examples in the literature of DNA surface density optimization for flat surface sensors [144-146].

In situ synthesis of DNA bioreceptors allows for a considerable increase in surface coverage with biomolecules within the porous silicon substrate. Given the constrained geometry within mesoscale pores, as well as the aspect ratio and secondary structure of DNA oligos, the surface coverage realized via in situ synthesis likely is not the optimal coverage for sensing. If bioreceptor density is too low, the likelihood of a biorecognition event occurring is also low, reducing the output signal. If surface coverage is exceedingly high, however, effects resulting from the surface crowding (e.g. steric hindrance, electrostatic repulsion) may reduce the number of biorecognition events, and thus also produce a low signal. There is only one example of surface density optimization in porous silicon photonic devices. Bonnano and DeLouise observed improved sensitivity at bioreceptor coverage around 57% in porous silicon; however, the bioreceptor in that

particular study was an antibody – for which the crowding effects may be quite different than observed with DNA bioreceptors [147].

4.1.1 Hybridization efficiency

Figure 4.1 shows hybridization efficiency data for in situ synthesized DNA probes and directly infiltrated probes in porous silicon waveguide with different average pore diameters to shed light on the role of size dependence and surface coverage in target molecule detection. In this set of experiments, the in situ synthesized DNA were immobilized in the porous silicon waveguides utilized in Chapter 3 with approximately 40% surface coverage while the pre-synthesized DNA was directly infiltrated into porous silicon membrane waveguides similar to those described in [62] with about 10% surface coverage. Hybridization efficiency is defined here as the ratio of the waveguide resonance shift after PNA attachment to the resonance shift after probe immobilization. For example, based on the resonance shifts discussed in Section 3.2.2 due to target attachment and the in situ synthesized probe DNA shifts discussed in Section 2.3.4, we find that the hybridization efficiency for the 8mer molecules is approximately 25% while that for 16mer molecules is approximately 10%. Due to sample to sample variations, it is estimated that these hybridization efficiencies are accurate to within 10% based on the typical variation observed in DNA probe and target shift. In a similar manner, as shown in Figure 4.1, hybridization experiments have shown that the hybridization efficiency of 16mer PNA molecules in 15 nm and 60 nm pores is approximately 50% and 70%, respectively, in porous silicon membrane waveguides functionalized by traditional infiltration of pre-synthesized DNA baroreceptor oligos [110].

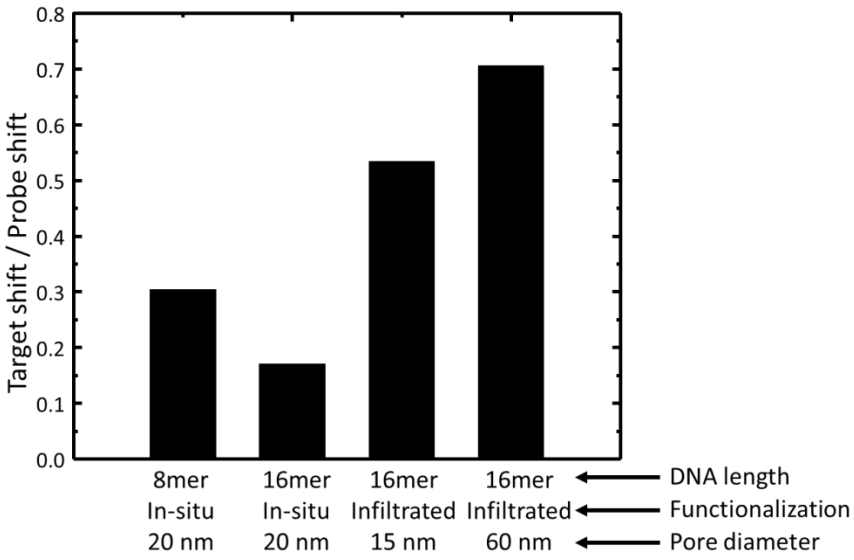

Figure 4.1: Hybridization efficiencies of various sensing systems toward 10-μM PNA solution: (a) 8mer target exposed to high in situ synthesized probe density in 20 nm pores of traditional two-layer porous waveguide, (b) 16mer target exposed to relatively high in situ synthesized probe density in 20 nm pores of traditional two-layer porous silicon waveguide, (c) 16mer target exposed to relatively low probe density in 15 nm pores of porous silicon membrane waveguide, and (d) 16mer target exposed to relatively low probe density in 60 nm pores of porous silicon membrane waveguide. Figure adapted from [110].

There are three primary conclusions that can be drawn from the hybridization efficiency comparison. First, when comparing hybridization efficiency in pores with similar diameters, the pores with lower probe density (i.e., 15 nm diameter pores with direct probe DNA infiltration) experience larger hybridization efficiency. This trend is consistent with prior reports [148], although the overall hybridization efficiency may be slightly lower in porous media. Second, unlike planar surfaces on which consistent hybridization efficiencies are achieved as long as the probe density remains constant (regardless of the method utilized to obtain the particular probe density) [149], when comparing pores with similar probe density but different pore size (e.g., 15 nm and 60 nm pores with direct probe infiltration), we find that hybridization efficiency is greater in the larger pores. This increased hybridization efficiency can be attributed in part to the extra

space available for the target molecule to move within the pores. Third, although the hybridization efficiency is significantly lower in the waveguides with high probe density, the overall resonance shift in response to target infiltration is larger. Although the fraction of DNA bioreceptors that capture target oligos is smaller, the magnitude of the signal is larger as a result of the higher number of available receptor molecules. When considering the most appropriate pore diameter and probe coverage for sensors utilizing porous materials, a modest probe surface density and slight compromise in hybridization efficiency along with sufficient pore diameter to enable molecular infiltration and binding is likely to yield the highest detection sensitivity. Hence, tuning DNA bioreceptor density is believed to be a key parameter for improved detection sensitivity.

4.1.2 Tuning DNA probe density on flat substrates

For emerging applications of planar DNA oligo sensor arrays and molecular recognition applications, it has been shown that surface density plays a crucial role. Both thermodynamic and kinetic equilibrium of receptor to target hybridization is strongly dependent on surface density [93, 148, 150-152]. It is interesting to note that the thermodynamics of DNA hybridization are not simply a function of sequence, but also of the nearest-neighbor interactions when the oligos are anchored on a surface. This nearest-neighbor interaction can affect thermodynamics of hybridization [153], and efficient duplex formation may be hindered by molecular crowding on the surface potentially slowing the kinetics of hybridization dramatically [148]. Electrostatic models have been developed to describe the effect of surface density on DNA hybridization [154].

The process of immobilizing DNA bioreceptors on a sensor surface is complex, with the resulting density being determined by electrostatic effects between

oligonucleotides and the surface. In order for surface kinetics and thermodynamics of oligonucleotide sensor arrays to be studied, careful control of the DNA surface density must be achieved and quantified. There are a number of approaches for controlling DNA surface density that have been described in the literature for flat substrates. Perhaps the most straight-forward approach to controlling surface DNA probe density involves controlling the concentration of pre-synthesized DNA probes in the incubation solution. By exposing the substrates to a range of DNA probe concentrations, a varied DNA surface density can be achieved and quantified by electrochemical means or via fluorescent tags on the immobilized DNA [155-157]. Other approaches involve the use of a single DNA solution concentration, but varying the substrate incubation time [158], ionic strength of the solution [148, 159], or an applied electrostatic field at the surface [148, 160].

For applications that involve the use of in situ DNA synthesis methods, the control of DNA surface density is more complex [161]. The most popular method currently employed for controlled oligonucleotide in situ synthesis involves light-directed synthesis. In this method, the 5' protecting group is modified to include a photolabile group, such as 2-(2-nitrophenyl)propoxycarbonyl [162] or (methyl-2-nitrophenyl)propoxycarbonyl [163]. During the synthesis cycle, these groups can be selectively removed by irradiation with light. On a flat surface DNA microarray, directing the light to deprotect specific regions of the substrate allows for spatial control of DNA synthesis. Further, a few researchers have looked at the dose-dependence of light-directed deprotection of the 5' photolabile group, and have demonstrated control of the surface density achieved by in situ synthesis by varying the UV light exposure time

[93]. This method may be particularly promising because it has been applied not only on glass slides, but also on silanized glass substrates, functionalized amorphous carbon, and glassy carbon as well [93], though not yet on a porous substrate such as porous silicon.

It is important to note that because attachment of DNA oligos to a sensor surface is highly dependent on oligo-to-surface interactions, it can be exceedingly difficult to apply a technique analyzed on one type of surface to another. Differences in the properties of various substrates – gold, glass slides, silicon – and the protocols developed for particular surfaces and conditions, may not transfer directly to new surfaces and applications. Even on a single material, significant differences in surface heterogeneity have been shown to make reproducibility a challenge. Other factors such as oligo length and conformation also play a role [164]. There are significant challenges in applying the previously described techniques to a porous surface compared to a flat surface. The primary impediment is that incubation time and concentration, electrostatic field application, and photo-patterning are all techniques that might not be applied uniformly through the three dimensional sensing surface of porous silicon waveguides. For example, if incubation time is varied, the time required for oligonucleotide diffusion from the top mesopores to the waveguide remains difficult to control. A surface density gradient may result across the depth of the porous silicon optical structure. For this reason, the functionalization method selected for this work controls the surface density by controlling the silanziation step – functionalizing the porous silicon with a uniform, two-component monolayer coating, only one of which is active for in situ probe DNA synthesis. This approach has been employed in a number of applications [165-167], but not previously in a porous silicon optical device for control of DNA surface density.

4.2 Porous silicon functionalization with two-component monolayer

4.2.1 Triethoxysilane-based two-component monolayers

In order to tune the surface density of DNA synthesized by the phosphoramidite in situ synthesis method, it is necessary to tune the density of –OH terminating silane monomers attached to the porous silicon waveguides. As discussed in Chapter 2, the silane monolayer serves a dual purpose: facilitating bioreceptor attachment while protecting the oxidized porous silicon substrate from dissolution in aqueous media. For this reason, it is not sufficient to simply reduce the incubation time in silane solution to achieve a lower surface coverage. A second monomer, inert to phosphoramidite synthesis, must also be introduced into the monolayer to preserve the porous silicon waveguide stability in aqueous solutions required for sensing experiments.

A very common method for formation of two-component self-assembled monolayers involves the deposition of a first component of the monolayer followed by a separate deposition of a second monomer which effectively back-fills into the gaps remaining in the monolayer left from the first deposition. This backfilling approach has been used in a number of applications, including some triethoxy-based monolayers for oligonucleotide sensors [168-170]. For this reason, first attempts at producing a dual functionality mixed silane monolayer utilized a two-step silanization procedure, combining the previously described hydroxyl terminating TEOS-HBA silane with octyltriethoxysilane (OTES), an alkyl-terminating monomer inert to phosphoramidite DNA synthesis. Attempts were made to produce a sub-monolayer with the first silane attached, and backfill with the second.

Figure 4.2 summarized the results of a two-step silanization experiment. The porous silicon waveguides were etch, oxidized, and cleaned as described in Chapter 2.

The waveguides were incubated first in a solution of 4% OTES in toluene for one hour in an effort to deposit a sub-monolayer. Samples were then washed with toluene and dried under nitrogen. In the second step, waveguides were incubated in a 4% solution of TEOS-HBA in 95% ethanol/5% water for four hours. Samples were subsequently washed with ethanol and dried under nitrogen. Resonance angle position was monitored via prism coupling before and after each step in the functionalization. Despite waveguides being functionalized concurrently and under the same conditions, considerable sample to sample variation was observed, with some samples showing a considerably larger shift in resonance angle indicating comparatively higher coverage with monomer. Similar inconsistencies were observed with TEOS-HBA silanization was performed as the first of the two steps and when lower percentage silane solutions were used for incubation.

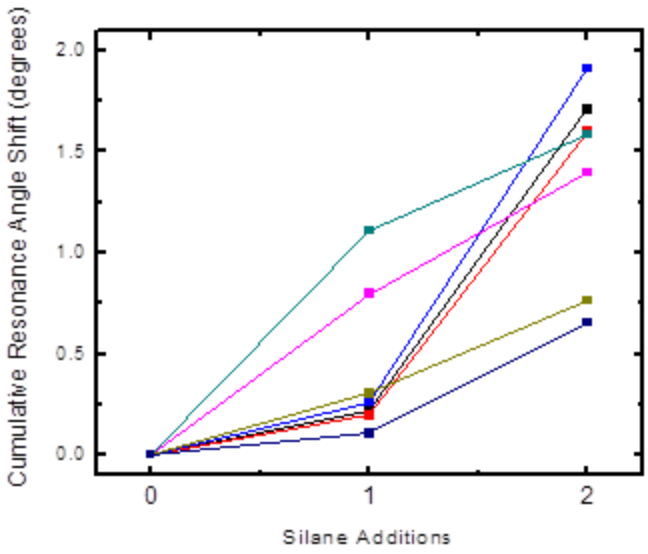

Figure 4.2: In the first silanization addition, a sub-monolayer of OTES is added to porous silicon waveguides. In the second silanization addition, TEOS-HBA back-fills into the sub-monolayer. Despite the consistent experimental conditions, considerably variation in sub-monolayer coverage is observed across porous silicon waveguide samples.

Two-step silanization with TEOS-HBA and OTES was not successful in producing mixed monolayers for control of in situ synthesized DNA surface density. Although consistent and robust TEOS-HBA silanization could be achieved through the processing described in Chapter 2, that work involved saturating samples with silane and removing unstable multilayers. When working below the saturation level, it became apparent that the previously described aggregation of monomers in solvent and moisture sensitivity [90] hamper the repeatability of sub-monolayer formation. Attempts were also made to produce mixed triethoxy-based monolayers with TEOS-HBA and OTES by depositing the monomers simultaneously from a single solution; however, a solvent compatible with both monomers was not found. Poor solubility of one or both of the monomers in incubation solvents resulted in cloudy silanization solutions and large variance in resonance angle shift upon mixed monolayer formation on the porous silicon waveguides. In order to tune DNA density through the silane functionalization, a more tunable surface chemistry is necessary.

4.2.2 Trichlorosilane-based two-component monolayers

In an effort to reduce the sample to sample variations likely resulting from the aggregation of monomer in the silanization solution [78, 91, 95, 171, 172], and alternative to the TEOS-HBA surface functionalization was sought. In contrast to the triethoxy-based monomers, literature reports indicated that trichloro-based monomers exhibit better control and reproducibility when the monolayer is deposited from an organic solvent. Oligomer aggregates tend to form when bonding between two or more monomers is initiated by reaction at a triethoxy group with the water solvent [90]. Reducing moisture content in the incubation solution and switching to

alkyltrichlorosilane monomers is a promising approach to increase monolayer uniformity and repeatability, and ultimately allow for control of a mixed silane monolayer to be formed on the porous silicon waveguides. Though there are only a limited number of reports on mixed monolayers of derived alkyltrichlorosilane monomers, it has been observed that the composition of the monolayer is generally equal to the composition of the incubation solution [173-176]. This competitive absorption approach to mixed monolayer formation is also desirable because it is a single step process and eliminates the variables introduced in any washing steps that would occur prior to back-filling with the second monomer [169].

The trichlorosilane selected for this work, trichloroacetic acid dodecyltrichlorosilane [177] can be deposited onto the porous silicon substrate with a protecting group on the –OH terminus, which subsequently can be converted to the hydroxyl under mild conditions. The selected molecule was synthesized in the two-step process outlined below, adapted from a synthetic preparation used in Professor Kane Jennings's group at Vanderbilt University. All reagents were obtained from Fisher Scientific and used as received. The synthesis is begun by combining 6.6 mmol of undecylenyl alcohol and 9.9 mmol of pyridine under nitrogen and stirring for 30 minutes at 0°C in a salt and ice water bath. After 30 minutes, 14.5mL of a 0.5 M solution of trichloroacetyl chloride in dichloromethane was added drop-wise to the mixture and the solution was stirred for overnight for 17 hours.

After the reaction is completed, the solution is rinsed with distilled water, 5 M hydrochloric acid, saturated sodium bicarbonate solution, and finally 5 M sodium chloride solution. The product is concentrated using the rotary evaporator and purified by

column chromatography, eluted using ethyl acetate, to give the colorless oil trichloroacetic acid undec-10-enylester. The final product was achieved by combining 5.8 mmol of trichloroacetic acid undec-10-enylester, 0.05 grams of 0.12 M H_2PtCl_6 in dry tetrahydrofuran, and 17.4 mmol of trichlorosilane under nitrogen in the glove box. The mixture was stirred for 4 hours. The product was separated and purified by vacuum distillation. The product is analyzed by proton NMR to assess the success of the synthesis and purification. Figure 4.3 outlines the synthesis process.

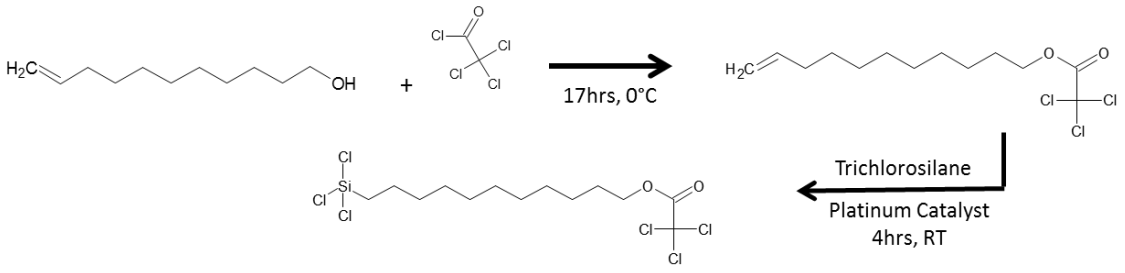

Figure 4.3: Synthesis route for trichloroacetic acid dodecyltrichlorosilane.

4.2.3 Formation of a Two-Component Silane Monolayer

Prior to incubation in the two-component silanization solution, thermally oxidized porous silicon waveguides are thoroughly cleaned to remove any organic residue and completely hydroxylate the sample. Piranha etch, a 3:1 mixture of concentrated sulfuric acid to 30% hydrogen peroxide, is prepared by adding hydrogen peroxide to the sulfuric acid in a glass beaker. The reaction is highly exothermic and should be handled with caution and kept within the fume hood. Porous silicon samples are soaked in the solution at elevated temperature for one hour. Following the piranha etch, waveguides rinsed with deionized water, then methanol, and finally are carefully dried under nitrogen gas.

The two-component trichloroacetic acid dodecyltrichlorosilane and octyltrichlorosilane monolayer can be formed by immersing the substrate in a 1 mM solution of the mixed monomers in toluene under nitrogen for 5 hours. This reaction can proceed in a glass reaction vessel sealed with a septum. Afterward, the sample is sequentially rinsed with toluene and methanol, and finally dried under nitrogen. Figure 4.4 illustrates a mixed monolayer formed on a flat substrate from alkyltrichlorosilanes in solution. One component of the monolayer is inert and the other contains a head group that can be converted to a hydroxyl for further functionalization.

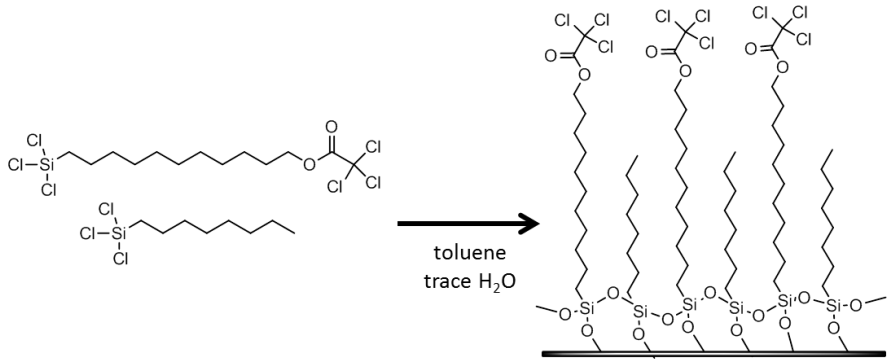

Figure 4.4: In the presence of trace amounts of water in toluene, mixed solutions of alkyltrichlorosilane monomers assemble on the substrate to form a monolayer of the same composition as the incubation solution.

The trichloroacetic acid head group on the deposited monolayer is readily converted to a hydroxyl end group by immersion of porous silicon waveguides functionalized with this monomer into a sodium bicarbonate solution. The conversion takes place over the course of a one hour soak in 10 mL deionized water, 10 mL ethanol, and 0.15 g of sodium bicarbonate. Figure 4.5 shows the head group conversion from trichloroacetic acid to hydroxyl head group by monitoring, via prism coupling, the resonance blue shift that occurs during the conversion. A progressive blue shift result

during the conversion as the bulky trichloroacetic acid head group is removed in the sodium bicarbonate deprotection solution. The resonance shift saturates when the conversion is complete. On similarly prepared flat surfaces with a trichloroacetic acid dodecyltrichlorosilane monolayer, contact angle measurements verify that soaking in sodium bicarbonate solution produced hydroxyl terminating groups in the monolayer.

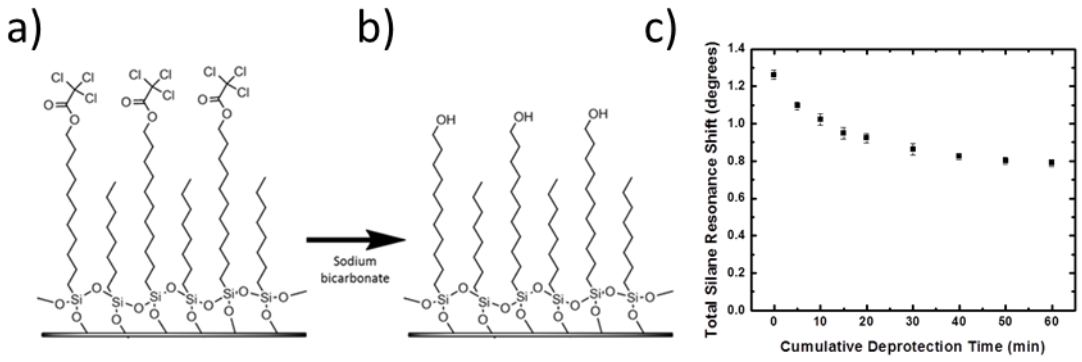

Figure 4.5: (a) Silane monolayer is produced with partial hydroxyl termination by depositing specified ratios of a two component monolayer. (b) Upon exposure to sodium bicarbonate solution, the head group of one of the mixed monolayer components is converted to the –OH termination required for in situ DNA synthesis. (c) The cumulative resonance shift measured via prism coupling for a 100% trichloroacetic acid dodecyltrichlorosilane monolayer averaged over four measurement spots. Soaking in the sodium bicarbonate deprotection solution removes the bulky trichloroacetic acid head group and blue shifts the resonance angle over the course of an hour of incubation.

To produce a two-component mixed monolayer, specific ratios of the two different monomers are introduced at the silanization step. For example, to achieve a monolayer composed of 25% silane active towards phosphoramidite DNA synthesis and 75% of an inert monomer, the silanization solution is modified to contain 0.25 mM trichloroacetic acid dodecyltrichlorosilane and 0.75 mM of octyltrichlorosilane, which is inert towards DNA synthesis. For a monolayer with 50% of molecules available for DNA synthesis, the silanization solution contains 0.50 mM trichloroacetic acid dodecyltrichlorosilane and 0.50 mM of octyltrichlorosilane. On a flat surface, contact

angle measurements verify that the monomers are deposited onto the surface in a ratio very close to that prepared in the silanization solution [177].

4.3 Characterization of two-component monolayer

In order to analyze the trichloro- derived monolayers in porous silicon waveguides, an analytical tool for surface chemistry and binding states is required. For this analysis, x-ray photoelectron spectroscopy is utilized to determine the composition of the monolayers. The photoelectric effect is at the foundation of this technique, using x-rays to eject electrons from the inner-shell orbitals with which they interact. Photoelectron spectroscopies are single photon in, single electron out processes where the energy of the photon for all types of electromagnetic radiation is given by the relation $E = hv$. When a monochromatic source of radiation is applied, a photon is absorbed by an atom in a surface molecule under analysis. As a result, an inner shell electron is emitted (ionization). By analyzing the distribution of the kinetic energies at which the emitted photoelectrons leave the surface, a photoelectron spectrum can be recorded. Characteristic binding energies of the detected electrons allow each element present in the sample to be identified and counted. It is critically important to note that this analytical technique is a surface technique. While x-ray penetration depth may be micrometers into the substrate, only those photo-emitted electrons in the top ~10nm of the substrate escape the surface before reabsorption within the material. All XPS measurements were completed in collaboration with Robert Harl from the Department of Chemical and Biomolecular Engineering at Vanderbilt University, and in consultation with Professor Bridget Rogers. All data was acquired using a 50 W x-ray beam. Charge neutralization was accomplished with 1.1 eV e^- and 10 eV Ar^+.

4.3.1 Surface coverage by trichlorosilane-based monomers

X-ray photoelectron spectroscopy allows for the analysis of the packing density and relative composition of silane monomers on porous silicon substrates. Figure 4.6 below shows the XPS survey data for alkyltrichlorosilane-derived mixed monolayers of various compositions.

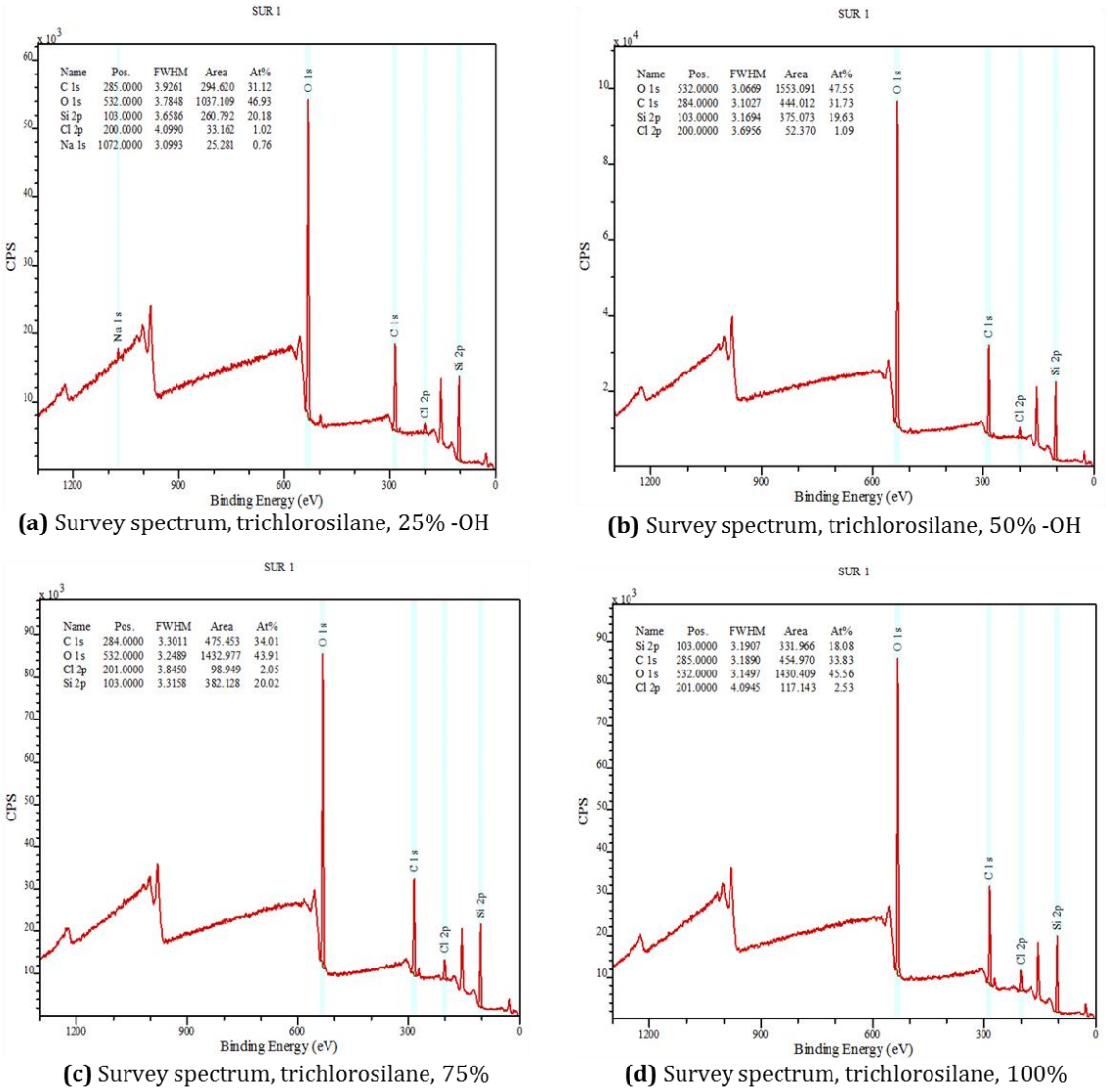

(a) Survey spectrum, trichlorosilane, 25% -OH

(b) Survey spectrum, trichlorosilane, 50% -OH

(c) Survey spectrum, trichlorosilane, 75%

(d) Survey spectrum, trichlorosilane, 100%

Figure 4.6: XPS survey spectra for two-component mixed monolayers on porous silicon following sodium bicarbonate treatment to remove the trichloroacetic acid head group. Inset (a) shows a surface with a solution of 25% trichloroacetic acid dodecyltrichlorosilane and 75% octyltrichlorosilane. Inset (b) shows a sample silanized in 50% trichloroacetic acid dodecyltrichlorosilane and 50% octyltrichlorosilane, while inset (c) was incubated in 75% trichloroacetic acid dodecyltrichlorosilane and (d) in 100% trichloroacetic acid dodecyltrichlorosilane. The relative intensities of the carbon and silicon peaks may be used to analyze the packing densities from sample to sample.

In order to assess the relative surface coverage for the trichlorosilane-derived mixed monolayers, a standard methodology for surface comparison across samples must be developed. The atomic percentages calculated from the survey scans can be used to

determine the relative quantities of two atoms on a single porous silicon sample under XPS analysis. Taking the ratio of carbon from the monolayers to the silicon background provides a measure of surface coverage with the monomers on the porous silicon surface.

Comparing the packing densities formed by the different self-assembled monomers is not possible by directly comparing only the carbon content of the spectra. If monomers are of similar length, however, then the carbon to silicon ratio may instead be used as a proxy for packing density, and as the packing density of the SAM increases, the carbon to silicon ratio will increase as well [165]. Because the monomers used in this study are of different lengths, the C/Si ratio calculated must also be normalized to account for length differences in the monolayers of octyltrichlorsilane (8 carbons) and trichloroacetic acid dodecyltrichlorosilane (11 carbons, after conversion to hydroxyl). Table 4.1 illustrates the normalization of the C/Si ratio used to compensate for the varying carbon chain lengths of the monomers. Once normalized, it is clear that there low variation in the packing density even as the ratio of the two components of the monolayer is varied. This sample to sample consistency is maintained despite the bulky head group of the trichloroacetic acid dodecyltrichlorosilane monomer, and adds further evidence of higher uniformity and repeatability for silane monolayer formation. Interestingly, the mixed silane monolayers deposited from trichlorosilanes in solution also display resistance to dissolution in phosphoramidite DNA synthesis solution without the need for hydrolyzing and extended annealing.

Sample Silane	Average number of carbons per chain	C/Si ratio	C/Si normalized by C atoms in monomer
Trichlorosilane, 25% -OH	8.75	1.54	0.176
Trichlorosilane, 50%-OH	9.50	1.62	0.171
Trichlorosilane, 75% -OH	10.25	1.70	0.166
Trichlorosilane, 100% -OH	11	1.87	0.170

Table 4.1: C/Si ratios for the various surface treatments are normalized by the average number of carbons per chain. Given the low Cl content on each of these samples treated with sodium bicarbonate solution, full deprotection of the trichloroacetate group is assumed in these calculations.

Survey data from XPS measurement of the mixed silane samples was also used to verify the higher surface coverage with the trichloroacetic acid dodecyltrichlorosilane monomer by comparing the relative magnitudes of the carbon peaks. On a flat surface, contact angle measurements verified that low percent hydroxyl terminal surfaces were produced when silanized in low percent hydroxyl incubation solutions of the same composition. In Figure 4.7, carbon content is compared for a series of four substrates: two flat surface silicon substrates of varied mixed silane composition and two porous silicon substrates of varied mixed silane composition. For the flat surface samples, it is noted that the 75% hydroxyl samples show approximately three times larger than the signal observed from the 25% hydroxyl sample. This may indicate a higher degree of coverage with the longer (i.e. more carbons) trichloroacetic acid dodecyltrichlorosilane monomer than the shorter inert monomer. This corroborates the contact angle measurements for flat surface samples with the mixed silane coating. A similar difference in the 25% hydroxyl and 75% hydroxyl samples on porous silicon is observed. This supported the hypothesis that controlled, mixed silane monolayers may be deposited on

porous silicon under conditions similar to those used on flat substrates. Note also that the porous surface provides for a higher coverage with monomer even within the nominal probing depth of XPS analysis when compared with the flat surface substrates.

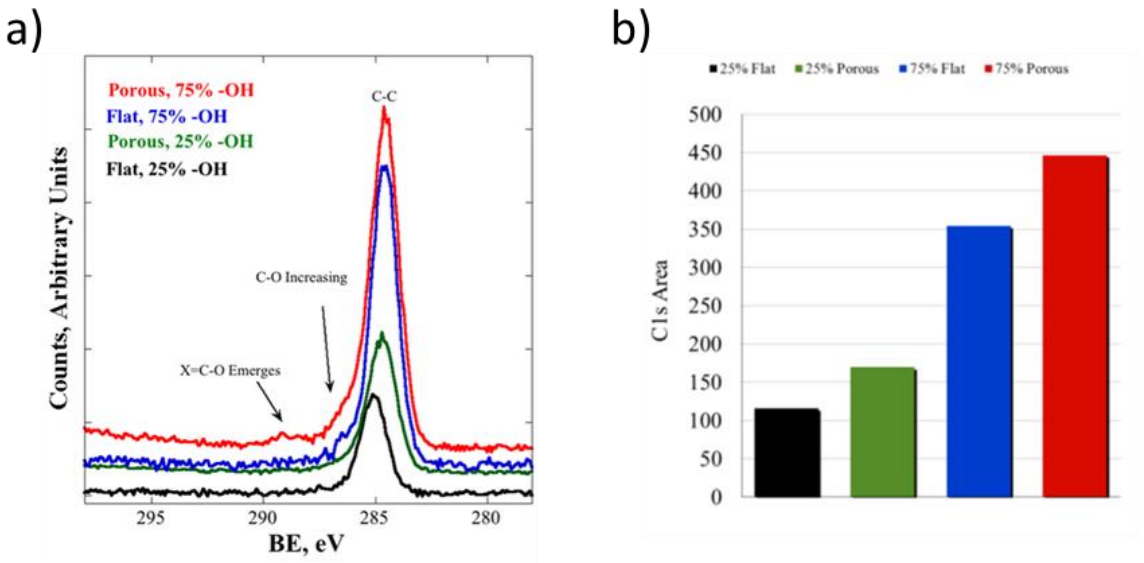

Figure 4.7: (a) XPS spectra for both flat and porous substrates with 25% and 75% silanized surface active toward DNA synthesis are shown. Characteristic peaks for the two distinct trichlorosilane monomers utilized in the mixed monolayer are indicated. (b) The integrated area of the C1s peak provides an estimation of the ratio of the two silanes found within the pores. Because the DNA-synthesis-active monomer contains a longer alkyl chain, greater C1s peak area indicates higher coverage with the DNA-synthesis-active end group.

4.3.2 Quantifying surface DNA vs. silane ratio

Figure 4.8 illustrates the expected surface coverage of a mixed silane monolayer where one monomer component has a hydroxyl head group and the other monomer component is an alkyl (inert) chain. When such a two-component monolayer is introduced, only the fraction of the surface that is hydroxyl functionalized will be active towards the in situ DNA synthesis process, effectively decreasing the DNA bioreceptor surface density. In the constrained pore geometry, there is reason to expect that a lower

surface density than previously achieved (Chapter 3) may improve sensitivity, allowing for more target oligos to be captured for detection. This approach will be analyzed in this chapter by preparing porous silicon waveguide sensors with a range of monomer ratios forming two-component monolayers, synthesizing DNA within the pores, and then testing the detection sensitivity towards oligo targets of a specified concentration.

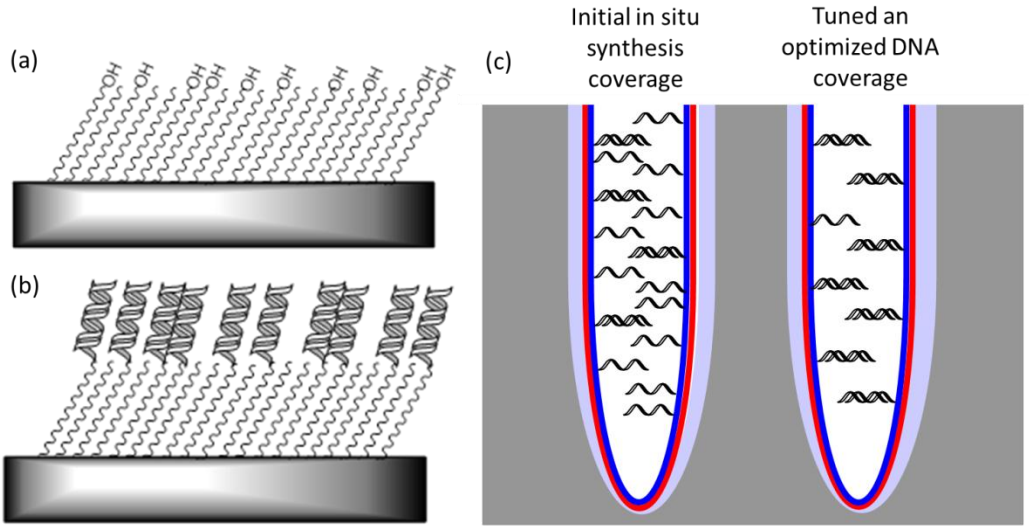

Figure 4.8: Schematic of (a) surface functionalization of mixed trichlorosilanes deposited on a flat surface and (b) DNA receptor and target bound after in situ synthesis on the substrate. DNA attaches only to –OH terminal functional groups on the silane. (c) Due to molecule crowding effects that are accentuated in cylindrical pores, a reduced surface spacing of the active component of the mixed silane and accordingly probe DNA, is expected to increase the number of DNA probes that can hybridize.

Porous silicon waveguides with dual functionality mixed monolayers are used as substrates for in situ DNA synthesis to determine the relative quantity of DNA attached for each surface. In order to quantify the DNA attached to each porous substrate, the acid-labile, dimethoxytrityl (DMT) protecting group on the 5'-hydroxyl end of the synthesized nucleoside can be collected during in situ DNA synthesis. Upon treatment with the trichloroacetic acid, the 5' end of the nucleoside is detritylated and the wash from this step can be collected for analysis. Quantification of the dimethoxytrityl (DMT)

cation in acetonitrile solvent can be accomplished by measuring its absorbance. The quantity of DMT cation measured by the analysis method gives a minimum limit for the number of nucleosides attached in the preceding coupling step in the synthesis, and the maximum number of nucleosides that remain available for next coupling step in the DNA synthesis sequence. The Applied Biosystems 392 Nucleic Acid Synthesizer has a trityl collection port built in to the system. The synthesis cycle procedure is modified to allow for collection of wash solutions of the DMT in acetonitrile as the synthesis proceeds.

The DMT cation has a maximum absorbance at 498 nm and an extinction coefficient of 70,000 M^{-1} cm^{-1} in acetonitrile solvent. The cation can be quantified spectrophotometrically and the molar amount of cation calculated using Beer's Law:

$$A = \varepsilon C l$$

where A is the absorbance, ε is the extinction coefficient for the molecule, C is the concentration of the molecule in solution, and l is path length of which the beam passes through the solution. Absorbance is measured spectroscopically, allowing the equation to be solved for concentration. With a molar concentration known, it is possible to determine the number of trityl cations in the collected solution, and thus the number of in situ synthesized DNA chains initiated.

Absorbance data for the DMT cation collected from mixed silane porous silicon substrates was collected using a Varian Cary 5000 UV-VIS-NIR spectrophotometer. During in situ DNA synthesis, DMT-containing fractions were collected after base addition. Fractions for each base were combined and diluted up to 10 mL using 0.1M p-toluenesulfonic acid in acetonitrile. A 1 mL quartz cell filled with the DMT solution was placed in the spectrophotometer and absorbance at 498 nm was recorded. Background

absorbance for acetonitrile solution alone was recorded and subtracted from the sample absorbance measurements. Absorbance measurements for the trityl cation cleaved from the first and second nucleotide additions in a synthesis are measured and averaged. These absorbance values for each porous silicon waveguide functionalization are listed in Table 4.2. From the absorbance, moles of initiated DNA oligo chains for the various surface compositions are calculated.

Mixed monolayer composition	Absorbance	DNA synthesized (nmol)	Surface Density (molecules/ cm^2)
10% Hydroxyl-terminating	0.046	6.57	7.23×10^{12}
25% Hydroxyl-terminating	0.082	11.71	1.29×10^{13}
50% Hydroxyl-terminating	0.094	13.42	1.48×10^{13}
75% Hydroxyl-terminating	0.141	20.14	2.22×10^{13}
100% Hydroxyl-terminating	0.183	26.14	2.88×10^{13}

Table 4.2: Absorbance and concentration data for DMT cation collected following in situ DNA synthesis on mixed silane monolayer porous silicon substrates with varying hydroxyl content. Porous silicon waveguide surface area is estimated using BET surface area calculated by nitrogen adsorption isotherms.

In addition to quantifying the DNA sequences synthesized within the porous silicon waveguide, it is essential to accurately estimate the internal surface area in the porous silicon structure to predict bioreceptor surface density. Reasonable estimates of the internal surface area can be made by approximating the pores as cylinders, and calculating the total area of cylinder walls of diameter equal to the average pore size that can compose the porous percentage of the layer composition. Alternatively, nitrogen adsorption isotherms may be measured and analyzed using BET (or Brunauer, Emmett,

and Teller) theory. Adsorption is a surface-based phenomenon where molecules adhere to a surface creating a thin mono- or multi- layer film. As this process is related to surface energy, describing the amount of adsorbate as a function or pressure at constant temperature produces an isotherm from which information about the total energy of the adsorbed molecule thin layer can be deduced. Given pore sizes below ~50nm in diameter and a narrow pore size distribution, total pore surface area can be estimated from the constructed nitrogen adsorption-desorption isotherm [178-180]. This approach has previously been applied to porous silicon mesoporous structures for total internal surface area analysis [43, 181, 182].

In order to achieve isotherms for BET analysis, porous samples much be degasses at high temperature for 16 hours to eliminate moisture from the sample which interferes with nitrogen gas adsorption. A minimum of 0.5 grams of sample is necessary, with pore thickness of at least 20 μm for waveguides etched under standards conditions. When nitrogen adsorption is used to approximate the surface area of the 2cm diameter porous silicon waveguide biosensor used for in situ DNA synthesis experiments, the BET surface area for the waveguide layer is $0.65cm^2$ per 1nm depth. This for the 240nm thick high index porous layer, the internal pore surface area is approximated as $157cm^2$. For the low index cladding layer, the internal pore surface is approximated as $390cm^2$.

The porous silicon substrates (waveguide + cladding) used in this work have an estimated internal surface area of $547cm^2$. This calculation approximates the pores as cylinders and estimates the total internal surface using the average pore diameter, porosity, and pore depth, combining the estimated surface are for both the waveguiding and cladding layers of porous silicon. The calculated surface densities achieved via in situ

synthesis of DNA oligonucleotides in porous silicon are listed in Table 4.2. These results seem consistent with other reports of oligonucleotide synthesis in porous silicon without tunable surface chemistry [100, 103, 183]. On flat surface sensors, a number of examples of DNA bioreceptor density optimizations can be found in the literature, often in the range of 10^{12} molecules/cm^2 for nucleic acid sequences 20-25mer in length [148, 155, 159, 184]. For analysis of a comparatively short DNA probe and hybridization to PNA (thus, reduced nearest-neighbor electrostatic effects) this DNA probe density range is reasonable for sensor optimization.

4.4 PNA sensing and probe density optimization

Hybridization experiments between the controlled density, in situ synthesized DNA bioreceptors and 100% antisense PNA targets were conducted. As shown in Figure 4.9, the sensitivity of the porous silicon waveguide sensors toward 100% complementary, 16mer target PNA (500nM solution) depends on the bioreceptor surface density. Highest detection sensitivity, as indicated by the largest measured resonance shift, was achieved for the sample prepared in 25% trichloroacetic acid dodecyltrichlorosilane incubation solution. The mixed silane samples with a tuned, lower probe DNA density clearly show a higher sensitivity than the single functionality samples (highest DNA bioreceptor coverage) with a high of the surface active to probe synthesis. This trend is consistent with prior reports on flat surfaces, where hybridization efficiencies have been observed as low as 10% for a high-density DNA probe coverage of approximately 1.2×10^{13} molecules/cm^2 and 50% for a low-density DNA probe coverage of approximately 3×10^{12} molecules/cm^2. Improvements in detection limits for the optical sensing of nucleic acids through careful control of surface chemistry provide further advantages of the

porous silicon waveguide sensor platform for fast, selective detection of small-molecule targets. At the optimal surface coverage with DNA probe, detection of 25nM of 16mer PNA target is predicted, and detection of 125nM target PNA in solution has been demonstrated.

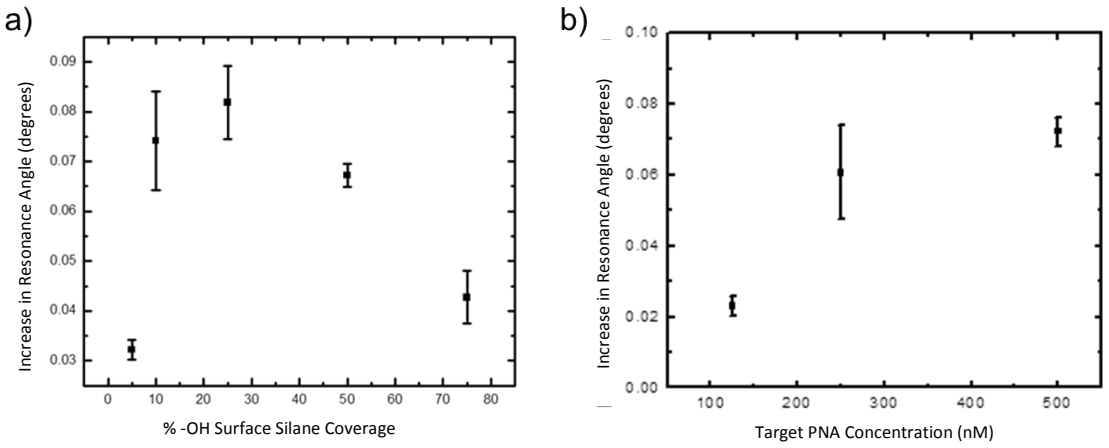

Figure 4.9: (a) Percent hydroxyl groups in SAMs on porous silicon waveguides versus resonance shift upon hybridization to 500nM 16mer PNA target. Controlling the DNA bioreceptor density by applying a mixed-functionality alkyltrichlorosilane SAM allows for an optimization of the DNA surface density to be achieved around 25% hydroxyl coverage. (b) Sensitivity curve for a porous silicon waveguide optimally functionalized with in situ synthesized DNA bioreceptors. Detection of 125nM concentration of target 16mer PNA is achieved.

Chapter 5

5. APTAMER-BASED SENSING IN POROUS SILICON WAVEGUIDES

While there is interest in sensing devices towards DNA targets, both as a model system for sensing devices as well as for actual clinical applications, expanding porous silicon waveguide sensing to targets other than nucleic acids also relevant. One area in which porous silicon waveguides with in situ synthesized DNA bioreceptors may prove particularly useful is in aptamer-based sensing. While the ability of DNA single strands to bind to complementary DNA to form duplexes is well known, these nucleic acid structures are also capable of binding non-nucleic acid target molecules with a high selectivity and high affinity. Aptamers are nucleic acid sequence structures, often between 15 and 60 bases in length, whose complex three-dimensional structure produced by Watson-Crick and non-canonical intramolecular interactions promotes the binding of a specific target [185]. As such, the three-dimensional structure functions much like the "lock" in the lock-and-key example introduced in Chapter 1, a quasi-rigid structure into which a molecular "key" of the correct shape may fit. Aptamers exist for a number of possible chemical and biological targets, with no proposed upper limit of the target size.

Selecting small molecules of interest (such as toxin molecules) and functionalizing a waveguide with the appropriate targeted nucleic acid aptamer sequence could allow for all of the advantages of this system for small molecule detection that have been discussed previously. There are some limited reports in the literature of aptamer-based sensing on planar substrates, and very little work in label-free biosensing, and no examples of aptamer in porous materials for biosensing. In order to incorporate an aptamer into a porous silicon waveguide for the label-free detection of a small molecule,

several aspects of the binding chemistry warrant investigation. As observed with DNA-DNA and DNA-PNA synthesis and binding, coverage of porous silicon waveguides with the aptamer bioreceptor will be monitored by change in resonance angle via prism coupling. Upon binding of the target molecule, a shift in resonance angle related to the change in refractive index of the porous layer will result.

5.1 Introduction to aptamers

Theoretically, a high affinity and selectivity aptamer could be found for any desired target, given a large enough library of oligos to search. This is a significant advantage of aptamers compared with other bioreceptor classes, such as antibodies. In practice, a number of aptamers have been proposed and demonstrated for a range of target types, from small ions [186, 187], nucleotides [188-190], and oligopeptides [191], to the larger organic dyes[192], viruses [193-197], whole cells [198, 199], and antibiotics [200, 201]. Even given a relatively short 25mer oligo, the number of different DNA sequences possible is 4^{25}. Systematic evolution of ligands by exponential enrichment, known as SELEX [202-204], is a technique for selecting and amplifying sequences with binding affinity to the target. This allows for a large oligo library to be narrowed down to a few sequences of interest. Aptamer binding to a number of target molecules has been described, and as a result it is possible to draw from successful aptamer sequences reported in the literature [205] within an aptamer database rather than utilizing the time-consuming and complex SELEX process to generate new aptamers for sensing.

Generally, the detection sensitivity of aptamers to small molecule targets found in the literature vary considerably depending on the target, sequence, and experimental conditions. Most commonly, binding affinities are reported to be in the micromolar

range. For small molecule targets, aptamers for citrulline and arginine have reported affinities from 0.3 to 65 μM [206-208], some ATP aptamers have affinities of 6 μM [189, 209-211], and aptamers against dopamine have a reported affinity of 2.8 μM [212-215]. When the target is a nucleic acid-binding molecule or derivative, affinities in the nanomolar or sub-nanomolar range are possible.

For label-free analysis using aptamers, a number of possible signal transduction mechanisms have been utilized. In these systems, aptamers may be immobilized on solid supports either through modification of the 3'- or 5'- end of the aptamer oligo. Typically, this immobilization step is the most challenging and cumbersome step in the label-free aptasensor preparation [216]. Given that the aptamer-target binding interaction occurs at a surface-solution interface, it should not be surprising that many of the transduction mechanisms applied to aptasensing involve changes in interfacial properties. Electrochemical aptasensors have been well described, often relying on changes in surface capacitance induced by electron-transfer mechanisms [217-223]. Solution-surface interface changes might also be transduced by gravimetric analysis of piezoelectric materials. Some high-sensitivity surface acoustic wave sensors have been used as substrates for aptamers against thrombin, with sensitivities in the μM range [224, 225]. Microcantilevers are a rapidly developing area of aptamer-based sensing. Because aptamers undergo a significantly larger conformational change than do antibodies upon target binding, they have been demonstrated to be a much better bioreceptor for systems where transduction depends upon surface stress-induced bending. Aptamer-based microcantilevers have been used to detect hepatitis C virus helicase [193] and Taq polymerase [226] in the pM range. Optical detection of aptamer-based target capture

measured by surface-plasmon resonance (SPR) spectroscopy has been demonstrated for micromolar solutions of Tat protein [195, 227, 228]. These SPR systems involved immobilized aptamers within a microfluidics channel or microarray. An alternative optical measurement technique involves solution phase – wherein DNA aptamers are affixed to a metal complex and the presence of target molecules induces a conformational change in the bound aptamer, changing the degree of intercalcation and thus the optical properties of the metal complex solution. Both large [229] and small [230] targets have been detected in this manner, and both solution luminescence [229-234] and color [215, 227, 235-238] have been used as quantitative indicators of target. Sensitivities from μM to pM have been reported.

Aptamers have been utilized not only for detection, but also for therapeutics [202, 239, 240] and chemical separations [241-245]. In therapeutics, aptamers may be administered as medications that bind to specific cell component cites and interfere with nucleic acid replication. As an example, the aptamer known as AS-1411 has been shown to selectively bind a nucleolin found on cancer cells. The aptamer inhibits mRNA production by these cells and slows tumor growth [246]. Though only about two decades have passed since the discovery of aptamers, there is already at least one aptamer-based therapy available, and aptamer therapeutics are currently undergoing clinical trials [247, 248]. This is a remarkably fast development of medical technology. There are high expectations that therapeutic applications may surpass sensing applications for aptamer use. Unlike proteins, modification of aptamers to improve in vivo stability in physiologic conditions is possible, while maintaining the nucleic acid's structure and function. They

also may be synthesized chemically (via phosphoramidite synthesis, for example) and thus do not involve culturing of animal cells.

5.2 Effects of DNA bioreceptor secondary structure on hybridization

The secondary structure, or folding, of nucleic acid oligos is fundamental to mechanism of aptamer-based sensing. DNA folding and intramolecular hairpin formation is the source of the molecular surface grooves into which molecular targets may be fit and captured by the aptamer. In Chapter 3, the challenges introduced by ssDNA secondary structure were discussed, and the importance of designing probe and target oligos without such intramolecular interaction was noted. For ssDNA oligos to act as aptamers, intramolecular interaction is essential. Intramolecular base-pairing will stabilize the single strand conformations within oligos anchored to the substrate surface. In order to incorporate DNA aptamers into porous silicon waveguide it is important to understand these structural effects on hybridization and, by extension, small molecule binding, under the incubation conditions utilized in previous experiments.

In order to investigate the effects of hairpin formation, three DNA bioreceptor and target sequence sets are investigated, one with no predicted hairpins (P0) above room temperature, one containing a 3mer hairpin (P3), and one with a 4mer hairpin (P4). Hairpins of 3mer and 4mer simulate the secondary structure of aptamers. Applying the method described in Section 3.1.3, a 16mer PNA aptamer target is designed with no secondary structure under the conditioned employed in sensing experiments. This PNA sequence is 5’-TCC ATC GAT ACC AGA A-3’ and is obtained from Biosynthesis Inc. as a custom oligo without modification. Figure 5.1 shows the selected sequences and illustrates the formation of intramolecular hairpins in selected sequences.

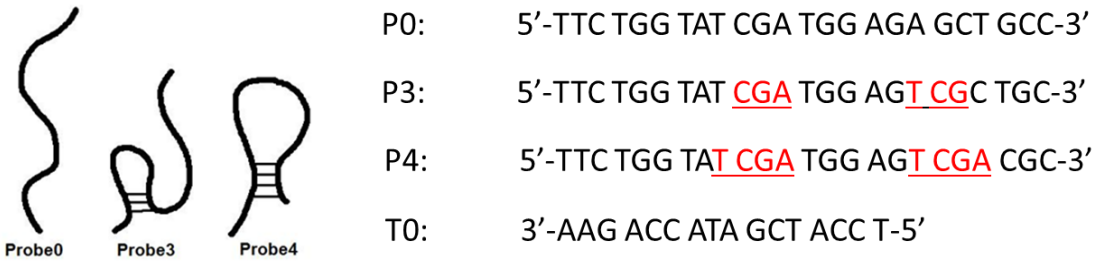

Figure 5.1: A series of 24mer DNA probes are designed to hybridize to a 100% complementary 16mer PNA sequence. The P0 probe contains no secondary structure and can be approximated as a random coil. The P3 sequence contains a 3 base pair hairpin with melting temperature 42.4°C. The P4 sequence contains a 4 base pair hairpin with melting temperature 49.7°C. The bases forming hairpins are underlined and in red.

The 24mer DNA sequences are designed to hybridize to the same 16mer PNA target to allow to direct comparison between experiments. At room temperature, both the P3 and P4 probe are expected to have possible hairpin conformations. For these sequences, there may be more than one hairpin conformation possible, but only the lowest energy structures are considered for simplicity. The 3 base pair hairpin in sequence P3 has a melting temperature of 42.4°C, and the 4 base pair hairpin in sequence P4 has a melting temperature of 49.7°C. Above these temperatures, sequences P3 and P4 would be expected to, like P0, behave as random coils.

Porous silicon waveguides were fabricated as described in Section 2.1.1 and functionalized with a mixed silane monolayer as described in Section 4.2.3 with 25% of the silane monomers having hydroxyl termination. The porous silicon waveguides were used as substrates for in situ DNA synthesis of the 24mer DNA sequences described in Figure 5.1. Each of three porous silicon waveguides was functionalized with a different 24mer sequence. The average shift in resonance angle measured after 24mer in situ DNA probe attachment to the waveguides was 0.64° measured by prism coupling. The porous silicon waveguides with in situ 24mer DNA were deprotected in 50:50

ethanol/ethylenediamine solution for 30 minutes and were subsequently used for detection of the 16mer PNA target.

All three in situ synthesized 24mer DNA sequences on porous silicon waveguides were exposed to 5 μM of target 16mer PNA in buffer solution at room temperature for one hour. Following incubation, samples were rinsed with buffer, water, and then dried under nitrogen. For room temperature hybridization, only the P0 functionalized waveguide regularly produced a resolvable shift in resonance angle measured by prism coupling. In contrast, the same incubation experiment on the porous silicon waveguides functionalized with P0, P3, and P4 sequences was performed where the target PNA solution was heated before incubation to 80°C (above the hairpin melting temperatures) and then dropped onto the waveguides at elevated temperature for one hour incubation. After incubation, porous silicon waveguide samples were washed with buffer, water, and then dried under nitrogen.

For the elevated temperature incubation, all three bioreceptors – P0, P3, and P4 – demonstrated PNA target capture, and the resonance shifts associated with each porous silicon waveguide upon binding the target 16mer PNA were similar in magnitude, indicating that the secondary structures did not inhibit target capture when incubation solutions were heated prior to the one hour incubation. Figure 5.2 shows the resonance angle shifts observed for the P0, P3, and P4 bioreceptors after target capture from heated incubation solution. Because it was not performed in real-time, this experiment does not give a full picture of the complex hybridization kinetics for DNA with secondary structure; however, it does provide evidence that incubation conditions may be controlled

to reduce the effect of secondary structure on target capture. This result is consistent with reports from the literature for hybridization on flat surfaces and in solution [143, 249].

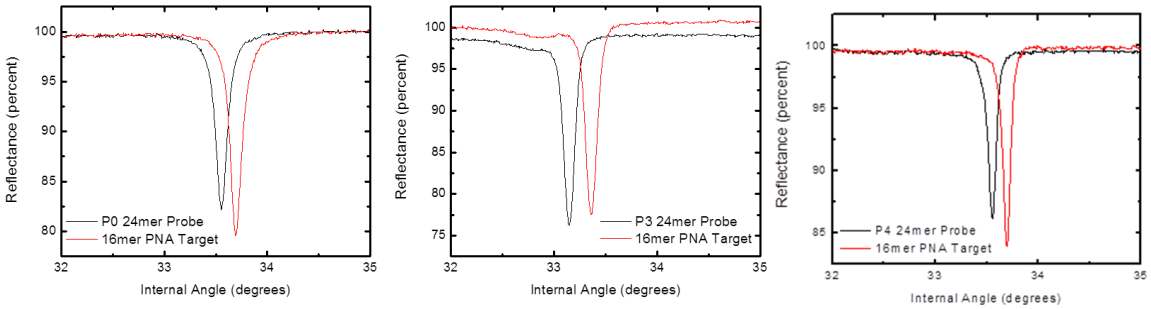

Figure 5.2: Resonance shift upon hybridization to target for porous silicon waveguides with P0, P3, and P4 DNA probes in situ synthesized within the pores. All three sensors demonstrate a shift in resonance, indicating that the designed secondary structure in the P3 and P4 DNA probes does not inhibit target capture for one hour incubation in target when incubation solutions are initially heated above the hairpin melting temperatures.

5.3 Porous silicon waveguide aptasensor for adenosine detection

5.3.1 Adenosine sensors

The nucleotide adenine plays a crucial role in cellular metabolism, active transport, and the mechanical work of myocardial cells. The adenine derivatives of adenosine, adenosine diphosphate (ADP), and adenosine triphosphate (ATP) have important applications in studies of cardiac ischemia. A number of aptamers-based sensing platforms for adenosine detection have been reported in the literature. Many of these examples are electrochemical detectors [219, 250, 251]. Colorimetric detection schemes have also been described [235, 236, 252]. In such systems, the selective aggregation of DNA-functionalized gold nanoparticles occurs in the presence of adenosine. The resulting color change from blue to red could be quantified for adenosine concentrations from 100μM to 1mM [235, 236]. Aptamer-based detectors for adenosine

suffer the same limitations as all small molecule aptasensor – low aptamer to target binding affinity in comparison to large molecule targets. Small changes at the solution-surface interface upon target capture means that signal is weak, and detection limits beyond mM and μM are difficult to achieve in a label-free system.

5.3.2 In situ adenosine aptamer synthesis

Adenosine is a commonly selected small molecule target for aptamer-based biosensors. As such, oligonucleotide sequences reported in the literature have been selected (via SELEX processes) with high binding affinity towards adenosine molecules [189, 219, 235, 236, 253]. These sequences have been used both in solution platforms [235, 236, 254] and surface-anchored platforms [188, 250, 251, 253]. Commonly, adenosine aptamers are utilized in the stationary phase for separation columns for adenosine purification [243, 244, 255]. For a porous silicon waveguides sensor platform, the DNA sequence selected and synthesized as the aptamer for adenosine detection is the same as that studied in other detection platforms.

For all surface functionalization for aptamer sensing, a mixed silane monolayer approach is utilized, as described in Chapter 4. In these experiments, the two component monolayer contains 11-acetoxyundecyltrichlorosilane as the active monomer towards phosphoramidite DNA synthesis, and octyltrichlorosilane remains as the inert alkyltrichlorosilane in the SAM (Figure 5.3). The adjustment in the active component of the monolayer for the aptasensor application compared to the former nucleic acid target sensing experiments was made for ease of synthesis. The synthesis protocol was adapted from [256]. Both monomers utilized for the aptasensing experiments are available from Gelest, and are used as received. Once opened, monomer bottles are regularly degasses

and stored under nitrogen. The silanization procedure for 11-acetoxyundecyltrichlorosilane SAMs is similar to the procedures described in Chapter 4. Porous silicon waveguides are incubated 80 μL of silane monomer in 10 mL dry toluene for 4 hours. Following incubation, samples are rinsed with toluene, then methanol, and dried under nitrogen gas. The resulting SAM will have the same composition as the incubation solution, so ratios of 11-acetoxyundecyltrichlorsilane to octyltrichlorosilane may be controlled by tuning their ratios in the incubation solution. Following silanization, the acetoxy head group is converted to hydroxyl by incubation in 10% sulfuric acid in a solution of 10mL water and 10mL methanol for 30 minutes at 50°C. Functionalized waveguides were annealed at 200°C in air for one hour. This protocol produces a mixed SAM with controlled hydroxyl head group content. For all aptamer work, a 25% hydroxyl SAM composition is utilized, under the assumption that the steric effects described in Chapter 4 would affect aptasensing in the same way that steric effects affect nucleic acid hybridization. Porous surface functionalization is monitored by tracking the change in resonance angle of the waveguide by prism coupling.

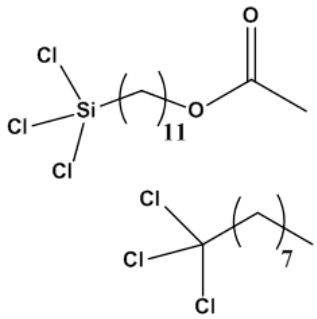

Figure 5.3: Trichlorosilanes shown above are deposited in specified ratios from anhydrous toluene solution. The acetoxy group is removed by soak in 10% acid alcohol solution, converting it to a hydroxyl end group.

After the two component silanization, porous silicon waveguides are used as a substrate for in situ DNA aptamer synthesis. The aptamer sequence 3'-TGG AAG GAG GCG TTA TGA GGG GGT CCA-5' previously described in the literature to capture adenosine is synthesized via the phosphoramidite method. Figure 5.4 shows the progressive shift in resonance angle from the oxidized porous silicon surface to the silanized surface to the aptamer-functionalized surface based on prism coupling measurements. Analysis of the trityl cation cleaved during the synthesis, as described in Section 4.3.2, indicates a high rate of sequence completion, with approximately 75% of the initiated DNA oligo chains reaching completion.

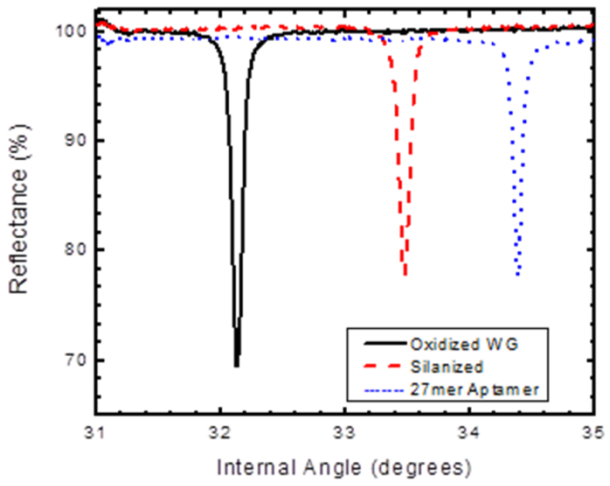

Figure 5.4: Attenuated total reflectance is measured for porous silicon waveguides throughout the functionalization process by prism coupling. As the mixed alkylsilane SAM is attached and the DNA aptamer is synthesized in the pores, the waveguide resonance shifts to higher angle, indicating increasing effective index of the waveguide due to the added species.

As previously observed with DNA-DNA and DNA-PNA sensing, the DNA aptamer sequence must be deprotected before use. Again, a 50:50 ethanol and

ethylenediamine solution is used to deprotect the DNA phosphate backbone. Porous silicon waveguides functionalized with DNA are immersed in the deprotection solution for 30 minutes, then washed thoroughly with ethanol and dried under nitrogen.

5.3.3 Detection of adenosine on porous silicon aptasensor

Buffer solutions play an important role in stabilizing the negatively charged backbone the DNA aptamer, promoting target binding. For all adenosine detection experiments, buffer solution conditions were utilized from a report on buffer optimization for adenosine aptamers [257]. Adenosine, obtained from Fisher Scientific, was dissolved in 20mM Tris acetate buffer containing 150mM NaCl and 5mM $MgCl_2$. Aptamer-functionalized porous silicon waveguides were rinsed sequentially with water and ethanol, then dried under nitrogen prior to all measurements. Prior to incubation, adenosine-containing buffer solutions were heated to 60°C. While at elevated temperature, incubation solution was dropped into the aptamer-functionalized porous silicon surface. Waveguides were the incubated in adenosine-containing buffer solutions for one hour in the refrigerator, allowing the incubation solution to cool to 4°C. The heating step is used to anneal any pre-sensing hairpin formations, ensuring that the ssDNA has the potential to bind to the target. The waveguides are then incubated in buffer solution alone at 4°C for 30 minutes, and finally washed with deionized water. The adenosine capture mechanism by the 27mer DNA aptamer is illustrated in Figure 5.5. Aptamer-based detection of adenosine occurs when an intramolecular hairpin forms in the ssDNA sequence anchored to the porous silicon. The hairpin loop creates a conformational structure that acts as the “lock” to a two adenosine molecule “key”. The presence of adenosine within the hairpin stabilizes the secondary structure of the aptamer.

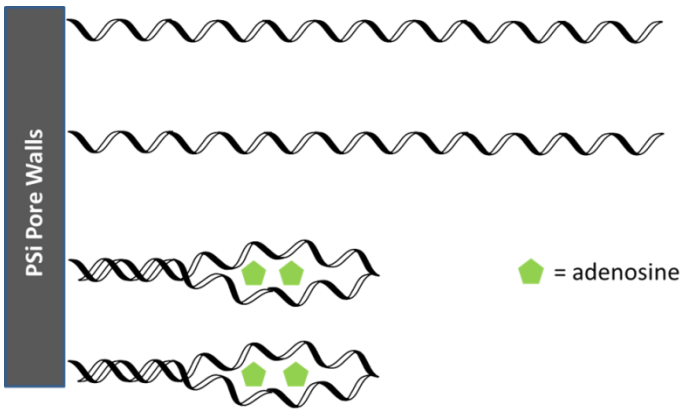

Figure 5.5: Aptamer binding mechanism for adenosine. In the presence of the small molecule, ssDNA binds the target. The addition of adenosine to the porous silicon waveguide pores changes the effective refractive index of the waveguide, which can be monitored by prism coupling.

After incubation in buffer solutions containing adenosine, samples were rinsed, dried, and measured by prism coupling. The change in resonance angle after adenosine exposure was recorded for several spots on the aptamer-functionalized porous silicon waveguide. In Figure 5.6, the change in resonance angle is plotted versus the concentration of adenosine in buffer solution. A resonance shift was observed for concentrations of adenosine as low as 10 μM. This detection sensitivity is comparable to some of the most sensitive aptamer-based adenosine detection platforms previously reported [235, 236, 251]. With the high available surface area for adenosine capture, this sensitivity is achieved without the incorporation of labels or signal amplifiers. Aptamer functionalized porous silicon waveguides may also be denatured and reused for further sensing experiments. Heating waveguides above 50°C in buffer solution for one hour was sufficient to remove any captured adenosine from the surface and return the resonance angle peak back towards the initial position prior to sensing.

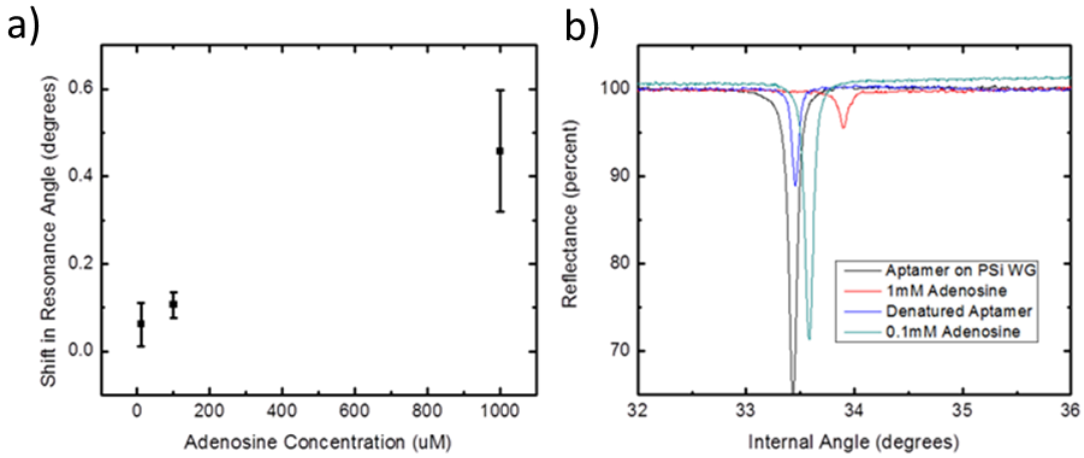

Figure 5.6: (a) Measured shift in resonance angle upon exposure of aptamer-functionalized porous silicon waveguides to different concentrations of adenosine target. The smallest concentration of adenosine in buffer that produced a resolvable shift is 10μM. (b) The aptamer functionalized waveguides may be denatured and re-used for multiple exposures to target molecules.

In an alternative detection mechanism, a nucleic acid hybridized to the aptamer can be displaced, producing a blue shift in the reflectance spectrum, as schematically illustrated in Figure 5.7 [250, 258, 259]. For this experiment, the same porous silicon waveguide and aptamer functionalization was used, but prior to adenosine exposure, samples were incubated in 25μM of a complementary nucleic acid sequence at 4°C in HEPES buffer. The sequence 3'-CCC AGG TTC TCT-5' is capable of hybridizing to a portion of the in situ synthesized adenosine aptamer [250]. The resonance angle in the reflectance spectrum was monitored via prism coupling. After duplex formation, the functionalized porous silicon waveguides was incubated in 100μM adenosine in buffer solution as described above. As shown in Figure 5.5, the result was a blue shift in the reflectance spectrum as the 12mer nucleic acid sequence was displaced by the smaller adenosine molecule. This competitive displacement provides an interesting alternative detection scheme and the opportunity to amplify signal from small molecule capture by

utilizing longer nucleic acid complements, as the displacement of larger nucleic acid complements would produce a greater change in the effective refractive index and thus an even larger change in resonance angle [67].

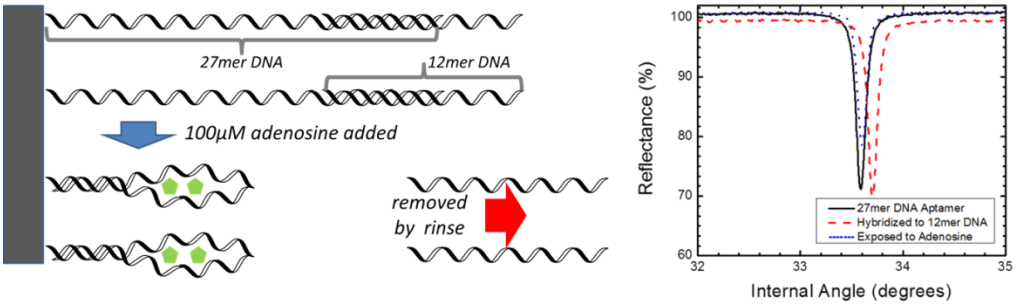

Figure 5.7: Indirect detection platform for adenosine is constructed using DNA aptamer partially hybridized with complementary 12mer DNA. The concentration of adenosine is monitored via displacement of a 12mer nucleic acid target from the hybridized duplex. Detection limits for this mechanism have been in the 10-50 μM range.

5.3.4 Aptasensor specificity

In order to demonstrate the specific target binding achieved with the adenosine aptamer, the porous silicon waveguide aptasensor was incubated in a saturated target solution of uridine, a commonly used control molecule for adenosine sensors due to its size and structural similarities [236]. As can be seen in Figure 5.8, exposure to uridine did not result in a measurable shift in the resonance angle measured by prism coupling; thus, uridine has not been bound by the aptamer. Additionally, exposure to the buffer solution alone does not produce a shift in resonance angle. As summarized in Figure 5.6, the porous silicon waveguide aptasensor selectively binds to adenosine, and not to uridine or buffer components. After exposure to the negative control uridine, aptamer functionalized porous silicon waveguides were again exposed to adenosine, producing a shift in

resonance angle, and indicating that the aptamer maintains its functionality throughout the control experiments. Captured adenosine may be removed from the aptasensor by denaturing in buffer solution at 50°C in the buffer solution for one hour, and the resonance angle peak moves back in the direction of the initial position prior to adenosine addition.

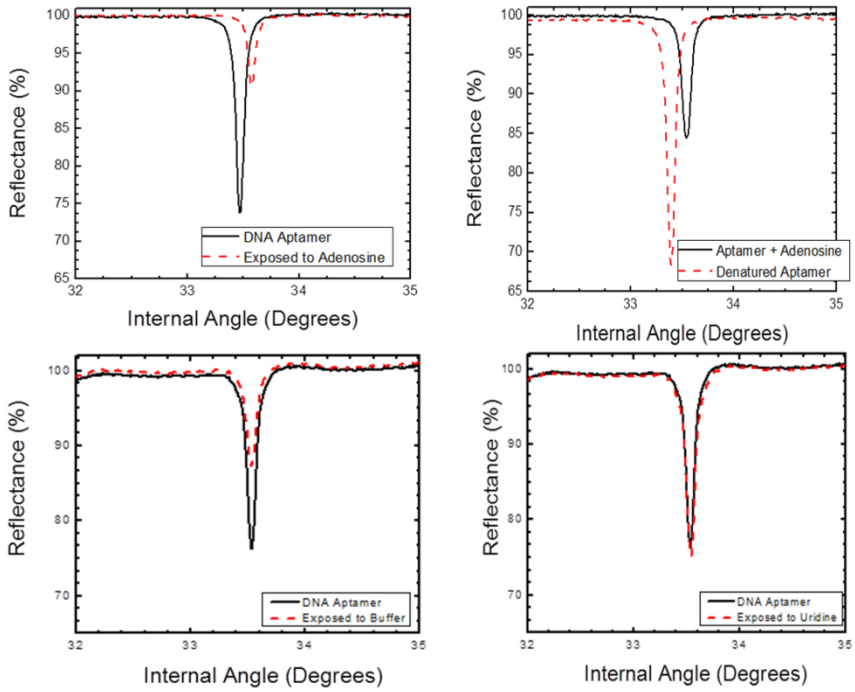

Figure 5.8: With DNA aptamer synthesized within the porous silicon waveguide, shifts in reflectance angle are monitored to detect target binding and denaturing. Representative figures from repeated experiments are shown. (a) Resonance angle shift upon exposure to adenosine in buffer solution demonstrating target capture. (b) Denaturing the bound aptamer/target pair at elevated temperature shifts the resonance to lower angle, returning the reflectance angle position to near the initial position prior to target binding. (c) No shift is observed upon exposure to buffer. (d) No shift is observed upon exposure to the structurally similar uridine, demonstrating the selectivity of the aptamer. All sensing experiments shown were performed on a single aptamer-functionalized porous silicon waveguide.

5.4 Aptamer for ochratoxin detection

After demonstrating selective aptamer-based detection of a small molecule target, which provides a strong indication that aptamers maintain their functionality even while

confined within mesoporous silicon, another small molecule target with a greater clinical significance was explored. In the work that follows, the selected target in Ochratoxin A (OTA), a mycotoxin with molecular weight 403.81 grams per mole, produced most commonly by Aspergillus ochraceus, Aspergillus carbonarius, and Penicillum verrucosum [260-263]. As discussed previously, mesoporous silicon optical structures with aptamer functionalization can only be used for detecting small molecules due to the infiltration challenges faced by large molecules. The longer aptamer sequences are synthesized base-by-base in situ, achieving bioreceptor functionality within the pores while circumventing the infiltration challenges. The target, in this case OTA, must be infiltrated unmodified as a whole species, so selection of a small target (or adjusting the pore size accordingly) is critical to achieving efficient target infiltration [110].

The toxin can be found as a contaminant in improperly stored food commodities, including grains, coffee, wine, and beans. Because of its high degree of cytotoxicity, maximum permissible levels of OTA in food commodities are set frequently in the μg/kg range. Because of the high toxicity, it is important to avoid the risks associated with OTA consumption, and developing analytical tools for the detection and quantification of OTA in raw materials is of considerable importance. Additionally, much of the morbidity and mortality associated with OTA consumption occurs in the developing world. For this reason, there is a need for highly specific and sensitive OTA detectors that are durable and long-lasting, and do not require sophisticated equipment or highly trained personnel. For selective detection of small molecule toxins, the label-free porous silicon waveguide platform may be particularly advantageous. Details of common detection schemes for OTA and their respective sensitivities will be addressed in Section 5.3.2.

5.4.1 Mycotoxin overview

Mycotoxins are a broad class of low-molecular weight secondary metabolites produced by a number of fungi species present in feed stock. The term encompasses metabolites with wide variations in structure and biological effects, but all can cause disease and death in humans. A number of excellent reviews [264-266] have been published on the topic of mycotoxins, their production, and their biological effects. The presence of the initial fungus contamination in feed depends upon environmental moisture, storage temperature and time, geographic location, and the presences of rodents and other pests. Poor storage conditions of raw foodstuffs can result in an overgrowth of fungus and contamination with produced mycotoxins. Due to their high toxicity, good control of these contaminants is desired by international regulatory agencies.

The symptoms produced by mycotoxins depend on the type of toxin, the duration of exposure, age and health of the exposed person, and a number of other factors. Vitamin deficiencies can result in more severe mycotoxicity, and exposure to mycotoxins may also leave the affected individual more susceptible to opportunistic infections and disease. Disease causes by mycotoxins is much more common in the developing world than in developed countries. Exposure occurs by eating contaminated foods. There are almost no treatments currently available for mycotoxicity, so reducing the possibility of exposure is critical in reducing the burden of the disease.

In this work, the focus will be on Ochratoxin A. This toxin has been found as a contaminant in barley, oats, rye, wheat, coffee beans, and some wines. This toxin primarily acts on the kidneys, and can result in significant nephrotoxic effects with chronic exposure [263, 267]. Humans have been shown to have a long half-life for

elimination of OTA from the body [268]. It has been suspected in severe kidney diseases such as Balkan endemic nephropathy (BEN), a progressive and untreatable deterioration of kidney function observed in rural regions of Bulgaria, Yugoslavia, and Romania. At its peak, the average mortality rate from BEN in Bulgaria was reported to be 10.6 per 1000 [269].

Structurally, the OTA molecule is composed of a para-chlorophenolic ring attached to a dihydoiso-coumarin group on one side and amide-linked to an L-phenylalanine group on the other (Figure 5.9). It is believed that OTA uptake within the body occurs primarily through plasma proteins such as albumin, which has a strong binding affinity to OTA in the non-ionized form [270, 271]. In the bloodstream, approximately 99% of OTA present is bound to serum proteins. Some of the additional small proteins that show an affinity for OTA are quite small, and can easily pass through the glomerular membrane of the kidney, perhaps explaining the nephrotoxicity of the molecule [272]. One major mechanism by which OTA damages the kidneys is by DNA adduct formation. When chemical carcinogens such as OTA covalently bond to the organism's DNA, there is an increased likelihood of mutations, thus an increased frequency of cancers [273-275].

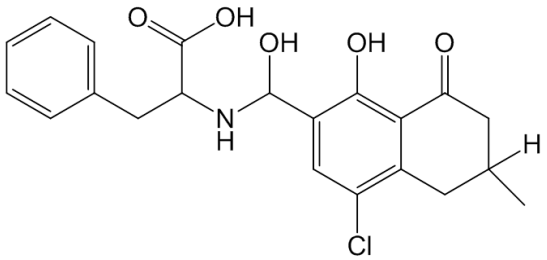

Figure 5.9: Chemical structure of Ochratoxin A (OTA).

5.4.2 Ochratoxin A detection

Over the past few decades, a number of analytical methods for OTA detection have been developed [276]. The most commonly used methods utilize fluorescent labels, specifically high-performance liquid chromatography fluorescence [277-279] and thin-layer chromatography fluorescence [277, 280, 281]. Some labeled detection schemes have reported limit of detection in ng/kg [282], but more commonly the detection limits are reported in the 1-10 μg/kg range [283]. As discussed in Chapter 1, the complex labeling techniques make such measurement schemes difficult to apply outside of the laboratory where rapid detection of small molecule toxins may be most critical. Hence, for OTA detection in developing countries, the additional sample preparation becomes a significant barrier to widespread implementation. Immunoassays have become an increasingly popular alternative [284-286], but antibody procurement, preparation, and storage remains time consuming and expensive as well. Perhaps some of the most promising developments in OTA sensing have been the surface plasmon resonance (SPR) immunosensors for OTA contamination is foodstuffs, where mycotoxins including OTA have been detected in the μg/kg concentration range [287] using the mycotoxin-specific antibodies immobilized by the Biacore system.

5.4.3 In situ synthesis of OTA aptamer

For preparation of an aptamer-based sensor for adenosine, a mixed silane surface with 25% hydroxyl-terminal groups (as described for hybridization optimization in Chapter 4) is used for in situ synthesis of an ochratoxin A aptamer. The procedure for silanization is the same as described in Section 5.2.2. The resulting mixed two-

component silane monolayer is converted to partial hydroxyl functionality by immersion in 10% sulfuric acid in methanol and water solution at 50°C for 30 minutes.

Once hydroxyl termination is achieved on the silanized porous silicon waveguides, the samples may be used as substrates for in situ DNA synthesis. The sequence selected as the DNA aptamer has been well-described in the literature for selective detection of OTA [217, 234, 237, 244, 288-290]. The DNA sequence 5'-GAT CGG GTG TGG GTG GCG TAA AGG GAG CAT CGG ACA-3' is synthesized on the porous silicon waveguide via the phosphoramidite method. The DNA aptamer is deprotected and prepared for target capture by a 30 minute soak in 50:50 ethanol and ethylenediamine solution. Figure 5.10 shows the evolution of the resonance peak position throughout the aptamer-functionalization procedure.

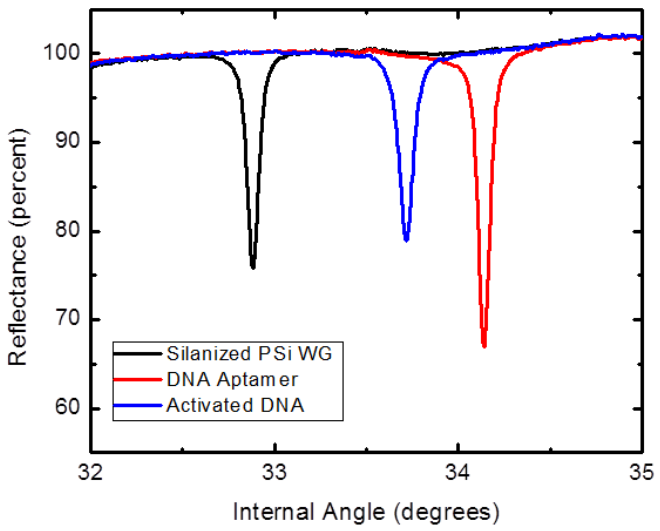

Figure 5.10: As DNA aptamer for OTA is attached to the porous silicon waveguide, resonance angle measured by prism coupling increases. Upon deprotection, there is a shift to lower resonance angle as some material is lost in this step. After deprotection, the in situ synthesized DNA aptamer is active towards target capture.

5.4.4 OTA detection

Ochratoxin A, 99% purity, was obtained from Arcos Organics. A stock solution of ochratoxin was prepared by diluting with 1x phosphate buffered saline (PBS). The PBS buffer stock solution is prepared from standard buffer tablets obtained from Fisher Scientific. The buffer composition is 137mmol/L sodium chloride, 2.7 mmol/L potassium chloride, 10mmol/L disodium hydrogen phosphate, 2 mmol/L potassium dihydrogen phosphate in water at pH 7.4. Due to the high level of toxicity, it was important to eliminate potential contact with ochratoxin dust. The solution was stored under nitrogen and all equipment that came into contact with the solution was stored separately from general laboratory glassware, and sterilized with a bleach solution after use.

Aptamer-functionalized porous silicon waveguides were exposed to 1μM solutions of OTA in PBS buffer. Incubation experiments were completed in sealed petri dishes and all solution transfers and washing steps were contained within the chemical fume hood. Prior to incubation, OTA-containing buffer solution was heated gently above 60°C, and then introduced onto the porous silicon waveguide. After 1 hour incubation, porous silicon waveguides were washed sequentially with buffer, water, and ethanol, and then dried under nitrogen. Changes in the effective optical thickness were monitored by prism coupling at each step in the sample preparation. Figure 5.11 illustrates a typical shift in the resonance peak on a functionalized porous silicon waveguide following exposure to OTA target solution for one hour. Incubation and rinsing are performed with solutions at 4°C to promote formation of the intramolecular hairpin responsible for OTA capture.

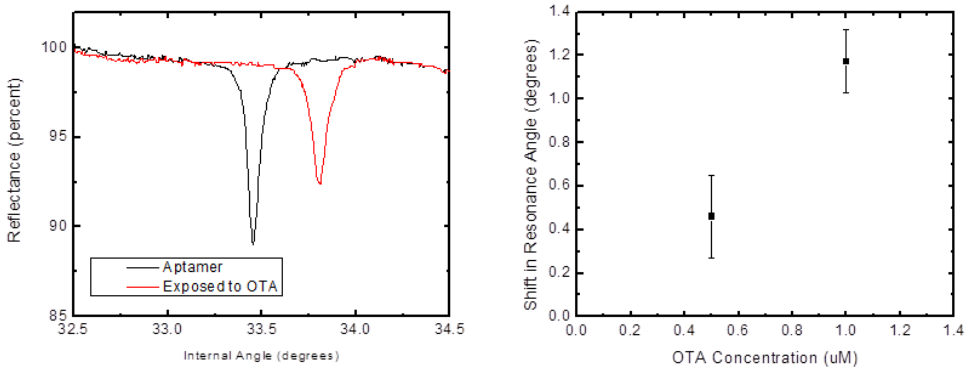

Figure 5.11: At left, the shift in resonance angle upon exposure to 1μM Ochratoxin A in PBS buffer is shown. At right, the concentration dependence of the OTA resonance shift is demonstrated for two different target concentrations in PBS buffer solution.

Following exposure to 1μM OTA in buffer solution, an average shift in resonance angle of 1.1725°±0.1446° is observed for several aptamer to target exposures. Samples may be denatured by heating above 50°C for one hour in buffer solution and reused for additional sensing experiments. Given the resolution of the Metricon prism coupler, detection limits at or below 100nM are likely possible for OTA in this aptamer-based sensing configuration. Compared with international thresholds for allowable OTA in foodstuffs, the predicted detection limit is below the cut-off for many food categories (liquorice extract and spices) though does not reach the EU cut-off for raw cereals, which is approximately an order of magnitude lower. It is, however, well above the levels previously shown to have sub-acute and chronic toxicities [267]. For this reason, optical detection of ochratoxin a within porous silicon waveguides has the potential to be used as a rapid and inexpensive screening tool to prevent OTA contaminated foodstuffs from entering the food supply in low-resources areas. This is achieved before sensor optimization, and without the inclusion of signal amplification or labels. For label-free detection of OTA, the detection sensitivity afforded by changes in the reflectance

spectrum of aptamer-functionalized porous silicon waveguides rivals many of the previously reported detection schemes, many of which involve more complex chemical work-up or measurements [217, 234, 237, 288-290].

Chapter 6

6. CONCLUSIONS AND FUTURE WORK

6.1 Conclusions and research contributions

Highly sensitive and selective detection of nucleic acids and small molecules has been demonstrated by applying in situ synthesis of DNA oligos to porous silicon optical structures. Step-wise synthesis of DNA oligonucleotides [89] and hybridization to in situ synthesized DNA bioreceptors was demonstrated for the first time in porous silicon waveguides [104, 110] by measuring an angular shift in resonance. The large surface area available for biomolecule attachment in porous waveguides and strong field confinement in the region where biomolecules are immobilized make high sensitivity label-free DNA detection possible. The high surface coverage achieved by in situ synthesis requires that surface density of DNA bioreceptors be tuned in order to limit steric crowding and improve detection sensitivities [110]. Improved sensitivity to ~25nM of 16mer oligo targets was demonstrated by controlling DNA bioreceptor density through mixed silane monolayer functionalization. Additionally, a first demonstration of DNA aptamer-based detection in porous silicon waveguides was reported. Aptamers synthesized in situ retained their functionality within mesoporous optical structures, and selective and sensitive detection of the small molecules adenosine and ochratoxin A was demonstrated.

6.2 Future research opportunities

6.2.1 Kinetic and thermodynamic studies of DNA bioreceptors in flow cells

With the recent development of an all-porous silicon grating and waveguide [291], it is now possible to incorporate a flow cell onto a porous silicon waveguide biosensor while allowing for coupling of light in to the porous silicon waveguide for

biosensing. In such an experimental setup, real time sensing of biomolecule target capture may be monitored without sacrificing any of the sensitivity advantages obtained through the porous silicon waveguide scheme. Previous work from the Weiss group has demonstrated the feasibility of attaching a flow cell to an all porous silicon grating coupled waveguide. Initial work with this system monitored the kinetics of silanization, DNA bioreceptor infiltration, and hybridization to complementary PNA targets.

This work incorporating the porous silicon waveguide with a flow cell opens up the possibility for exciting studies of fundamental kinetic and thermodynamic properties of target binding by surface-anchored aptamers. Although there are many studies of the effects of secondary structure of nucleic acid sequences on solution phase hybridization kinetics[143], there have been only a few studies completed for surface-bound nucleic acids [144, 249]. As previously noted, there are no other studies looking at optimal DNA bioreceptor density in porous silicon, and similarly, no studies of DNA hybridization or aptamer-based binding kinetics or thermodynamics in porous silicon optical structures.

The analysis of the kinetics and thermodynamics of aptamer-based detection in porous silicon is of considerable importance. Understanding of binding properties is essential to the expansion of the technology beyond the laboratory and into point-of-care and diagnostic applications. When DNA-based biosensors incorporate structured probes, the secondary structure effects may significantly impact target capture efficiency and reaction time. For the further development of aptamer-based porous silicon biosensors, quantitative characterization of the effects of intramolecular interactions in the nucleic acid aptamer on hybridization under physiologic (or other biosensor-relevant) environment is crucial.

6.2.2 Corrosion-enhanced aptasensing in porous silicon

Many aptamer-based small molecule detection platforms utilize signal enhancement to overcome the challenges presented by lower affinity of nucleic acid aptamers to small molecule targets. Attaching fluorescent labels to the nucleic acid aptamers is a common method of enhancing target binding signal [292-294]. Other signal enhancement strategies involve reporter molecule displacement [250, 254, 259], improved binding avidity through bifunctional aptamer attachment [295], and biocatalytic strategies such as redox cycling [296-298]. In order to compete with the sensitivity achieve in labeled sensing platforms, signal enhancement strategies will almost certainly need to be incorporated into developing label-free optical aptasensors.

In porous silicon, the oxidative corrosion mechanism referenced in Chapter 2 has been used for signal enhancement [40, 41] for detection of DNA hybridization, as the negatively charged sugar-phosphate backbone of the DNA induces corrosion at the porous silicon surface. This corrosion mechanism – and thus the sensitivity to target binding – can be enhanced by incorporating a catalytic, electron transferring label, such as certain transition metal complexes [42]. The rate of oxidative corrosion has been shown to be strongly dependent upon the distance between the transition metal complex and the porous silicon surface. For this reason, a catalytic label may be attached to a selected in situ synthesized aptamer on porous silicon optical structures. Upon target binding, the resulting conformational change in the nucleic acid sequence may significantly enhance oxidative corrosion as the label in pulled in close proximity to the pore walls as target binding occurs. Similar mechanisms relying on changes in label to substrate distance changing upon aptamer binding have been described in the literature

[188, 234, 299]. Oxidative enhancement of aptamer-based sensing would limit reusability of porous silicon aptamer-functionalized biosensors, but, based on oxidative corrosion studies with DNA hybridization, could potentially allow for colorimetric detection in dilute solutions of small molecule targets by aptamer binding.

6.2.3 In situ synthesis of nucleic acids in porous silicon for drug delivery

Although the dissolution of porous silicon substrates in aqueous media presented challenges in biosensing that needed to be addressed by altering the silanization process, in applications such as drug delivery, the degradation of porous silicon to silicic acid is advantageous [300]. Porous silicon is a biocompatible material and under physiologic conditions will degrade to nontoxic polyatomic ions [301] that can be readily cleared from the body by the kidneys. Coupled with the high surface to area ratio achieved in nano- and meso- porous silicon, the material has the potential to be an exceptional drug delivery platform. There have been a number of examples of porous silicon nanoparticles used for drug delivery [87, 167, 302-305].

Recently, nucleic acid therapeutics has gained attention, as the understanding of RNA in biological processing and control has increased. Complementary, small interfering (siRNA) have been designed to exert control and regulate expression of certain genes of respiratory viruses [306, 307]. This approach of interfering with gene expression as a method of antiviral therapy is an exciting new approach in human therapeutics. Recently, a double-blind placebo controlled clinical trial was completed, demonstrating that siRNA delivered to the lungs had a therapeutic effect in limiting the replication of respiratory syncytial virus [308]. In vitro and in vivo work has shown siRNAs with antiviral effects on influenza, coronaviruses, measles, and parainfluenza as

well [309-315]. Peptide nucleic acids have also been shown to have these therapeutic effects [316-319].

One of the major challenges in nucleic acid therapeutics has been achieving a high loading of the oligos into the drug delivery agent, and selectively depositing it in to the target region [307]. In situ synthesis may be an excellent option for preparing porous silicon particles for drug delivery applications, as a considerably higher loading of oligos can be achieved than by infiltration of pre-synthesized molecules of comparable length. Additionally, pore diameters in such drug delivery systems could be tuned to small enough diameters to control release time of the therapeutic agents without interfering with loading efficiency [320]. As was demonstrated previously, pore diameter does not inhibit step by step synthesis of nucleic acid oligos in porous silicon substrates. In situ synthesis in nano- and meso- porous silicon particles could be an effective new approach in nucleic acid therapeutics.

6.3 Prospects of biosensor research in porous silicon

Biosensor research is a rapidly growing field with the potential to reach a broad range of applications including medical diagnostics, environmental monitoring, food safety and quality control. Porous silicon is an especially promising material for biosensing applications because of the ease and control with which porous silicon nanostructures can be fabricated, with precise control of the optical and morphological characteristics. Other advantages of the material are the small sizes necessary for sensing, CMOS compatibility, and potential for mass fabrication. Over the past decade a number of proof of principle studies have been published, applying porous silicon as a substrate for biomolecule detection. Advances in biochemistry will allow the researcher to better

understand the kinetics and thermodynamics of receptor to target binding and improve upon the surface chemistries utilized in porous silicon biosensing devices. Advances in nucleic acid-based porous silicon biosensors has allowed for better control of surface chemistry, and as a result improved detection sensitivity. Small molecule targets have been expanded beyond complementary nucleic acids to biologically relevant compounds and toxins. Combined with coming advances in the design and fabrication of porous silicon photonic structures and integration into flow cell and microarray systems, there is considerable promise in porous silicon biosensors. This practical and convenient material will continue to see growth in biosensing applications.

Appendix A: In Situ DNA Synthesis Procedure

For use with flow cell on ABI model 392 DNA/RNA synthesizer.

Step	Description	Function Number	Time (seconds)
1	Begin	106	
2	18 to Waste	64	7
3	18 to Column	42	120
4	Reverse Flush	2	96
5	Block Flush	1	8
6	Phos Prep	101	6
7	Col 1 On	140	
8	Block Vent	111	4
9	Tet to Waste	58	3.4
10	B+Tet to Column	33	4
11	Wait	103	240
12	Block Flush	1	6
13	Tet to Column	34	2
14	Wait	103	240
15	B+Tet to Column	33	4
16	Wait	103	240
17	Push to Column	43	
18	Column 1 Off	141	
-------	--------	--------	--------
29	Wait	103	75

30	Cap Prep	102	6
31	18 to Waste	64	8
32	Reverse Flush	2	60
33	Block Flush	1	60
34	Cap to Column	39	20
35	Wait	103	240
36	18 to Waste	64	8
37	Reverse Flush	2	60
38	Block Flush	1	6
39	15 to Column	41	16
40	Wait	103	240
41	18 to Waste	64	8
42	Block Flush	1	6
43	Wait	103	15
44	18 to Column	42	120
45	Flush to Waste	4	8
46	18 to Column	42	120
47	Reverse Flush	2	60
48	Block Flush	1	6
49	Start Detrityl	105	
50	18 to Waste	64	8
51	18 to Column	42	120
52	Reverse Flush	2	60
53	Block Flush	1	6

54	Trityl Advance	112	
55	Waste - Port	109	
56	Advance FC	120	
57	Advance FC	120	
58	Advance FC	120	
59	Advance FC	120	
60	End Advance	113	
61	14 to Column	40	12
62	Wait	103	240
63	Trityl Flush	3	60
64	14 to Column	40	12
65	Wait	103	240
66	Trityl Flush	3	60
67	14 to Column	40	12
68	Wait	103	240
69	Trityl Flush	3	60
70	14 to Column	40	12
71	Wait	103	240
72	Trityl Flush	3	60
73	18 to Column	42	120
74	Trityl Flush	3	96
75	Waste – Bottle	110	
76	18 to Column	42	120
77	Reverse Flush	2	60

78	Block Flush	1	8
79	End	107	

APPENDIX B: POROSITY, ETCH CURRENT, AND EFFECTIVE REFRACTIVE INDEX OF POROUS SILICON

Within the Weiss Group, calibration curves for the porous silicon electrochemical etch process have been developed to correlate etch current and porosity. Similarly, calibration curves were developed relating porosity and Bruggeman Effective Refractive Index (ERI). This analysis was completed by Dr. Guoguang Rong and additional details can be found in his thesis entitled, "Label-free Nanoscale Biosensing Using a Porous Silicon Waveguide". Graphs are included here only as a tool for estimating the resulting porosity and ERI for waveguides fabricated for this research.

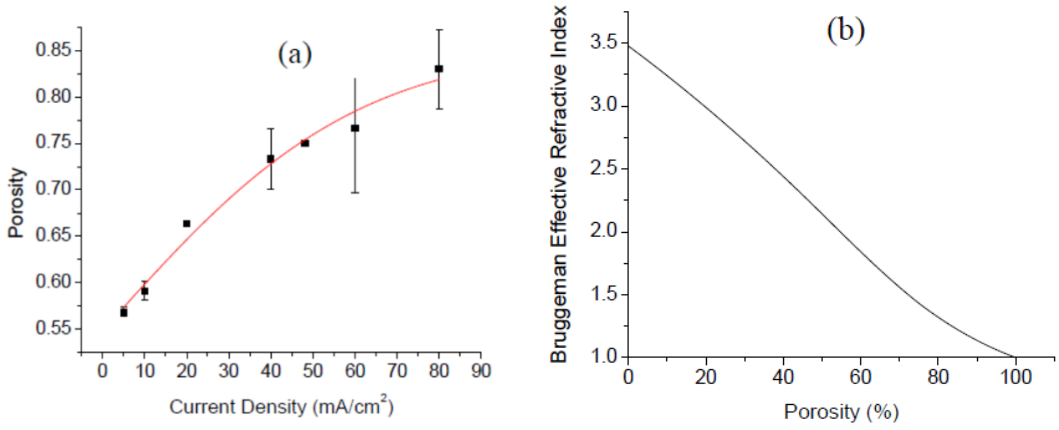

(a) Porous silicon porosity that results from the application of different current densities during electrochemical etching. (b) Bruggeman effective refractive index at different porous silicon porosities, assuming a wavelength of 1550 nm.

REFERENCES

[1] K. Cammann, U. Lemke, A. Rohen, J. Sander, H. Wilken, and B. Winter, "Chemical Sensors and Biosensors - Principles and Applications," *Angewandte Chemie-International Edition in English,* vol. 30, pp. 516-539, May 1991.

[2] D. Grieshaber, R. MacKenzie, J. Voros, and E. Reimhult, "Electrochemical biosensors - Sensor principles and architectures," *Sensors,* vol. 8, pp. 1400-1458, Mar 2008.

[3] N. V. Lavrik, M. J. Sepaniak, and P. G. Datskos, "Cantilever transducers as a platform for chemical and biological sensors," *Review of Scientific Instruments,* vol. 75, pp. 2229-2253, Jul 2004.

[4] N. J. Ronkainen, H. B. Halsall, and W. R. Heineman, "Electrochemical biosensors," *Chemical Society Reviews,* vol. 39, pp. 1747-1763, 2010.

[5] A. Jane, R. Dronov, A. Hodges, and N. H. Voelcker, "Porous silicon biosensors on the advance," *Trends in Biotechnology,* vol. 27, pp. 230-239, 2009.

[6] R. Ince and R. Narayanaswamy, "Analysis of the performance of interferometry, surface plasmon resonance and luminescence as biosensors and chemosensors," *Analytica Chimica Acta,* vol. 569, pp. 1-20, 2006.

[7] S. M. Weiss, G. Rong, and J. L. Lawrie, "Current status and outlook for silicon-based optical biosensors," *Physica E-Low-Dimensional Systems & Nanostructures,* vol. 41, pp. 1071-1075, 2009.

[8] Z. Rosenzweig and R. Kopelman, "Analytical properties and sensor size effects of a micrometer-sized optical fiber glucose biosensor," *Analytical Chemistry,* vol. 68, pp. 1408-1413, Apr 1996.

[9] S. L. R. Barker, R. Kopelman, T. E. Meyer, and M. A. Cusanovich, "Fiber-optic nitric oxide-selective biosensors and nanosensors," *Analytical Chemistry,* vol. 70, pp. 971-976, Mar 1998.

[10] M. Boncheva, C. Duschl, W. Beck, G. Jung, and H. Vogel, "Formation and characterization of lipopeptide layers at interfaces for the molecular recognition of antibodies," *Langmuir,* vol. 12, pp. 5636-5642, Nov 1996.

[11] M. M. F. Choi, "Progress in Enzyme-Based Biosensors Using Optical Transducers," *Microchimica Acta,* vol. 148, pp. 107-132, 2004.

[12] K. Aslan, J. R. Lakowicz, and C. D. Geddes, "Tunable plasmonic glucose sensing based on the dissociation of Con A-aggregated dextran-coated gold colloids," *Analytica Chimica Acta,* vol. 517, pp. 139-144, Jul 26 2004.

[13] I. Klimant, P. Belser, and O. S. Wolfbeis, "Novel Metal-organic Ruthenium(II) Diimine Complexes for Use as Longwave Excitable Luminescent Oxygen Probes," *Talanta,* vol. 41, pp. 985-991, Jun 1994.
[14] C. Preininger, I. Klimant, and O. S. Wolfbeis, "Optical-fiber Sensor for Biological Oxygen-demand," *Analytical Chemistry,* vol. 66, pp. 1841-1846, Jun 1 1994.
[15] H. Y. Aboul-Enein, R. I. Stefan, and J. F. van Staden, "Chemiluminescence-based (bio) sensors - An overview," *Critical Reviews in Analytical Chemistry,* vol. 29, pp. 323-331, 1999.
[16] D. B. Papkovsky, A. N. Ovchinnikov, V. I. Ogurtsov, G. V. Ponomarev, and T. Korpela, "Biosensors on the basis of luminescent oxygen sensor: the use of microporous light-scattering support materials," *Sensors and Actuators B-Chemical,* vol. 51, pp. 137-145, Aug 1998.
[17] C. Sumner, A. Sabot, K. Turner, and S. Krause, "A transducer based on enzyme-induced degradation of thin polymer films monitored by surface plasmon resonance," *Analytical Chemistry,* vol. 72, pp. 5225-5232, Nov 1 2000.
[18] S. Cagnin, M. Caraballo, C. Guiducci, P. Martini, M. Ross, M. SantaAna, D. Danley, T. West, and G. Lanfranchi, "Overview of Electrochemical DNA Biosensors: New Approaches to Detect the Expression of Life," *Sensors,* vol. 9, pp. 3122-3148, Apr 2009.
[19] J. Wang, "Electrochemical nucleic acid biosensors," *Analytica Chimica Acta,* vol. 469, pp. 63-71, Sep 2002.
[20] J. Wang, "Electrochemical biosensors: Towards point-of-care cancer diagnostics," *Biosensors & Bioelectronics,* vol. 21, pp. 1887-1892, Apr 15 2006.
[21] J. J. Gooding, "Electrochemical DNA hyhridization biosensors," *Electroanalysis,* vol. 14, pp. 1149-1156, Sep 2002.
[22] E. Wilkins and P. Atanasov, "Glucose monitoring: State of the art and future possibilities," *Medical Engineering & Physics,* vol. 18, pp. 273-288, Jun 1996.
[23] M. Mascini, I. Palchetti, and G. Marrazza, "DNA electrochemical biosensors," *Fresenius' Journal of Analytical Chemistry,* vol. 369, pp. 15-22, 2001.
[24] Z. H. Shen, M. C. Huang, C. D. Xiao, Y. Zhang, X. Q. Zeng, and P. G. Wang, "Nonlabeled quartz crystal microbalance biosensor for bacterial detection using carbohydrate and lectin recognitions," *Analytical Chemistry,* vol. 79, pp. 2312-2319, Mar 2007.
[25] I. Willner, F. Patolsky, Y. Weizmann, and B. Willner, "Amplified detection of single-base mismatches in DNA using micro gravimetric quartz-crystal-microbalance transduction," *Talanta,* vol. 56, pp. 847-856, Apr 2002.

[26] A. Janshoff, H.-J. Galla, and C. Steinem, "Piezoelectric Mass-Sensing Devices as Biosensors—An Alternative to Optical Biosensors?," *Angewandte Chemie International Edition,* vol. 39, pp. 4004-4032, 2000.
[27] R. Raiteri, M. Grattarola, H.-J. Butt, and P. Skládal, "Micromechanical cantilever-based biosensors," *Sensors and Actuators B: Chemical,* vol. 79, pp. 115-126, 2001.
[28] K. K. Jensen, H. Orum, P. E. Nielsen, and B. Norden, "Kinetics for hybridization of peptide nucleic acids (PNA) with DNA and RNA studied with the BIAcore technique," *Biochemistry,* vol. 36, pp. 5072-5077, Apr 1997.
[29] Y. Abdiche, D. Malashock, A. Pinkerton, and J. Pons, "Determining kinetics and affinities of protein interactions using a parallel real-time label-free biosensor, the Octet," *Analytical Biochemistry,* vol. 377, pp. 209-217, Jun 2008.
[30] K. Elovsson, Z. C. Pei, and T. Aastrup, "Cell-Based Biosensors: A Quartz Crystal Microbalance Approach to Membrane Protein Interaction Studies," *American Laboratory,* vol. 43, pp. 26-+, Jun-Jul 2011.
[31] J. Sterling, "Roche all set to launch XCELLigence system," *Genetic Engineering & Biotechnology News,* vol. 28, pp. 34-35, Apr 2008.
[32] A. Uhlir, "Electrolytic Shaping of Germanium and Silicon," *Bell System Technical Journal,* vol. 35, pp. 333-347, 1956.
[33] L. T. Canham, "Silicon Quantum Wire Array Fabrication by Electrochemical and Chemical Dissolution of Wafers," *Applied Physics Letters,* vol. 57, pp. 1046-1048, 1990.
[34] W. Theiss, "Optical properties of porous silicon," *Surface Science Reports,* vol. 29, pp. 95-192, 1997.
[35] M. J. Sailor and E. C. Wu, "Photoluminescence-Based Sensing With Porous Silicon Films, Microparticles, and Nanoparticles," *Advanced Functional Materials,* vol. 19, pp. 3195-3208, Oct 2009.
[36] N. F. Starodub, L. L. Fedorenko, V. M. Starodub, S. P. Dikij, and S. V. Svechnikov, "Use of the silicon crystals photoluminescence to control immunocomplex formation," *Sensors and Actuators B-Chemical,* vol. 35, pp. 44-47, Sep 1996.
[37] G. Di Francia, V. La Ferrara, S. Manzo, and S. Chiavarini, "Towards a label-free optical porous silicon DNA sensor," *Biosensors & Bioelectronics,* vol. 21, pp. 661-665, 2005.
[38] S. Chan, S. R. Horner, P. M. Fauchet, and B. L. Miller, "Identification of gram negative bacteria using nanoscale silicon microcavities," *Journal of the American Chemical Society,* vol. 123, pp. 11797-11798, Nov 2001.
[39] S. Chan, P. M. Fauchet, Y. Li, L. J. Rothberg, and B. L. Miller, "Porous silicon microcavities for biosensing applications," *Physica Status Solidi a-Applied Research,* vol. 182, pp. 541-546, Nov 2000.

[40] V. S. Y. Lin, K. Motesharei, K. P. S. Dancil, M. J. Sailor, and M. R. Ghadiri, "A porous silicon-based optical interferometric biosensor," *Science,* vol. 278, pp. 840-843, Oct 1997.
[41] C. Steinem, A. Janshoff, V. S. Y. Lin, N. H. Volcker, and M. R. Ghadiri, "DNA hybridization-enhanced porous silicon corrosion: mechanistic investigators and prospect for optical interferometric biosensing," *Tetrahedron,* vol. 60, pp. 11259-11267, Nov 29 2004.
[42] N. H. Voelcker, I. Alfonso, and M. R. Ghadiri, "Catalyzed oxidative corrosion of porous silicon used as an optical transducer for ligand-receptor interactions," *Chembiochem,* vol. 9, pp. 1776-1786, 2008.
[43] A. Janshoff, K. P. S. Dancil, C. Steinem, D. P. Greiner, V. S. Y. Lin, C. Gurtner, K. Motesharei, M. J. Sailor, and M. R. Ghadiri, "Macroporous p-type silicon Fabry-Perot layers. Fabrication, characterization, and applications in biosensing," *Journal of the American Chemical Society,* vol. 120, pp. 12108-12116, Nov 1998.
[44] K. P. S. Dancil, D. P. Greiner, and M. J. Sailor, "A porous silicon optical biosensor: Detection of reversible binding of IgG to a protein A-modified surface," *Journal of the American Chemical Society,* vol. 121, pp. 7925-7930, Sep 1999.
[45] L. De Stefano, L. Rotiroti, I. Rendina, L. Moretti, V. Scognamiglio, M. Rossi, and S. D'Auria, "Porous silicon-based optical microsensor for the detection of L-glutamine," *Biosensors & Bioelectronics,* vol. 21, pp. 1664-1667, Feb 2006.
[46] A. Tinsley-Bown, R. G. Smith, S. Hayward, M. H. Anderson, L. Koker, A. Green, R. Torrens, A. S. Wilkinson, E. A. Perkins, D. J. Squirrell, S. Nicklin, A. Hutchinson, A. J. Simons, and T. I. Cox, "Immunoassays in a porous silicon interferometric biosensor combined with sensitive signal processing," *Physica Status Solidi a-Applications and Materials Science,* vol. 202, pp. 1347-1356, 2005.
[47] C. Pacholski, M. Sartor, M. J. Sailor, F. Cunin, and G. M. Miskelly, "Biosensing using porous silicon double-layer interferometers: Reflective interferometric Fourier transform spectroscopy," *Journal of the American Chemical Society,* vol. 127, pp. 11636-11645, Aug 2005.
[48] L. Moretti, I. Rea, L. De Stefano, and I. Rendina, "Periodic versus aperiodic: Enhancing the sensitivity of porous silicon based optical sensors," *Applied Physics Letters,* vol. 90, 2007.
[49] M. A. Anderson, A. Tinsley-Bown, P. Allcock, E. A. Perkins, P. Snow, M. Hollings, R. G. Smith, C. Reeves, D. J. Squirrell, S. Nicklin, and T. I. Cox, "Sensitivity of the optical properties of porous silicon layers to the refractive index of liquid in the pores," *Physica Status Solidi a-Applied Research,* vol. 197, pp. 528-533, 2003.

[50] P. J. Reece, M. Gal, H. H. Tan, and C. Jagadish, "Optical properties of erbium-implanted porous silicon microcavities," *Applied Physics Letters,* vol. 85, pp. 3363-3365, 2004.
[51] G. Lerodel, P. Reece, A. Bruyant, and M. Gal, "Strong light confinement in microporous photonic silicon structures," in *Materials Research Society Symposium*, 2004, pp. W1.7.1-W1.7.6.
[52] L. A. DeLouise, P. M. Kou, and B. L. Miller, "Cross-correlation of optical microcavity biosensor response with immobilized enzyme activity. Insights into biosensor sensitivity," *Analytical Chemistry,* vol. 77, pp. 3222-3230, May 2005.
[53] H. Ouyang, M. Christophersen, R. Viard, B. L. Miller, and P. M. Fauchet, "Macroporous silicon microcavities for macromolecule detection," *Advanced Functional Materials,* vol. 15, pp. 1851-1859, Nov 2005.
[54] H. Ouyang, L. A. DeLouise, B. L. Miller, and P. M. Fauchet, "Label-free quantitative detection of protein using macroporous silicon photonic bandgap biosensors," *Analytical Chemistry,* vol. 79, pp. 1502-1506, Feb 2007.
[55] L. M. Bonanno and L. A. DeLouise, "Whole blood optical biosensor," *Biosensors & Bioelectronics,* vol. 23, pp. 444-448, Oct 2007.
[56] M. J. Sailor and J. R. Link, ""Smart dust'': nanostructured devices in a grain of sand," *Chemical Communications,* pp. 1375-1383, 2005.
[57] M. M. Orosco, C. Pacholski, G. M. Miskelly, and M. J. Sailor, "Protein-coated porous-silicon photonic crystals for amplified optical detection of protease activity," *Advanced Materials,* vol. 18, pp. 1393-+, Jun 2006.
[58] L. Z. Gao, N. Mbonu, L. L. Cao, and D. Gao, "Label-free colorimetric detection of Gelatinases on nanoporous silicon photonic films," *Analytical Chemistry,* vol. 80, pp. 1468-1473, Mar 2008.
[59] K. A. Kilian, T. Bocking, K. Gaus, J. King-Lacroix, M. Gal, and J. J. Gooding, "Hybrid lipid bilayers in nanostructured silicon: a biomimetic mesoporous scaffold for optical detection of cholera toxin," *Chemical Communications,* pp. 1936-1938, 2007.
[60] J. J. Saarinen, S. M. Weiss, P. M. Fauchet, and J. E. Sipe, "Optical sensor based on resonant porous silicon structures," *Optics Express,* vol. 13, pp. 3754-3764, May 2005.
[61] H. F. Arrand, T. M. Benson, A. Loni, R. Arens-Fischer, M. Kruger, M. Thonissen, H. Luth, and S. Kershaw, "Novel liquid sensor based on porous silicon optical waveguides," *IEEE Photonics Technology Letters,* vol. 10, pp. 1467-1469, Oct 1998.
[62] G. G. Rong, J. D. Ryckman, R. L. Mernaugh, and S. M. Weiss, "Label-free porous silicon membrane waveguide for DNA sensing," *Applied Physics Letters,* vol. 93, p. 3, Oct 2008.

[63] Y. Jiao and S. M. Weiss, "Design parameters and sensitivity analysis of polymer-cladded porous silicon waveguides for small molecule detection," *Biosensors & Bioelectronics,* vol. 25, pp. 1535-1538, 2010.
[64] X. Wei, C. Kang, M. Liscidini, G. Rong, S. T. Retterer, M. Patrini, J. E. Sipe, and S. M. Weiss, "Grating couplers on porous silicon planar waveguides for sensing applications," *Journal of Applied Physics,* vol. 104, Dec 15 2008.
[65] G. Rong, A. Najmaie, J. E. Sipe, and S. M. Weiss, "Nanoscale porous silicon waveguide for label-free DNA sensing," *Biosensors & Bioelectronics,* vol. 23, pp. 1572-1576, 2008.
[66] G. Rong and S. M. Weiss, "Biomolecule size-dependent sensitivity of porous silicon sensors," *Physica Status Solidi a-Applications and Materials Science,* vol. 206, pp. 1365-1368, Jun 2009.
[67] G. Rong and S. M. Weiss, "Influence of biomolecule size on performance of nanostructured sensing devices," in *Proceedings of SPIE*, 2007, p. 647717.
[68] V. Lehmann, *Electrochemistry of silicon: instrumentation, science, materials and applications*. Weinheim, Germany: Wiley-VCH, 2002.
[69] V. Lehmann and U. Gosele, "Porous Silicon Formation - A Quantum Wire Effect," *Applied Physics Letters,* vol. 58, pp. 856-858, Feb 25 1991.
[70] M. I. J. Beale, N. G. Chew, M. J. Uren, A. G. Cullis, and J. D. Benjamin, "Microstructure and Formation Mechanism of Porous Silicon," *Applied Physics Letters,* vol. 46, pp. 86-88, 1985 1985.
[71] R. L. Smith and S. D. Collins, "Porous Silicon Formation Mechanisms," *Journal of Applied Physics,* vol. 71, pp. R1-R22, Apr 15 1992.
[72] T. Unagami, "Formation Mechanism of Porous Silicon Layer by Anodization in HF Solution," *Journal of the Electrochemical Society,* vol. 127, pp. 476-483, 1980 1980.
[73] X. G. Zhang, "Morphology and formation mechanisms of porous silicon," *Journal of the Electrochemical Society,* vol. 151, pp. C69-C80, Jan 2004.
[74] L. T. Canham, "Bioactive silicon structure fabrication through nanoetching techniques," *Advanced Materials,* vol. 7, pp. 1033-&, Dec 1995.
[75] T. Bocking, K. A. Kilian, K. Gaus, and J. J. Gooding, "Modifying Porous Silicon with Self-Assembled Monolayers for Biomedical Applications: The Influence of Surface Coverage on Stability and Biomolecule Coupling," *Advanced Functional Materials,* vol. 18, pp. 3827-3833, 2008.
[76] J. M. Buriak, "Organometallic chemistry on silicon and germanium surfaces," *Chemical Reviews,* vol. 102, pp. 1271-1308, 2002.

[77] K. A. Kilian, T. Boecking, and J. J. Gooding, "The importance of surface chemistry in mesoporous materials: lessons from porous silicon biosensors," *Chemical Communications,* pp. 630-640, 2009.
[78] W. Wang and M. W. Vaughn, "Morphology and amine accessibility of (3-aminopropyl) triethoxysilane films on glass surfaces," *Scanning,* vol. 30, pp. 65-77, Mar-Apr 2008.
[79] S. Sharma and T. A. Desai, "Nanostructured antifouling poly(ethylene glycol) films for silicon-based microsystems," *Journal of Nanoscience and Nanotechnology,* vol. 5, pp. 235-243, Feb 2005.
[80] M. P. Stewart and J. M. Buriak, "Photopatterned hydrosilylation on porous silicon," *Angewandte Chemie-International Edition,* vol. 37, pp. 3257-3260, 1998.
[81] J. H. Song and M. J. Sailor, "Functionalization of nanocrystalline porous silicon surfaces with aryllithium reagents: Formation of silicon-carbon bonds by cleavage of silicon-silicon bonds," *Journal of the American Chemical Society,* vol. 120, pp. 2376-2381, Mar 1998.
[82] N. Y. Kim and P. E. Laibinis, "Derivatization of porous silicon by Grignard reagents at room temperature," *Journal of the American Chemical Society,* vol. 120, pp. 4516-4517, May 1998.
[83] J. E. Bateman, R. D. Eagling, D. R. Worrall, B. R. Horrocks, and A. Houlton, "Alkylation of porous silicon by direct reaction with alkenes and alkynes," *Angewandte Chemie-International Edition,* vol. 37, pp. 2683-2685, 1998.
[84] M. P. Stewart, E. G. Robins, T. W. Geders, M. J. Allen, H. C. Choi, and J. M. Buriak, "Three methods for stabilization and functionalization of porous silicon surfaces via hydrosilylation and electrografting reactions," *Physica Status Solidi a-Applied Research,* vol. 182, pp. 109-115, Nov 2000.
[85] J. Salonen, E. Laine, and L. Niinisto, "Thermal carbonization of porous silicon surface by acetylene," *Journal of Applied Physics,* vol. 91, pp. 456-461, Jan 2002.
[86] V. Torres-Costa, R. J. Martin-Palma, J. M. Martinez-Duart, J. Salonen, and V. P. Lehto, "Effective passivation of porous silicon optical devices by thermal carbonization," *Journal of Applied Physics,* vol. 103, p. 4, Apr 2008.
[87] J. Salonen, L. Laitinen, A. M. Kaukonen, J. Tuura, M. Bjorkqvist, T. Heikkila, K. Vaha-Heikkila, J. Hirvonen, and V. P. Lehto, "Mesoporous silicon microparticles for oral drug delivery: Loading and release of five model drugs," *Journal of Controlled Release,* vol. 108, pp. 362-374, Nov 2005.
[88] B. Sciacca, S. D. Alvarez, F. Geobaldo, and M. J. Sailor, "Bioconjugate functionalization of thermally carbonized porous silicon using a radical

coupling reaction," *Dalton Transactions,* vol. 39, pp. 10847-10853, 2010 2010.
[89] J. L. Lawrie, Z. Xu, G. G. Rong, P. E. Laibinis, and S. M. Weiss, "Synthesis of DNA oligonucleotides in mesoporous silicon," *Physica Status Solidi a-Applications and Materials Science,* vol. 206, pp. 1339-1342, Jun 2009.
[90] B. Y. Chow, D. W. Mosley, and J. M. Jacobson, "Perfecting imperfect "monolayers": Removal of siloxane multilayers by CO2 snow treatment," *Langmuir,* vol. 21, pp. 4782-4785, 2005.
[91] J. A. Howarter and J. P. Youngblood, "Optimization of silica silanization by 3-aminopropyltriethoxysilane," *Langmuir,* vol. 22, pp. 11142-11147, 2006.
[92] J. L. Lawrie and S. M. Weiss, "Stabilization of hydroxyl-terminated silane in porous silicon for in-situ DNA synthesis," *Physica Status Solidi c,* vol. 8, pp. 1851-1855, 2011.
[93] S. Chen, M. F. Phillips, F. Cerrina, and L. M. Smith, "Controlling Oligonucleotide Surface Density in Light-Directed DNA Array Fabrication," *Langmuir,* vol. 25, pp. 6570-6575, Jun 2009.
[94] M. F. Phillips, M. R. Lockett, M. J. Rodesch, M. R. Shortreed, F. Cerrina, and L. M. Smith, "In situ oligonucleotide synthesis on carbon materials: stable substrates for microarray fabrication," *Nucleic Acids Research,* vol. 36, p. 9, Jan 2008.
[95] R. M. Pasternack, S. R. Amy, and Y. J. Chabal, "Attachment of 3-(Aminopropyl)triethoxysilane on Silicon Oxide Surfaces: Dependence on Solution Temperature," *Langmuir,* vol. 24, pp. 12963-12971, Nov 2008.
[96] N. Tillman, A. Ulman, and T. L. Penner, "Formation of Multilayers by Self-assembly," *Langmuir,* vol. 5, pp. 101-111, Jan-Feb 1989.
[97] E. T. Vandenberg, L. Bertilsson, B. Liedberg, K. Uvdal, R. Erlandsson, H. Elwing, and I. Lundstrom, "Structure of 3-Aminopropyl Triethoxy Silane on Silicon-Oxide," *Journal of Colloid and Interface Science,* vol. 147, pp. 103-118, Nov 1991.
[98] L. H. Lie, S. N. Patole, A. R. Pike, L. C. Ryder, B. A. Connolly, A. D. Ward, E. M. Tuite, A. Houlton, and B. R. Horrocks, "Immobilization and synthesis of DNA on Si(111), nanocrystalline porous silicon and silicon nanoparticles," *Faraday Discussions,* vol. 125, pp. 235-251, 2004.
[99] F. Bessueille, V. Dugas, V. Vikulov, J. P. Cloarec, E. Souteyrand, and J. R. Martin, "Assessment of porous silicon substrate for well-characterized sensitive DNA chip implement," *Biosensors and Bioelectronics,* vol. 21, pp. 908-916, 2005.
[100] S. McInnes, S. Graney, Y.-L. Khung, and N. H. Voelcker, "Porous silicon microparticles as an alternative support for solid phase DNA synthesis," *Proceedings of SPIE,* vol. 6036, pp. 445-454, 2006.

[101] D. Rekesh, Y. Lyubchenko, L. S. Shlyakhtenko, and S. M. Lindsay, "Scanning tunneling microscopy of mercapto-hexyl-oligonucleotides attached to gold," *Biophysical Journal,* vol. 71, pp. 1079-1086, 1996.
[102] Y. Hayakawa, S. Wakabayashi, H. Kato, and R. Noyori, "The Allylic Protection Method in Solid-phase Oligonucleotide Synthesis - An Efficient Preparation of Solid-anchored DNA Oligomers," *Journal of the American Chemical Society,* vol. 112, pp. 1691-1696, 1990.
[103] I. Rea, G. Oliviero, J. Amato, N. Borbone, G. Piccialli, I. Rendina, and L. De Stefano, "Direct Synthesis of Oligonucleotides on Nanostructured Silica Multilayers," *Journal of Physical Chemistry C,* vol. 114, pp. 2617-2621, Feb 2010.
[104] J. L. Lawrie, Z. Xu, P. E. Laibinis, M. Molinari, and S. M. Weiss, "DNA Oligonucleotide Synthesis in Mesoporous Silicon for Biosensing Applications," *Proceedings of SPIE,* vol. 7176, p. 71670R, 2009.
[105] M. J. Moorcroft, W. R. A. Meuleman, S. G. Latham, T. J. Nicholls, R. D. Egeland, and E. M. Southern, "In situ oligonucleotide synthesis on poly(dimethylsiloxane): a flexible substrate for microarray fabrication," *Nucleic Acids Research,* vol. 33, 2005.
[106] D. C. Tessier, S. Boughaba, M. Arbour, P. Roos, and G. Pan, "Improved surface sensing of DNA on gas-etched porous silicon," *Sensors and Actuators B-Chemical,* vol. 120, pp. 220-230, 2006.
[107] S. Chan, Y. Li, L. J. Rothberg, B. L. Miller, and P. M. Fauchet, "Nanoscale silicon microcavities for biosensing," *Materials Science & Engineering C-Biomimetic and Supramolecular Systems,* vol. 15, pp. 277-282, 2001.
[108] S. E. Letant, B. R. Hart, A. W. Van Buuren, and L. J. Terminello, "Functionalized silicon membranes for selective bio-organism capture," *Nature Materials,* vol. 2, pp. 391-396, 2003.
[109] A. Samoc, A. Miniewicz, M. Samoc, and J. G. Grote, "Refractive-index anisotropy and optical dispersion in films of deoxyribonucleic acid," *Journal of Applied Polymer Science,* vol. 105, pp. 236-245, 2007.
[110] J. L. Lawrie, Y. Jiao, and S. M. Weiss, "Size-Dependent Infiltration and Optical Detection of Nucleic Acids in Nanoscale Pores," *IEEE Transactions on Nanotechnology,* vol. 9, pp. 596-602, Sep 2010.
[111] R. K. Saiki, D. H. Gelfand, S. Stoffel, S. J. Scharf, R. Higuchi, G. T. Horn, K. B. Mullis, and H. A. Erlich, "Primer-directed Enzymatic Amplification of DNA with a Thermostable DNA-Polymerase," *Science,* vol. 239, pp. 487-491, Jan 1988.
[112] J. G. Wetmur and N. Davidson, "Kinetics of Renaturation of DNA," *Journal of Molecular Biology,* vol. 31, pp. 349-&, 1968.
[113] L. E. Morrison and L. M. Stols, "Sensitive Fluorescence-based Thermodynamic and Kinetic Measurements of DNA Hybridization in Solution," *Biochemistry,* vol. 32, pp. 3095-3104, Mar 1993.

[114] Y. Okahata, M. Kawase, K. Niikura, F. Ohtake, H. Furusawa, and Y. Ebara, "Kinetic measurements of DNA hybridisation an an oligonucleotide-immobilized 27-MHz quartz crystal microbalance," *Analytical Chemistry,* vol. 70, pp. 1288-1296, Apr 1998.
[115] J. Xu and S. L. Craig, "Thermodynamics of DNA hybridization on gold nanoparticles," *Journal of the American Chemical Society,* vol. 127, pp. 13227-13231, Sep 2005.
[116] O. Gotoh and Y. Tagashira, "Stabilities of Nearest-neighbor Doublets in Double-helical DNA Determined by Fitting Calculated Melting Profiles to Observed Profiles," *Biopolymers,* vol. 20, pp. 1033-1042, 1981.
[117] H. T. Allawi and J. SantaLucia, "Thermodynamics and NMR of internal GT mismatches in DNA," *Biochemistry,* vol. 36, pp. 10581-10594, Aug 1997.
[118] R. Owczarzy, Y. You, B. G. Moreira, J. A. Manthey, L. Y. Huang, M. A. Behlke, and J. A. Walder, "Effects of sodium ions on DNA duplex oligomers: Improved predictions of melting temperatures," *Biochemistry,* vol. 43, pp. 3537-3554, Mar 2004.
[119] P. A. Wright and D. Wynfordthomas, "The Polymerase Chain-reaction - Miracle or Mirage - A Critical Rreview of its Uses and Limitations is Diagnosis and Research," *Journal of Pathology,* vol. 162, pp. 99-117, Oct 1990.
[120] A. K. Bej, M. H. Mahbubani, and R. M. Atlas, "Amplification of Nucleic-acids by Polymerase Chain-Reaction (PCR) and Other Methods and Their Applications," *Critical Reviews in Biochemistry and Molecular Biology,* vol. 26, pp. 301-334, 1991.
[121] T. G. Drummond, M. G. Hill, and J. K. Barton, "Electrochemical DNA sensors," *Nature Biotechnology,* vol. 21, pp. 1192-1199, Oct 2003.
[122] A. J. Thiel, A. G. Frutos, C. E. Jordan, R. M. Corn, and L. M. Smith, "In situ surface plasmon resonance imaging detection of DNA hybridization to oligonucleotide arrays on gold surfaces," *Analytical Chemistry,* vol. 69, pp. 4948-4956, Dec 1997.
[123] E. Palecek, M. Fojta, M. Tomschik, and J. Wang, "Electrochemical biosensors for DNA hybridization and DNA damage," *Biosensors & Bioelectronics,* vol. 13, pp. 621-628, Sep 1998.
[124] J. Wang, P. E. Nielsen, M. Jiang, X. H. Cai, J. R. Fernandes, D. H. Grant, M. Ozsoz, A. Beglieter, and M. Mowat, "Mismatch sensitive hybridization detection by peptide nucleic acids immobilized on a quartz crystal microbalance," *Analytical Chemistry,* vol. 69, pp. 5200-5202, Dec 1997.
[125] I. Rea, A. Lamberti, I. Rendina, G. Coppola, M. Gioffre, M. Iodice, M. Casalino, E. De Tommasi, and L. De Stefano, "Fabrication and characterization of a porous silicon based microarray for label-free

optical monitoring of biomolecular interactions," *Journal of Applied Physics,* vol. 107, Jan 1 2010.
[126] I. Rea, E. Orabona, A. Lamberti, I. Rendina, and L. De Stefano, "A microfluidics assisted porous silicon array for optical label-free biochemical sensing," *Biomicrofluidics,* vol. 5, Sep 2011.
[127] L. De Stefano, P. Arcari, A. Lamberti, C. Sanges, L. Rotiroti, I. Rea, and I. Rendina, "DNA optical detection based on porous silicon technology: from biosensors to biochips," *Sensors,* vol. 7, pp. 214-221, Feb 2007.
[128] V. Vamvakaki and N. A. Chaniotakis, "DNA stabilization and hybridization detection on porous silicon surface by EIS and total reflection FT-IR spectroscopy," *Electroanalysis,* vol. 20, pp. 1845-1850, Sep 2008.
[129] J. D. Feng, W. J. Zhao, B. Su, and J. M. Wu, "A label-free optical sensor based on nanoporous gold arrays for the detection of oligodeoxynucleotides," *Biosensors & Bioelectronics,* vol. 30, pp. 21-27, Dec 2011.
[130] M. Archer, M. Christophersen, and P. M. Fauchet, "Macroporous silicon electrical sensor for DNA hybridization detection," *Biomedical Microdevices,* vol. 6, pp. 203-211, Sep 2004.
[131] J. E. Lugo, M. Ocampo, A. G. Kirk, D. V. Plant, and P. M. Fauchet, "Electrochemical sensing of DNA with porous silicon layers," *Journal of New Materials for Electrochemical Systems,* vol. 10, pp. 113-116, Apr 2007.
[132] J. H. Jin, K. Wong, I. Xagoraraki, J. B. Rose, and E. C. Alocilja, "Label free DNA-porous silicon biosensor for the detection of enteric adenoviruses," *Abstracts of the General Meeting of the American Society for Microbiology,* vol. 107, p. 631, 2007 2007.
[133] J.-H. Jin, D. Zhang, E. C. Alocilja, and D. L. Grooms, "Label-free DNA sensor on nanoporous silicon-polypyrrole chip for monitoring Salmonella species," *IEEE Sensors Journal,* vol. 8, pp. 891-895, May-Jun 2008.
[134] F. P. Mathew and E. C. Alocilja, "Porous silicon-based biosensor for pathogen detection," *Biosensors & Bioelectronics,* vol. 20, pp. 1656-1661, Feb 15 2005.
[135] D. Zhang and E. C. Alocilja, "Characterization of nanoporous silicon-based DNA biosensor for the detection of Salmonella Enteritidis," *IEEE Sensors Journal,* vol. 8, pp. 775-780, May-Jun 2008.
[136] Y. Jiao and S. M. Weiss, "Enhanced PNA detection sensitivity based on polymer-cladded porous silicon waveguide," *Proceedings of SPIE,* vol. 7553, p. 75530O, 2010.

[137] X. Wei and S. M. Weiss, "Guided mode biosensor based on grating coupled porous silicon waveguide," *Optics Express,* vol. 19, pp. 11330-11339, Jun 6 2011.
[138] F. Pellestor and P. Paulasova, "The peptide nucleic acids, efficient tools for molecular diagnosis (review)," *International Journal of Molecular Medicine,* vol. 13, pp. 521-525, Apr 2004.
[139] S. Shakeel, S. Karim, and A. Ali, "Peptide nucleic acid (PNA) - a review," *Journal of Chemical Technology and Biotechnology,* vol. 81, pp. 892-899, Jun 2006.
[140] J. Wang, "DNA biosensors based on peptide nucleic acid (PNA) recognition layers. A review," *Biosensors & Bioelectronics,* vol. 13, pp. 757-762, Oct 1 1998.
[141] X. Luo and I. M. Hsing, "Real Time Electrochemical Monitoring of DNA/PNA Dissociation by Melting Curve Analysis," *Electroanalysis,* vol. 21, pp. 1557-1561, Jul 2009.
[142] T. Takiya, Y. Seto, H. Yasuda, T. Suzuki, and K. Kawai, "An empirical approach for thermal stability (Tm) prediction of PNA/DNA duplexes," *Nucleic Acids Symposium Series,* vol. 48, pp. 131-132, November 1, 2004 2004.
[143] C. L. Chen, W. J. Wang, Z. Wang, F. Wei, and X. S. Zhao, "Influence of secondary structure on kinetics and reaction mechanism of DNA hybridization," *Nucleic Acids Research,* vol. 35, pp. 2875-2884, May 2007.
[144] L. K. Wolf, D. E. Fullenkamp, and R. M. Georgiadis, "Quantitative angle-resolved SPR imaging of DNA-DNA and DNA-drug kinetics," *Journal of the American Chemical Society,* vol. 127, pp. 17453-17459, 2005.
[145] P. Guedon, T. Livache, F. Martin, F. Lesbre, A. Roget, G. Bidan, and Y. Levy, "Characterization and optimization of a real-time, parallel, label-free, polypyrrole-based DNA sensor by surface plasmon resonance imaging," *Analytical Chemistry,* vol. 72, pp. 6003-6009, 2000.
[146] D. Piscevic, R. Lawall, M. Veith, M. Liley, Y. Okahata, and W. Knoll, "Oligonucleotide Hybridization Observed by Surface-Plasmon Optical Techniques," *Applied Surface Science,* vol. 90, pp. 425-436, 1995.
[147] L. M. Bonanno and L. A. DeLouise, "Steric crowding effects on target detection in an affinity biosensor," *Langmuir,* vol. 23, pp. 5817-5823, 2007.
[148] A. W. Peterson, R. J. Heaton, and R. M. Georgiadis, "The effect of surface probe density on DNA hybridization," *Nucleic Acids Research,* vol. 29, pp. 5163-5168, Dec 15 2001.
[149] J. E. Lugo, H. A. Lopez, S. Chan, and P. M. Fauchet, "Porous silicon multilayer structures: A photonic band gap analysis," *Journal of Applied Physics,* vol. 91, pp. 4966-4972, Apr 15 2002.

[150] J. H. Watterson, P. A. E. Piunno, C. C. Wust, and U. J. Krull, "Effects of oligonucleotide immobilization density on selectivity of quantitative transduction of hybridization of immobilized DNA," *Langmuir,* vol. 16, pp. 4984-4992, May 30 2000.
[151] P. Gong, G. M. Harbers, and D. W. Grainger, "Multi-technique comparison of immobilized and hybridized oligonucleotide surface density on commercial amine-reactive microarray slides," *Analytical Chemistry,* vol. 78, pp. 2342-2351, Apr 1 2006.
[152] C.-Y. Lee, P. Gong, G. M. Harbers, D. W. Grainger, D. G. Castner, and L. J. Gamble, "Surface coverage and structure of mixed DNA/alkylthiol monolayers on gold: Characterization by XPS, NEXAFS, and fluorescence intensity measurements," *Analytical Chemistry,* vol. 78, pp. 3316-3325, May 15 2006.
[153] K. Y. Wong and B. M. Pettitt, "A study of DNA tethered to surface by an all-atom molecular dynamics simulation," *Theoretical Chemistry Accounts,* vol. 106, pp. 233-235, Jul 2001.
[154] I. Y. Wong and N. A. Melosh, "An Electrostatic Model for DNA Surface Hybridization," *Biophysical Journal,* vol. 98, pp. 2954-2963, Jun 16 2010.
[155] F. Ricci, R. Y. Lai, A. J. Heeger, K. W. Plaxco, and J. J. Sumner, "Effect of molecular crowding on the response of an electrochemical DNA sensor," *Langmuir,* vol. 23, pp. 6827-6834, Jun 5 2007.
[156] R. J. White, N. Phares, A. A. Lubin, Y. Xiao, and K. W. Plaxco, "Optimization of electrochemical aptamer-based sensors via optimization of probe packing density and surface chemistry," *Langmuir,* vol. 24, pp. 10513-10518, Sep 16 2008.
[157] F. Cattaruzza, A. Cricenti, A. Flamini, M. Girasole, G. Longo, T. Prosperi, G. Andreano, L. Cellai, and E. Chirivino, "Controlled loading of oligodeoxyribonucleotide monolayers onto unoxidized crystalline silicon; fluorescence-based determination of the surface coverage and of the hybridization efficiency; parallel imaging of the process by Atomic Force Microscopy," *Nucleic Acids Research,* vol. 34, 2006 2006.
[158] A. W. Peterson, L. K. Wolf, and R. M. Georgiadis, "Hybridization of mismatched or partially matched DNA at surfaces," *Journal of the American Chemical Society,* vol. 124, pp. 14601-14607, Dec 11 2002.
[159] S. D. Keighley, P. Estrela, P. Li, and P. Mighorato, "Optimization of label-free DNA detection with electrochemical impedance spectroscopy using PNA probes," *Biosensors & Bioelectronics,* vol. 24, pp. 906-911, Dec 2008.
[160] A. Vainrub and B. M. Pettitt, "Surface electrostatic effects in oligonucleotide microarrays: Control and optimization of binding thermodynamics," *Biopolymers,* vol. 68, pp. 265-270, Feb 2003.

[161] X. L. Gao, E. Gulari, and X. C. Zhou, "In situ synthesis of oligonucleotide microarrays," *Biopolymers,* vol. 73, pp. 579-596, Apr 5 2004.
[162] A. Hasan, K. P. Stengele, H. Giegrich, P. Cornwell, K. R. Isham, R. A. Sachleben, W. Pfleiderer, and R. S. Foote, "Photolabile protecting groups for nucleosides: Synthesis and photodeprotection rates," *Tetrahedron,* vol. 53, pp. 4247-4264, Mar 24 1997.
[163] A. C. Pease, D. Solas, E. J. Sullivan, M. T. Cronin, C. P. Holmes, and S. P. A. Fodor, "Light-generated Oligonucleotide Arrays for Rapid DNA-Sequence Analysis," *Proceedings of the National Academy of Sciences of the United States of America,* vol. 91, pp. 5022-5026, May 24 1994.
[164] A. B. Steel, R. L. Levicky, T. M. Herne, and M. J. Tarlov, "Immobilization of nucleic acids at solid surfaces: Effect of oligonucleotide length on layer assembly," *Biophysical Journal,* vol. 79, pp. 975-981, Aug 2000.
[165] R. A. Shircliff, I. T. Martin, J. W. Pankow, J. Fennell, P. Stradins, M. L. Ghirardi, S. W. Cowley, and H. M. Branz, "High-Resolution X-ray Photoelectron Spectroscopy of Mixed Silane Monolayers for DNA Attachment," *ACS Applied Materials & Interfaces,* vol. 3, pp. 3285-3292, Sep 2011.
[166] H. Min, H. Yu, M. Son, D. W. Moon, and T. G. Lee, "Quantitative analysis of the surface composition of mixed self-assembled monolayers using ToF-SIMS and FT-IR analyses," *Surface and Interface Analysis,* vol. 43, pp. 397-401, Jan-Feb 2011.
[167] M. J. Sweetman, C. J. Shearer, J. G. Shapter, and N. H. Voelcker, "Dual Silane Surface Functionalization for the Selective Attachment of Human Neuronal Cells to Porous Silicon," *Langmuir,* vol. 27, pp. 9497-9503, Aug 2011.
[168] A. R. Lokanathan, S. Zhang, V. R. Regina, M. A. Cole, R. Ogaki, M. D. Dong, F. Besenbacher, R. L. Meyer, and P. Kingshott, "Mixed poly (ethylene glycol) and oligo (ethylene glycol) layers on gold as nonfouling surfaces created by backfilling," *Biointerphases,* vol. 6, pp. 180-188, Dec 2011.
[169] K. Mathauer and C. W. Frank, "Binary Self-Assembled Monolayers as Prepared by Successive Adsorption of Alkyl Trichlorosilanes," *Langmuir,* vol. 9, pp. 3446-3451, Dec 1993.
[170] X. J. Zhang and V. K. Yadavalli, "Surface immobilization of DNA aptamers for biosensing and protein interaction analysis," *Biosensors & Bioelectronics,* vol. 26, pp. 3142-3147, Mar 2011.
[171] A. Arranz, C. Palacio, D. Garcia-Fresnadillo, G. Orellana, A. Navarro, and E. Munoz, "Influence of surface hydroxylation on 3-aminopropyltriethoxysilane growth mode during chemical functionalization of GaN surfaces: An angle-resolved X-ray photoelectron spectroscopy study," *Langmuir,* vol. 24, pp. 8667-8671, Aug 2008.

[172] J. Y. Kim, P. Seidler, L. S. Wan, and C. Fill, "Formation, structure, and reactivity of amino-terminated organic films on silicon substrates," *Journal of Colloid and Interface Science,* vol. 329, pp. 114-119, Jan 2009.
[173] J. D. Legrange, J. L. Markham, and C. R. Kurkjian, "Effects of Surface Hydration on the Deposition of Silane Monolayers on Silica," *Langmuir,* vol. 9, pp. 1749-1753, Jul 1993.
[174] S. R. Wasserman, Y. T. Tao, and G. M. Whitesides, "Structure and Reactivity of Alkylsiloxane Monolayers Formed by Reaction of Alkyl Trichlorosilanes on Silicon Substrates," *Langmuir,* vol. 5, pp. 1074-1087, Jul-Aug 1989.
[175] K. Mathauer and C. W. Frank, "Naphthalene Chromophore Tethered in the Constrained Environment of a Self-Assembled Monolayer," *Langmuir,* vol. 9, pp. 3002-3008, Nov 1993.
[176] C. Rogero, B. T. Chaffey, E. Mateo-Marti, J. M. Sobrado, B. R. Horrocks, A. Houlton, J. H. Lakey, C. Briones, and J. A. Martin-Gago, "Silicon surface nanostructuring for covalent immobilization of biomolecules," *Journal of Physical Chemistry C,* vol. 112, pp. 9308-9314, Jun 2008.
[177] S. G. Vilt, Z. W. Leng, B. D. Booth, C. McCabe, and G. K. Jennings, "Surface and Frictional Properties of Two-Component Alkylsilane Monolayers and Hydroxyl-Terminated Monolayers on Silicon," *Journal of Physical Chemistry C,* vol. 113, pp. 14972-14977, Aug 2009.
[178] C. K. Lee, A. S. T. Chiang, and C. S. Tsay, "The characterization of porous solids from gas adsorption measurements," *Porous Ceramic Materials,* vol. 115, pp. 21-43, 1996.
[179] K. Sing, "The use of nitrogen adsorption for the characterisation of porous materials," *Colloids and Surfaces a-Physicochemical and Engineering Aspects,* vol. 187, pp. 3-9, Aug 2001.
[180] J. C. Groen, L. A. A. Peffer, and J. Perez-Ramirez, "Pore size determination in modified micro- and mesoporous materials. Pitfalls and limitations in gas adsorption data analysis," *Microporous and Mesoporous Materials,* vol. 60, pp. 1-17, Jun 2003.
[181] B. Coasne, A. Grosman, N. Dupont-Pavlovsky, C. Ortega, and M. Simon, "Adsorption in an ordered and non-interconnected mesoporous material: Single crystal porous silicon," *Physical Chemistry Chemical Physics,* vol. 3, pp. 1196-1200, 2001 2001.
[182] P. Kumar, T. Hofmann, K. Knorr, P. Huber, P. Scheib, and P. Lemmens, "Tuning the pore wall morphology of mesoporous silicon from branchy to smooth, tubular by chemical treatment," *Journal of Applied Physics,* vol. 103, Jan 2008.
[183] F. Bessueille, V. Dugas, V. Vikulov, J. P. Cloarec, E. Souteyrand, and J. R. Martin, "Assessment of porous silicon substrate for well-characterised

sensitive DNA chip implement," *Biosensors & Bioelectronics,* vol. 21, pp. 908-916, Dec 2005.
[184] J. H. Watterson, P. A. E. Piunno, and U. J. Krull, "Towards the optimization of an optical DNA sensor: control of selectivity coefficients and relative surface affinities," *Analytica Chimica Acta,* vol. 457, pp. 29-38, Apr 2002.
[185] T. Mairal, V. C. Ozalp, P. L. Sanchez, M. Mir, I. Katakis, and C. K. O'Sullivan, "Aptamers: molecular tools for analytical applications," *Analytical and Bioanalytical Chemistry,* vol. 390, pp. 989-1007, Feb 2008.
[186] C.-W. Liu, C.-C. Huang, and H.-T. Chang, "Highly Selective DNA-Based Sensor for Lead(II) and Mercury(II) Ions," *Analytical Chemistry,* vol. 81, pp. 2383-2387, Mar 15 2009.
[187] Y. Xiang, A. Tong, and Y. Lu, "Abasic Site-Containing DNAzyme and Aptamer for Label-Free Fluorescent Detection of Pb2+ and Adenosine with High Sensitivity, Selectivity, and Tunable Dynamic Range," *Journal of the American Chemical Society,* vol. 131, pp. 15352-15357, Oct 28 2009.
[188] J. W. Chen, X. P. Liu, K. J. Feng, Y. Liang, J. H. Jiang, G. L. Shen, and R. Q. Yu, "Detection of adenosine using surface-enhanced Raman scattering based on structure-switching signaling aptamer," *Biosensors & Bioelectronics,* vol. 24, pp. 66-71, Sep 2008.
[189] D. E. Huizenga and J. W. Szostak, "A DNA Aptamer That Binds Adenosine and ATP," *Biochemistry,* vol. 34, pp. 656-665, Jan 17 1995.
[190] M. Koizumi and R. R. Breaker, "Molecular recognition of cAMP by an RNA aptamer," *Biochemistry,* vol. 39, pp. 8983-8992, Aug 1 2000.
[191] J.-P. Xu, Z.-G. Song, Y. Fang, J. Mei, L. Jia, A. J. Qin, J. Z. Sun, J. Ji, and B. Z. Tang, "Label-free fluorescence detection of mercury(II) and glutathione based on Hg2+-DNA complexes stimulating aggregation-induced emission of a tetraphenylethene derivative," *Analyst,* vol. 135, pp. 3002-3007, 2010 2010.
[192] S. L. Stead, H. Ashwin, B. Johnston, J. A. Tarbin, M. Sharman, J. Kay, and B. J. Keely, "An RNA-Aptamer-Based Assay for the Detection and Analysis of Malachite Green and Leucomalachite Green Residues in Fish Tissue," *Analytical Chemistry,* vol. 82, pp. 2652-2660, Apr 1 2010.
[193] K. S. Hwang, S.-M. Lee, K. Eom, J. H. Lee, Y.-S. Lee, J. H. Park, D. S. Yoon, and T. S. Kim, "Nanomechanical microcantilever operated in vibration modes with use of RNA aptamer as receptor molecules for label-free detection of HCV helicase," *Biosensors & Bioelectronics,* vol. 23, pp. 459-465, Nov 30 2007.

[194] M. Labib, A. S. Zamay, D. Muharemagic, A. V. Chechik, J. C. Bell, and M. V. Berezoyski, "Aptamer-Based Viability Impedimetric Sensor for Viruses," *Analytical Chemistry,* vol. 84, pp. 1813-1816, Feb 21 2012.
[195] G. Lautner, Z. Balogh, V. Bardoczy, T. Meszaros, and R. E. Gyurcsanyi, "Aptamer-based biochips for label-free detection of plant virus coat proteins by SPR imaging," *Analyst,* vol. 135, pp. 918-926, 2010 2010.
[196] S. Lee, Y. S. Kim, M. Jo, M. Jin, D.-k. Lee, and S. Kim, "Chip-based detection of hepatitis C virus using RNA aptamers that specifically bind to HCV core antigen," *Biochemical and Biophysical Research Communications,* vol. 358, pp. 47-52, Jun 22 2007.
[197] X. Liu, Z. Cheng, H. Fan, S. Ai, and R. Han, "Electrochemical detection of avian influenza virus H5N1 gene sequence using a DNA aptamer immobilized onto a hybrid nanomaterial-modified electrode," *Electrochimica Acta,* vol. 56, pp. 6266-6270, Jul 15 2011.
[198] R. Joshi, H. Janagama, H. P. Dwivedi, T. Kumar, L. A. Jaykus, J. Schefers, and S. Sreevatsan, "Selection, characterization, and application of DNA aptamers for the capture and detection of Salmonella enterica serovars," *Molecular and Cellular Probes,* vol. 23, pp. 20-28, Feb 2009.
[199] G. A. Zelada-Guillen, S. V. Bhosale, J. Riu, and F. X. Rius, "Real-Time Potentiometric Detection of Bacteria in Complex Samples," *Analytical Chemistry,* vol. 82, pp. 9254-9260, Nov 2010.
[200] Y. S. Kim, J. H. Niazi, and M. B. Gu, "Specific detection of oxytetracycline using DNA aptamer-immobilized interdigitated array electrode chip," *Analytica Chimica Acta,* vol. 634, pp. 250-254, Feb 23 2009.
[201] Y. Wu, J.-k. Zhang, T. Fan, M. Li, B.-b. Zhang, K. Sun, and P. Wu, "Fast detection of antibiotics in milk by aptamer biosensor," *Shengwu Jiagong Guocheng,* vol. 8, pp. 48-52, May 2010.
[202] K.-T. Guo, A. Paul, C. Schichor, G. Ziemer, and H. P. Wendel, "Cell-SELEX: Novel perspectives of aptamer-based therapeutics," *International Journal of Molecular Sciences,* vol. 9, pp. 668-678, Apr 2008.
[203] S. M. Shamah, J. M. Healy, and S. T. Cload, "Complex target SELEX," *Accounts of Chemical Research,* vol. 41, pp. 130-138, Jan 2008.
[204] R. Stoltenburg, C. Reinemann, and B. Strehlitz, "SELEX-A (r)evolutionary method to generate high-affinity nucleic acid ligands," *Biomolecular Engineering,* vol. 24, pp. 381-403, Oct 2007.
[205] J. F. Lee, J. R. Hesselberth, L. A. Meyers, and A. D. Ellington, "Aptamer Database," *Nucleic Acids Research,* vol. 32, pp. D95-D100, 2004.
[206] P. Burgstaller, M. Kochoyan, and M. Famulok, "Structural probing and damage selection of citrulline- and arginine-specific RNA aptamers identify base positions required for binding," *Nucleic Acids Research,* vol. 23, pp. 4769-4776, Dec 11 1995.

[207] M. Famulok, "Molecular Recognition of Amino-acids by RNA-Aptamers - An L-Citrulline Binding RNA Motif and its Evolution into an L-Arginine Binder," *Journal of the American Chemical Society,* vol. 116, pp. 1698-1706, Mar 1994.
[208] A. Geiger, P. Burgstaller, H. vonderEltz, A. Roeder, and M. Famulok, "RNA aptamers that bind L-arginine with sub-micromolar dissociation constants and high enantioselectivity," *Nucleic Acids Research,* vol. 24, pp. 1029-1036, Mar 15 1996.
[209] T. Dieckmann, E. Suzuki, G. K. Nakamura, and J. Feigon, "Solution structure of an ATP-binding RNA aptamer reveals a novel fold," *RNA-A Publication of the RNA Society,* vol. 2, pp. 628-640, Jul 1996.
[210] P. L. Sazani, R. Larralde, and J. W. Szostak, "A small aptamer with strong and specific recognition of the triphosphate of ATP," *Journal of the American Chemical Society,* vol. 126, pp. 8370-8371, Jul 14 2004.
[211] X. Zuo, S. Song, J. Zhang, D. Pan, L. Wang, and C. Fan, "A target-responsive electrochemical aptamer switch (TREAS) for reagentless detection of nanomolar ATP," *Journal of the American Chemical Society,* vol. 129, pp. 1042-1043, Feb 7 2007.
[212] C. Mannironi, A. DiNardo, P. Fruscoloni, and G. P. TocchiniValentini, "In vitro selection of dopamine RNA ligands," *Biochemistry,* vol. 36, pp. 9726-9734, Aug 12 1997.
[213] C. Mannironi, C. Scerch, P. Fruscoloni, and G. P. Tocchini-Valentini, "Molecular recognition of amino acids by RNA aptamers: The evolution into an L-tyrosine binder of a dopamine-binding RNA motif," *RNA-A Publication of the RNA Society,* vol. 6, pp. 520-527, Apr 2000.
[214] R. Walsh and M. C. DeRosa, "Retention of function in the DNA homolog of the RNA dopamine aptamer," *Biochemical and Biophysical Research Communications,* vol. 388, pp. 732-735, Oct 30 2009.
[215] Y. Zheng, Y. Wang, and X. Yang, "Aptamer-based colorimetric biosensing of dopamine using unmodified gold nanoparticles," *Sensors and Actuators B-Chemical,* vol. 156, pp. 95-99, Aug 10 2011.
[216] S. Balamurugan, A. Obubuafo, S. A. Soper, and D. A. Spivak, "Surface immobilization methods for aptamer diagnostic applications," *Analytical and Bioanalytical Chemistry,* vol. 390, pp. 1009-1021, Feb 2008.
[217] L. Barthelmebs, A. Hayat, A. W. Limiadi, J.-L. Marty, and T. Noguer, "Electrochemical DNA aptamer-based biosensor for OTA detection, using superparamagnetic nanoparticles," *Sensors and Actuators B-Chemical,* vol. 156, pp. 932-937, Aug 2011.
[218] H. Cai, T. M. H. Lee, and I. M. Hsing, "Label-free protein recognition using an aptamer-based impedance measurement assay," *Sensors and Actuators B-Chemical,* vol. 114, pp. 433-437, Mar 30 2006.

[219] Y. Du, B. Li, H. Wei, Y. Wang, and E. Wang, "Multifunctional label-free electrochemical biosensor based on an integrated aptamer," *Analytical Chemistry,* vol. 80, pp. 5110-5117, Jul 1 2008.
[220] T. Hianik and J. Wang, "Electrochemical Aptasensors - Recent Achievements and Perspectives," *Electroanalysis,* vol. 21, pp. 1223-1235, Jun 2009.
[221] A. E. Radi, J. L. A. Sanchez, E. Baldrich, and C. K. O'Sullivan, "Reagentless, reusable, ultrasensitive electrochemical molecular beacon aptasensor," *Journal of the American Chemical Society,* vol. 128, pp. 117-124, Jan 11 2006.
[222] A. E. Radi, J. L. A. Sanchez, E. Baldrich, and C. K. O'Sullivan, "Reusable impedimetric aptasensor," *Analytical Chemistry,* vol. 77, pp. 6320-6323, Oct 1 2005.
[223] A.-E. Radi and C. K. O'Sullivan, "Aptamer conformational switch as sensitive electrochemical biosensor for potassium ion recognition," *Chemical Communications,* pp. 3432-3434, 2006 2006.
[224] A. Bini, M. Minunni, S. Tombelli, S. Centi, and M. Mascini, "Analytical performances of aptamer-based sensing for thrombin detection," *Analytical Chemistry,* vol. 79, pp. 3016-3019, Apr 1 2007.
[225] S. Tombelli, A. Bini, M. Minunni, and M. Mascini, "Piezoelectric Biosensors for Aptamer-Protein Interaction," in *Methods in Molecular Biology*. vol. 504, A. H. K. E. Rasooly, Ed., ed, 2009, pp. 23-36.
[226] C. A. Savran, S. M. Knudsen, A. D. Ellington, and S. R. Manalis, "Micromechanical detection of proteins using aptamer-based receptor molecules," *Analytical Chemistry,* vol. 76, pp. 3194-3198, Jun 1 2004.
[227] A. Sassolas, L. J. Blum, and B. D. Leca-Bouvier, "Optical detection systems using immobilized aptamers," *Biosensors & Bioelectronics,* vol. 26, pp. 3725-3736, May 15 2011.
[228] S. Tombelli, A. Minunni, E. Luzi, and M. Mascini, "Aptamer-based biosensors for the detection of HIV-1 Tat protein," *Bioelectrochemistry,* vol. 67, pp. 135-141, Oct 2005.
[229] Y. X. Jiang, X. H. Fang, and C. L. Bai, "Signaling aptamer/protein binding by a molecular light switch complex," *Analytical Chemistry,* vol. 76, pp. 5230-5235, Sep 1 2004.
[230] J. Wang, Y. X. Jiang, C. S. Zhou, and X. H. Fang, "Aptamer-based ATP assay using a luminescent light switching complex," *Analytical Chemistry,* vol. 77, pp. 3542-3546, Jun 1 2005.
[231] R. Freeman, X. Liu, and I. Winner, "Chemiluminescent and Chemiluminescence Resonance Energy Transfer (CRET) Detection of DNA, Metal Ions, and Aptamer-Substrate Complexes Using Hemin/G-Quadruplexes and CdSe/ZnS Quantum Dots," *Journal of the American Chemical Society,* vol. 133, pp. 11597-11604, Aug 3 2011.

[232] Y. Li, H. Qi, Y. Peng, Q. Gao, and C. Zhang, "Electrogenerated chemiluminescence aptamer-based method for the determination of thrombin incorporating quenching of tris(2,2 '-bipyridine)ruthenium by ferrocene," *Electrochemistry Communications,* vol. 10, pp. 1322-1325, Sep 2008.
[233] X. Ouyang, R. Yu, J. Jin, J. Li, R. Yang, W. Tan, and J. Yuan, "New Strategy for Label-Free and Time-Resolved Luminescent Assay of Protein: Conjugate Eu3+ Complex and Aptamer-Wrapped Carbon Nanotubes," *Analytical Chemistry,* vol. 83, pp. 782-789, Feb 1 2011.
[234] Z. Wang, N. Duan, X. Hun, and S. Wu, "Electrochemiluminescent aptamer biosensor for the determination of ochratoxin A at a gold-nanoparticles-modified gold electrode using N-(aminobutyl)-N-ethylisoluminol as a luminescent label," *Analytical and Bioanalytical Chemistry,* vol. 398, pp. 2125-2132, Nov 2010.
[235] S.-J. Chen, Y.-F. Huang, C.-C. Huang, K.-H. Lee, Z.-H. Lin, and H.-T. Chang, "Colorimetric determination of urinary adenosine using aptamer-modified gold nanoparticles," *Biosensors & Bioelectronics,* vol. 23, pp. 1749-1753, Jun 15 2008.
[236] J. W. Liu and Y. Lu, "Adenosine-dependent assembly of aptazyme-functionalized gold nanoparticles and its application as a colorimetric biosensor," *Analytical Chemistry,* vol. 76, pp. 1627-1632, Mar 15 2004.
[237] C. Yang, Y. Wang, J.-L. Marty, and X. Yang, "Aptamer-based colorimetric biosensing of Ochratoxin A using unmodified gold nanoparticles indicator," *Biosensors & Bioelectronics,* vol. 26, pp. 2724-2727, Jan 15 2011.
[238] W. Zhao, W. Chiuman, M. A. Brook, and Y. Li, "Simple and rapid colorimetric biosensors based on DNA aptamer and noncrosslinking gold nanoparticle aggregation," *Chembiochem,* vol. 8, pp. 727-731, May 7 2007.
[239] D. H. J. Bunka, O. Platonova, and P. G. Stockley, "Development of aptamer therapeutics," *Current Opinion in Pharmacology,* vol. 10, pp. 557-562, Oct 2010.
[240] S. M. Nimjee, C. P. Rusconi, and B. A. Sullenger, "Aptamers: An emerging class of therapeutics," in *Annual Review of Medicine*. vol. 56, ed, 2005, pp. 555-+.
[241] D. D. Buchanan, E. E. Jameson, J. Perlette, A. Malik, and R. T. Kennedy, "Effect of buffer, electric field, and separation time on detection of aptamer-ligand complexes for affinity probe capillary electrophoresis," *Electrophoresis,* vol. 24, pp. 1375-1382, May 2003.
[242] A. C. Connor and L. B. McGown, "Aptamer stationary phase for protein capture in affinity capillary chromatography," *Journal of Chromatography A,* vol. 1111, pp. 115-119, Apr 14 2006.

[243] Q. Deng, I. German, D. Buchanan, and R. T. Kennedy, "Retention and separation of adenosine and analogues by affinity chromatography with an aptamer stationary phase," *Analytical Chemistry,* vol. 73, pp. 5415-5421, Nov 15 2001.
[244] Q. Deng, C. J. Watson, and R. T. Kennedy, "Aptamer affinity chromatography for rapid assay of adenosine in microdialysis samples collected in vivo," *Journal of Chromatography A,* vol. 1005, pp. 123-130, Jul 11 2003.
[245] Q. Zhao, X.-F. Li, and X. C. Le, "Aptamer-modified monolithic capillary chromatography for protein separation and detection," *Analytical Chemistry,* vol. 80, pp. 3915-3920, May 15 2008.
[246] F. Mongelard and P. Bouvet, "AS-1411, a guanosine-rich oligonucleotide aptamer targeting nucleolin for the potential treatment of cancer, including acute myeloid leukemia," *Current Opinion in Molecular Therapeutics,* vol. 12, pp. 107-114, Feb 2010.
[247] A. D. Keefe, S. Pai, and A. Ellington, "Aptamers as therapeutics," *Nat Rev Drug Discov,* vol. 9, pp. 537-550, 2010.
[248] H. L. Deissler and G. E. Lang, "In vitro studies on the mechanism of action of VEGF and its inhibitors," *Klinische Monatsblatter Fur Augenheilkunde,* vol. 225, pp. 623-628, Jul 2008.
[249] Y. Gao, L. K. Wolf, and R. M. Georgiadis, "Secondary structure effects on DNA hybridization kinetics: a solution versus surface comparison," *Nucleic Acids Research,* vol. 34, pp. 3370-3377, 2006 2006.
[250] K. Feng, C. Sun, Y. Kang, J. Chen, J.-H. Jiang, G.-L. Shen, and R.-Q. Yu, "Label-free electrochemical detection of nanomolar adenosine based on target-induced aptamer displacement," *Electrochemistry Communications,* vol. 10, pp. 531-535, Apr 2008.
[251] D. W. Zhang, F. T. Zhang, Y. R. Cui, Q. P. Deng, S. Krause, Y. L. Zhou, and X. X. Zhang, "A label-free aptasensor for the sensitive and specific detection of cocaine using supramolecular aptamer fragments/target complex by electrochemical impedance spectroscopy," *Talanta,* vol. 92, pp. 65-71, Apr 2012.
[252] C. Teller, S. Shimron, and I. Willner, "Aptamer-DNAzyme Hairpins for Amplified Biosensing," *Analytical Chemistry,* vol. 81, pp. 9114-9119, Nov 1 2009.
[253] J. Wang and H. S. Zhou, "Aptamer-based Au nanoparticles-enhanced surface plasmon resonance detection of small molecules," *Analytical Chemistry,* vol. 80, pp. 7174-7178, Sep 15 2008.
[254] S. Zhang, J. Xia, and X. Li, "Electrochemical Biosensor for Detection of Adenosine Based on Structure-Switching Aptamer and Amplification with Reporter Probe DNA Modified Au Nanoparticles," *Analytical Chemistry,* vol. 80, pp. 8382-8388, Nov 15 2008.

[255] M. Michaud, E. Jourdan, C. Ravelet, A. Villet, A. Ravel, C. Grosset, and E. Peyrin, "Immobilized DNA aptamers as target-specific chiral stationary phases for resolution of nucleoside and amino acid derivative enantiomers," *Analytical Chemistry,* vol. 76, pp. 1015-1020, Feb 15 2004.
[256] J. S. Hargreaves, "Methods for Producing Multilayer Ligand Arrays," United States Patent, 2004.
[257] W. Xu and Y. Lu, "Label-Free Fluorescent Aptamer Sensor Based on Regulation of Malachite Green Fluorescence," *Analytical Chemistry,* vol. 82, pp. 574-578, Jan 15 2010.
[258] N. de-los-Santos-Alvarez, M. J. Lobo-Castanon, A. J. Miranda-Ordieres, and P. Tunon-Blanco, "Modified-RNA aptamer-based sensor for competitive impedimetric assay of neomycin B," *Journal of the American Chemical Society,* vol. 129, pp. 3808-+, Apr 4 2007.
[259] Z. Tang, P. Mallikaratchy, R. Yang, Y. Kim, Z. Zhu, H. Wang, and W. Tan, "Aptamer switch probe based on intramolecular displacement," *Journal of the American Chemical Society,* vol. 130, pp. 11268-11269, Aug 27 2008.
[260] P. Bayman, J. L. Baker, M. A. Doster, T. J. Michailides, and N. E. Mahoney, "Ochratoxin Production by the Aspergillus ochraceus Group and Aspergillus alliaceus," *Applied and Environmental Microbiology,* vol. 68, pp. 2326-2329, May 1, 2002 2002.
[261] A. Ciegler, D. J. Fennell, H. J. Mintzlaff, and L. Leistner, "Ochratoxin synthesis by<i>Penicillium species," *Naturwissenschaften,* vol. 59, pp. 365-366, 1972.
[262] F. S. Chu and B. J. Wilson, "Studies on Ochratoxins," *Critical Reviews in Toxicology,* vol. 2, pp. 499-524, 1973.
[263] R. R. Marquardt and A. A. Frohlich, "A review of recent advances in understanding ochratoxicosis," *Journal of Animal Science,* vol. 70, pp. 3968-88, December 1, 1992 1992.
[264] J. W. Bennett and M. Klich, "Mycotoxins," *Clinical Microbiology Reviews,* vol. 16, pp. 497-+, Jul 2003.
[265] M. Peraica, B. Radic, A. Lucic, and M. Pavlovic, "Toxic effects of mycotoxins in humans," *Bulletin of the World Health Organization,* vol. 77, pp. 754-766, 1999.
[266] N. W. Turner, S. Subrahmanyam, and S. A. Piletsky, "Analytical methods for determination of mycotoxins: A review," *Analytica Chimica Acta,* vol. 632, pp. 168-180, Jan 26 2009.
[267] A. E. Pohland, S. Nesheim, and L. Friedman, "Ochratoxin A - A Review - (Technical Report)," *Pure and Applied Chemistry,* vol. 64, pp. 1029-1046, Jul 1992.

[268] E. E. Creppy, "Human ochratoxicosis," *Journal of Toxicology Toxin Reviews,* vol. 18, pp. 277-293, Aug.-Nov. 1999.
[269] S. Ceovic, A. Hrabar, and M. Saric, "Epidemiology of Balkan Endemic Nephropathy," *Food and Chemical Toxicology,* vol. 30, pp. 183-188, Mar 1992.
[270] P. Galtier, M. Alvinerie, and J. L. Charpenteau, "The Pharmacokinetic Profiles of Ochratoxin-A in Pigs, Rabbits, and Chickens," *Food and Cosmetics Toxicology,* vol. 19, pp. 735-738, 1981 1981.
[271] S. Hagelberg, K. Hult, and R. Fuchs, "Toxicokinetics of Ochratoxin-A in Several Species and its Plasma-binding Properties," *Journal of Applied Toxicology,* vol. 9, pp. 91-96, Apr 1989.
[272] R. Stojkovic, K. Hult, S. Gamulin, and R. Plestina, "High-Affinity Binding of Ochratoxin-A to Plasma Constituents," *Biochemistry International,* vol. 9, pp. 33-38, 1984 1984.
[273] K. Hadjeba-Medjdoub, M. Tozlovanu, A. Pfohl-Leszkowicz, C. Frenette, R. J. Paugh, and R. A. Manderville, "Structure-Activity Relationships Imply Different Mechanisms of Action for Ochratoxin A-Mediated Cytotoxicity and Genotoxicity," *Chemical Research in Toxicology,* vol. 25, pp. 181-190, Jan 2012.
[274] A. Pfohl-Leszkowicz, V. Faucet-Marquis, M. Tozlovanu, F. Pont, M. Castegnaro, and R. Manderville, "Overview on molecular mechanism involved in ochratoxin A biotransformation and genotoxicity," *Abstracts of Papers of the American Chemical Society,* vol. 232, pp. 214-214, Sep 10 2006.
[275] A. Pfohl-Leszkowicz and R. A. Manderville, "An Update on Direct Genotoxicity as a Molecular Mechanism of Ochratoxin A Carcinogenicity," *Chemical Research in Toxicology,* vol. 25, pp. 252-262, Feb 2012.
[276] R. Krska, P. Schubert-Ullrich, A. Molinelli, M. Sulyok, S. Macdonald, and C. Crews, "Mycotoxin analysis: An update," *Food Additives and Contaminants,* vol. 25, pp. 152-163, 2008 2008.
[277] M. V. Howell and P. W. Taylor, "Determination of Aflatoxins, Ochratoxin-A, and Zearalenone in Mixed Feeds, With Detection by Thin-layer Chromatography or High-performance Liquid-chromatography," *Journal of the Association of Official Analytical Chemists,* vol. 64, pp. 1356-1363, 1981 1981.
[278] B. Zimmerli and R. Dick, "Determination of Ochratoxin-A at the PPT Level in Human Blood, Serum, Milk and Some Foodstuffs by High-performance Liquid-chromatography with Enhanced Fluorescence Detection and Immunoaffinity Column Cleanup - Methodology and Swiss Data," *Journal of Chromatography B-Biomedical Applications,* vol. 666, pp. 85-99, Apr 7 1995.

[279] S. Sforza, C. Dall'Asta, and R. Marchelli, "Recent advances in mycotoxin determination in food and feed by hyphenated chromatographic techniques/mass spectrometry," *Mass Spectrometry Reviews,* vol. 25, pp. 54-76, Jan-Feb 2006.
[280] A. A. Frohlich, R. R. Marquardt, and A. Bernatsky, "Quantitation of Ochratoxin-A - Use of Reverse Phase Thin-layer Chromatography for Sample Cleanup Followed by Liquid-Chromatography or Direct Fluorescence Measurement," *Journal of the Association of Official Analytical Chemists,* vol. 71, pp. 949-953, Sep-Oct 1988.
[281] K. Y. Lee, C. F. Poole, and A. Zlatkis, "Simultaneous Multi-mycotoxin Determination by High-performance Thin-layer Chromatography," *Analytical Chemistry,* vol. 52, pp. 837-842, 1980 1980.
[282] A. Leitner, P. Zollner, A. Paolillo, J. Stroka, A. Papadopoulou-Bouraoui, S. Jaborek, E. Anklam, and W. Lindner, "Comparison of methods for the determination of ochratoxin A in wine," *Analytica Chimica Acta,* vol. 453, pp. 33-41, Feb 18 2002.
[283] L. Monaci and F. Palmisano, "Determination of ochratoxin A in foods: state-of-the-art and analytical challenges," *Analytical and Bioanalytical Chemistry,* vol. 378, pp. 96-103, Jan 2004.
[284] J. Teren, J. Varga, Z. Hamari, E. Rinyu, and F. Kevei, "Immunochemical detection of ochratoxin A in black Aspergillus strains," *Mycopathologia,* vol. 134, pp. 171-176, 1996 1996.
[285] M. R. A. Morgan, R. A. Morgan, R. McNerney, and H. W. S. Chan, "Enzyme-linked Immunosorbent-assay of Ochratoxin-A in Barley," *Journal of the Association of Official Analytical Chemists,* vol. 66, pp. 1481-1484, 1983 1983.
[286] S. H. Alarcon, G. Palleschi, D. Compagnone, M. Pascale, A. Visconti, and I. Barna-Vetro, "Monoclonal antibody based electrochemical immunosensor for the determination of ochratoxin A in wheat," *Talanta,* vol. 69, pp. 1031-1037, Jun 15 2006.
[287] B. van der Gaag, S. Spath, H. Dietrich, E. Stigter, G. Boonzaaijer, T. van Osenbruggen, and K. Koopal, "Biosensors and multiple mycotoxin analysis," *Food Control,* vol. 14, pp. 251-254, 2003.
[288] J. A. Cruz-Aguado and G. Penner, "Determination of Ochratoxin A with a DNA Aptamer," *Journal of Agricultural and Food Chemistry,* vol. 56, pp. 10456-10461, Nov 26 2008.
[289] L. Bonel, J. C. Vidal, P. Duato, and J. R. Castillo, "An electrochemical competitive biosensor for ochratoxin A based on a DNA biotinylated aptamer," *Biosensors & Bioelectronics,* vol. 26, pp. 3254-3259, Mar 15 2011.
[290] H. Kuang, W. Chen, D. Xu, L. Xu, Y. Zhu, L. Liu, H. Chu, C. Peng, C. Xu, and S. Zhu, "Fabricated aptamer-based electrochemical "signal-off" sensor

of ochratoxin A," *Biosensors & Bioelectronics,* vol. 26, pp. 710-716, Oct 15 2010.
[291] X. Wei, J. W. Mares, G. Yangdong, D. Li, and S. M. Weiss, "Biomolecule kinetics measurements in flow cell integrated porous silicon waveguides " *Optical Society of America,* 2012.
[292] Q. P. Deng, C. Tie, Y. L. Zhou, and X. X. Zhang, "Cocaine detection by structure-switch aptamer-based capillary zone electrophoresis," *Electrophoresis,* vol. 33, pp. 1465-1470, May 2012.
[293] N. Yildirim, F. Long, C. Gao, M. He, H. C. Shi, and A. Z. Gu, "Aptamer-Based Optical Biosensor For Rapid and Sensitive Detection of 17 beta-Estradiol In Water Samples," *Environmental Science & Technology,* vol. 46, pp. 3288-3294, Mar 2012.
[294] R. A. Potyrailo, R. C. Conrad, A. D. Ellington, and G. M. Hieftje, "Adapting selected nucleic acid ligands (aptamers) to biosensors," *Analytical Chemistry,* vol. 70, pp. 3419-3425, Aug 1998.
[295] Y. H. Lao, K. Peck, and L. C. Chen, "Enhancement of Aptamer Microarray Sensitivity through Spacer Optimization and Avidity Effect," *Analytical Chemistry,* vol. 81, pp. 1747-1754, Mar 2009.
[296] Y. Xiang, Y. Y. Zhang, X. Q. Qian, Y. Q. Chai, J. Wang, and R. Yuan, "Ultrasensitive aptamer-based protein detection via a dual amplified biocatalytic strategy," *Biosensors & Bioelectronics,* vol. 25, pp. 2539-2542, Jul 2010.
[297] P. Hu, C. Z. Zhu, L. H. Jin, and S. J. Dong, "An ultrasensitive fluorescent aptasensor for adenosine detection based on exonuclease III assisted signal amplification," *Biosensors & Bioelectronics,* vol. 34, pp. 83-87, Apr 2012.
[298] J. L. He, Y. F. Yang, G. L. Shen, and R. Q. Yu, "Electrochemical aptameric sensor based on the Klenow fragment polymerase reaction for cocaine detection," *Biosensors & Bioelectronics,* vol. 26, pp. 4222-4226, Jun 2011.
[299] Y. Wang, Z. H. Li, H. Li, M. Vuki, D. K. Xu, and H. Y. Chen, "A novel aptasensor based on silver nanoparticle enhanced fluorescence," *Biosensors & Bioelectronics,* vol. 32, pp. 76-81, Feb 2012.
[300] L. T. Canham, "Nanoscale semiconducting silicon as a nutritional food additive," *Nanotechnology,* vol. 18, May 2007.
[301] S. H. C. Anderson, H. Elliott, D. J. Wallis, L. T. Canham, and J. J. Powell, "Dissolution of different forms of partially porous silicon wafers under simulated physiological conditions," *Physica Status Solidi a-Applied Research,* vol. 197, pp. 331-335, May 2003.
[302] E. J. Anglin, L. Y. Cheng, W. R. Freeman, and M. J. Sailor, "Porous silicon in drug delivery devices and materials," *Advanced Drug Delivery Reviews,* vol. 60, pp. 1266-1277, Aug 2008.

[303] L. M. Bonanno and L. A. DeLouise, "Tunable Detection Sensitivity of Opiates in Urine via a Label-Free Porous Silicon Competitive Inhibition Immunosensor," *Analytical Chemistry,* vol. 82, pp. 714-722, Jan 2010.
[304] C. A. Prestidge, T. J. Barnes, C. H. Lau, C. Barnett, A. Loni, and L. Canham, "Mesoporous silicon: a platform for the delivery of therapeutics," *Expert Opinion on Drug Delivery,* vol. 4, pp. 101-110, Mar 2007.
[305] H. A. Santos, J. Salonen, L. M. Bimbo, V. P. Lehto, L. Peltonen, and J. Hirvonen, "Mesoporous materials as controlled drug delivery formulations," *Journal of Drug Delivery Science and Technology,* vol. 21, pp. 139-155, Mar-Apr 2011.
[306] J. P. DeVincenzo, "The promise, pitfalls and progress of RNA-interference-based antiviral therapy for respiratory viruses," *Antiviral Therapy,* vol. 17, pp. 213-225, 2012.
[307] J. N. Leonard and D. V. Schaffer, "Antiviral RNAi therapy: emerging approaches for hitting a moving target," *Gene Therapy,* vol. 13, pp. 532-540, Mar 2006.
[308] J. DeVincenzo, R. Lambkin-Williams, T. Wilkinson, J. Cehelsky, S. Nochur, E. Walsh, R. Meyers, J. Gollob, and A. Vaishnaw, "A randomized, double-blind, placebo-controlled study of an RNAi-based therapy directed against respiratory syncytial virus," *Proceedings of the National Academy of Sciences of the United States of America,* vol. 107, pp. 8800-8805, May 11 2010.
[309] V. Bitko, A. Musiyenko, O. Shulyayeva, and S. Barik, "Inhibition of respiratory viruses by nasally administered siRNA," *Nature Medicine,* vol. 11, pp. 50-55, Jan 2005.
[310] E. J. Chapman, A. I. Prokhnevsky, K. Gopinath, V. V. Dolja, and J. C. Carrington, "Viral RNA silencing suppressors inhibit the microRNA pathway at an intermediate step," *Genes & Development,* vol. 18, pp. 1179-1186, May 15 2004.
[311] Q. Ge, L. Filip, A. L. Bai, T. Nguyen, H. N. Eisen, and J. Chen, "Inhibition of influenza virus production in virus-infected mice by RNA interference," *Proceedings of the National Academy of Sciences of the United States of America,* vol. 101, pp. 8676-8681, Jun 8 2004.
[312] L. Gitlin, S. Karelsky, and R. Andino, "Short interfering RNA confers intracellular antiviral immunity in human cells," *Nature,* vol. 418, pp. 430-434, Jul 25 2002.
[313] D. Palliser, D. Chowdhury, Q. Y. Wang, S. J. Lee, R. T. Bronson, D. M. Knipe, and J. Lieberman, "An siRNA-based microbicide protects mice from lethal herpes simplex virus 2 infection," *Nature,* vol. 439, pp. 89-94, Jan 5 2006.
[314] G. Randall, A. Grakoui, and C. M. Rice, "Clearance of replicating hepatitis C virus replicon RNAs in cell culture by small interfering RNAs,"

Proceedings of the National Academy of Sciences of the United States of America, vol. 100, pp. 235-240, Jan 7 2003.
[315] A. Shlomai and Y. Shaul, "Inhibition of hepatitis B virus expression and replication by RNA interference," *Hepatology,* vol. 37, pp. 764-770, Apr 2003.
[316] M. M. Fabani, C. Abreu-Goodger, D. Williams, P. A. Lyons, A. G. Torres, K. G. C. Smith, A. J. Enright, M. J. Gait, and E. Vigorito, "Efficient inhibition of miR-155 function in vivo by peptide nucleic acids," *Nucleic Acids Research,* vol. 38, pp. 4466-4475, Jul 2010.
[317] G. D. Ivanova, A. A. Arzumanov, J. J. Turner, M. M. Fabani, R. Abes, B. Lebleu, and M. J. Gait, *RNA targeting in cells by peptide conjugates of peptide nucleic acids (PNA)* vol. 10, 2008.
[318] J. J. Turner, M. Fabani, A. A. Arzumanov, G. Ivanova, and M. J. Gait, "Targeting the HIV-1 RNA leader sequence with synthetic oligonucleotides and siRNA: Chemistry and cell delivery," *Biochimica Et Biophysica Acta-Biomembranes,* vol. 1758, pp. 290-300, Mar 2006.
[319] J. J. Turner, S. Jones, M. M. Fabani, G. Ivanova, A. A. Arzumanov, and M. J. Gait, "RNA targeting with peptide conjugates of oligonucleotides, siRNA and PNA," *Blood Cells Molecules and Diseases,* vol. 38, pp. 1-7, Jan-Feb 2007.
[320] J. W. Mares and S. M. Weiss, "Diffusion dynamics of small molecules from mesoporous silicon films by real-time optical interferometry," *Applied Optics,* vol. 50, pp. 5329-5337, Sep 2011.